TESLA-FEL 2008-03

Fiber Laser Master Oscillators for Optical Synchronization Systems

Dissertation

zur Erlangung des Doktorgrades
des Department Physik
der Universität Hamburg

vorgelegt von

Axel Winter
aus Köln

Hamburg
2008

Gutachter der Dissertation	Prof. Dr. Peter Schmüser Prof. Dr. F. Ömer Ilday (Bilkent University, Ankara)
Gutachter der Disputation	Prof. Dr. Peter Schmüser Prof. Dr. Manfred Tonutti (RTWH Aachen)
Datum der Disputation	22. April 2008
Vorsitzender des Prüfungsausschusses	Dr. Klaus Petermann
Vorsitzender des Promotionsausschusses	Prof. Dr. Jochen Bartels
Dekan der Fakultät für Mathematik, Informatik und Naturwissenschaften	Prof. Dr Arno Frühwald

Abstract

New X-ray free electron lasers (e.g. the European XFEL) require a new generation of synchronization system to achieve a stability of the FEL pulse, such that pump-probe experiments can fully utilize the ultra-short pulse duration (50 fs). An optical synchronization system has been developed based on the distribution of sub-ps optical pulses in length-stabilized fiber links. The synchronization information is contained in the precise repetition frequency of the optical pulses. In this thesis, the design and characterization of the laser serving as laser master oscillator is presented. An erbium-doped mode-locked fiber laser was chosen. Amplitude and phase noise were measured and record-low values of 0.03 % and 10 fs for the frequency range of 1 kHz to the Nyquist frequency were obtained. Furthermore, an initial proof-of-principle experiment for the optical synchronization system was performed in an accelerator environment. In this experiment, the fiber laser wase phase-locked to a microwave reference oscillator and a 500 meter long fiber link was stabilized to 12 fs rms over a range of 0.1 Hz to 20 kHz. RF signals were obtained from a photodetector without significant degradation at the end of the link. Furthermore, the laser master oscillator for FLASH was designed and is presently in fabrication and the initial infrastructure for the optical synchronization system was setup.

Zusammenfassung

Freie Elektronen Laser wie z.B. der European XFEL produzieren Röntgenpulse mit einer Zeitdauer von einigen 10 Femtosekunden. Um diese Pulse für z.B. Pump-Probe Experimente mit höchster Zeitauflösung nutzen zu können, wird ein neuartiges Synchronisationssystem gebraucht, so dass eine Zeitstabilität des Röntgenpulses bezüglich des Probelasers von ebenfalls wenigen zehn Femtosekunden erreicht wird. Ein vielversprechender Ansatz basiert auf der Verteilung von optischen Pulsen mit einer Zeitdauer von ca. 100 Femtosekunden über längenstabilisierte Faserlinks. Die Synchronisationsinformation ist in der präzisen Repetitionsrate der Laserpulse enthalten. In dieser Arbeit wird sowohl Design als auch Charakterisierung des modengekoppleten Erbium-dotierten Faserlasers vorgestellt, der als "laser-master oscillator" des Systems benutzt werden soll. Eine der wichtigsten Eigenschaften ist das Amplituden- und Phasenrauschen dieser Laser. Es wurde zu 0.03% bzw. 10 fs in einem Frequenzbereich von 1 kHz bis zur Nyquistfrequenz vermessen, was eine bisher nicht erreichte Stabilität darstellt. Weiterhin wurde ein erster Test dieses Synchronisationskonzeptes in einer Beschleunigerumgebung durchgeführt. Ein Faserlaser wurde an die Mikrowellenreferenz des Beschleunigers gekoppelt und eine 500 Meter lange Glasfaserleitung wurde auf 12 fs stabiliert. Radiofrequenzsignale wurden aus den übertragenen optischen Signalen gewonnen, ohne das Phasenrauschen signifikant zu beeinträchtigen. Weiterhin wurde der "laser-master oscillator" für FLASH entworfen sowie die Infrastruktur für das optische Synchronisationssystem für FLASH aufgebaut.

Contents

1. Introduction and Motivation

The key mission of new free-electron lasers facilities such as the European X-ray Free-Electron Laser (XFEL) [Alt06] or the Free-Electron Laser in Hamburg (FLASH) is to produce ultra-short FEL pulses of between 20 fs and 100 fs duration at an unprecedented peak brilliance of up to (10^{33} photons/s/mm^2/0.1%BW). Most present day facilities depend on self amplified spontaneous emission (SASE), where spontaneous radiation from an electron bunch in an undulator is amplified in a highly nonlinear process to yield output peak powers in the GW range. Since the SASE process starts from noise, there are statistical timing and pulse energy fluctuations which cannot be compensated for.

A second option to create the FEL pulses is by modulating the electron beam with a high power laser beam at the desired output wavelength and to amplify only the modulated part of the electron beam (”seeded”-FEL’s). This approach is presently under development and will be implemented at FERMI [Bro07] and is proposed as an upgrade for FLASH [Sch07]. Laser systems operating at the desired FEL wavelength (typically tens of nanometers or shorter) are presently not available. High harmonics of the fundamental laser wavelength (often a titanium-sapphire laser with a wavelength of around 800 nm is used) produced in a gas cell are foreseen to produce seeding pulses with wavelengths down to around 30 nm. The seeding approach is presently not a viable option for facilities which produce x-ray pulses in the Angstrom range. For the seeding approach, the most important source of timing variations is the jitter between the laser system producing the laser pulses used to seed the FEL and the accelerator reference. This can be controlled by stabilizing the laser system with respect to the main accelerator reference.

1.1. The timing problem in modern accelerators

The short pulse duration of the FEL pulses opens a new road to time-resolved experiments with resolutions down to the ten femtosecond range [GAB+08]. These experiments are usually conducted by using a pump-probe approach. Most commonly, the FEL pulse is used to pump the sample and pulses from a dedicated short-pulse high-power optical laser system are used to probe the response with variable time delay. To

fully use the time resolution offered by the short FEL pulse durations, the synchronization between the FEL pulse and the probe laser system must be extremely tight, ideally on the order of the FEL pulse duration.

The timing jitter between the FEL pulse and the probe laser is dominated by:

- The timing jitter of the FEL pulse with respect to to the accelerator phase reference which is mainly caused by,
  - the stability of the laser system used to produce photoelectrons at the photocathode,
  - the stability of the radio frequency (RF) in the accelerating cavities,
  - jitter introduced by the bunch compression,
  - the jitter introduced by the SASE process.
- The timing jitter between the probe laser and the accelerator phase reference.

The electron bunches needs to enter the undulator with timing jitter comparable to the pulse duration, which requires point-to-point stabilization of various RF frequencies for the critical components (booster section, injector, bunch compressors and experimental area) with femtosecond precision. This translates to an amplitude and phase stability of the RF of 10^{-4} and 0.01 deg respectively in the cavities used to impose an energy chirp on the electron bunch. The required amplitude stability levels have almost been achieved in present day facilities, e.g. at JLAB and at FLASH [Lie05, Sim05]. The best phase stability reported for superconducting cavities is on the order of 0.03 °; improving this to the 0.01 ° level (21 fs at 1.3 GHz) seems feasible. However, in order to accurately measure the phase stability, one requires a high-quality reference with much smaller phase jitter than the signal to be measured. A key challenge is to provide this reference in facilities spanning a few kilometers in length.

These requirements appear to be beyond the capability of traditional RF distribution systems based on temperature-stabilized coaxial cables. A promising way to reach this goal was first suggested by Prof. Kärtner of MIT in 2004 [KM04]. It is based on an optical transmission system, depicted schematically in Figure 1.1. The centerpiece of the system is a mode-locked laser that emits a train of sub-picosecond light pulses with very low timing jitter. To further reduce the overall timing jitter of the laser, it is phase-locked to a microwave reference oscillator. The optical pulse train is distributed over actively length-stabilized optical fiber links to multiple remote locations. The precise repetition frequency of the pulse train contains the synchronization information. At the remote locations, the laser pulse train can be used directly for beam diagnostics [LHL+06], locking other laser systems with optical cross correlators or by directly seeding them with the transmitted pulse train [DK05], or generating highly-stable RF

signals [KL06]. This approach opens the road to long-term synchronization of various components in the accelerator to the 10 fs level over long distances (up to several kilometers).

One of the key components for the synchronization system is the source of the optical pulse train to be transmitted. It needs to supply a highly phase-stable optical pulse train with a reliability that is compatible with continuous accelerator operation. Most laser systems do not meet these requirements and the main part of this thesis has been devoted to design, built and evaluate a suitable laser system and to conduct a first test of a fiber optic distribution in a real accelerator environment.

In the following a linac-driven light source will be introduced and its main compo-

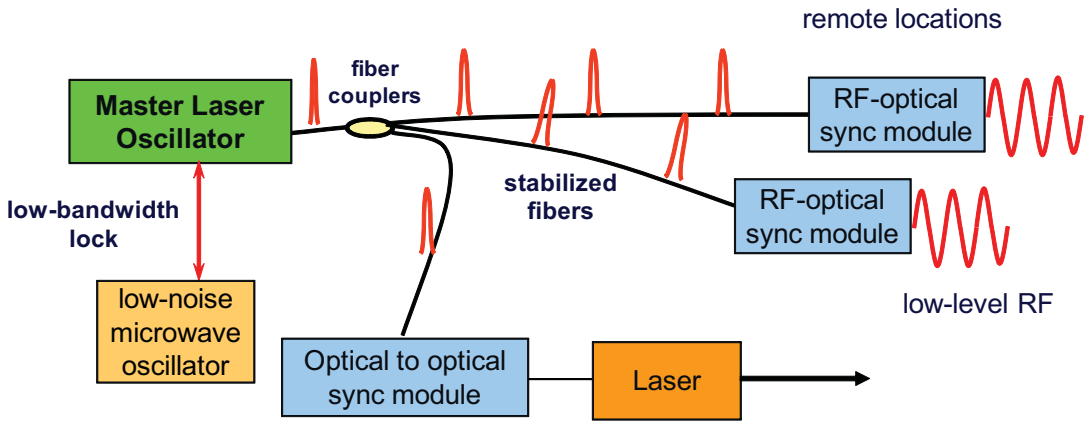

Figure 1.1.: Schematic overview of the optical synchronization system

nents explained. Taking the Free Electron Laser in Hamburg (FLASH) as an example, the main aspects regarding the time jitter of the electron beam are discussed. The general layout of the machine has been widely described in various sources, the description given here follows the one found in [Ste07]. Then an introduction to the theoretical foundations of propagation of ultra-short pulses in optical fibers and mode-locking is given. In chapter 3 the proposed fiber laser system for the laser master oscillator is described, followed by the characterization of the key properties of the laser system. In chapter 5 a first test in an accelerator environment will be presented followed by the design and layout of the laser master oscillator for FLASH.

1.2. The FLASH accelerator and free-electron laser

The free electron laser in Hamburg (FLASH) has recently been upgraded to a maximum electron energy of 1 GeV allowing to cover the wavelength range from 6.2 nm to 45 nm [TES02] with significant power also present in the third and fifth harmonic. The

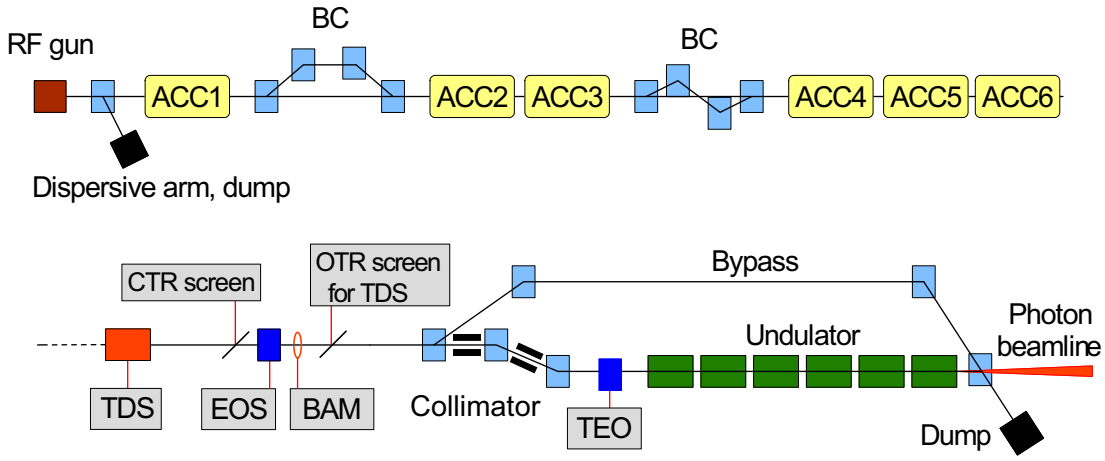

Figure 1.2.: Schematic layout of FLASH at DESY. The beam is accelerated to a maximum energy of 1 GeV in six acceleration modules ACC1 to ACC6 containing eight superconducting cavities each. The two bunch compression stages are denoted by BC. The accelerator is followed by a diagnostic section and the undulator to create the FEL radiation. Abbreviations for the experiments in the diagnostic section are explained in the text.

FEL is based on the principle of self amplified spontaneous emission (SASE), which opens the way to powerful FELs in the x-ray regime. Electron bunches of extremely high local charge density are needed to achieve laser saturation in the undulator magnet.

The FLASH linear accelerator and free electron laser consists of three main parts: the RF-photoinjector, the superconducting linac including the bunch compressors, and the undulators. A schematic overview of FLASH is shown in Fig. 1.2.

1.2.1. The photoinjector gun

A laser driven RF photo-cathode gun is used to produce the high current electron bunches with small transverse emittance and a small energy spread as they are needed for the operation of a SASE-FEL [SCG+02, FP02].

A high power, actively mode-locked Nd:YLF laser generates a series of pulses at a wavelength of 1047 nm. The pulses are frequency doubled twice in two nonlinear crystals to reach a wavelength of 262 nm with a pulse energy of up to 50 µJ and a pulse duration of 4 ps (rms). Three frequencies from the master oscillator (13.5 MHz, 108 MHz and 1.3 GHz) are used to mode-lock the Nd:YLF laser with a fundamental repetition rate of 27 MHz. The 13.5 MHz are used ensure that the laser operates at the fundamental repetition frequency, whereas the 108 MHz and 1.3 GHz are used to obtain a shorter pulse duration. Before amplification, the laser repetition rate is reduced to a maximum of 2.5 MHz. This is one of the systems that will greatly benefit from an optical synchronization system, since the residual timing jitter can be greatly re-

duced compared to conventional RF synchronization techniques by using optical cross correlators.

The laser beam is focused onto a cesium telluride (Cs_2Te) photo-cathode, where the pulses liberate electrons due to photo emission. The cathode is placed inside a $1\frac{1}{2}$-cell normal conducting copper RF structure operated at 1.3 GHz with a maximum accelerating gradient of up to 42 MV/m on the cathode. The high gradient is needed to rapidly accelerate the electrons to relativistic energies to reduce the emittance increase due to internal Coulomb forces. One solenoid coil is placed around the RF cavity to produce a longitudinal magnetic field of 0.163 T along the axis of the cavity. A small bucking coil at the back of the cathode is used to cancel the field at the cathode surface. The solenoid field focuses the accelerated electrons to counteract the effects of the internal Coulomb forces. This way it is possible to achieve a bunch charge of 0.5 to 1 nC with a normalized transverse emittance of only a few micrometers.

The electron bunches leave the gun with an energy of about 4.5 MeV per electron and an rms bunch length of about 4 ps and are injected into the first accelerating module.

1.2.2. The present RF-based synchronization system

Presently, all frequencies used in FLASH originate from a central master oscillator system located near the photoinjector laser. The central frequency is at 9.02777 MHz which is the 144^{th} subharmonic of the acceleration frequency of 1.3 GHz. All frequencies are transmitted via coaxial cables to their respective destinations. Since stability of the reference signal is critical for the regulation of the RF field inside the cavities, it is transported via temperature stabilized cables to minimize drifts.

At the present time, all lasers (injector laser, diagnostic lasers, pump-probe laser and the planned seed laser) are synchronized to the accelerator using RF techniques. The achievable short-term stability with these techniques is on the order of 50 fs. Drifts resulting from the transfer of the reference frequency via cables to the laser positions are however on the order of several hundred femtoseconds. Diagnostic and pump-probe laser systems are especially sensitive, since they are located at distances of up to 300 meters from the position of the master oscillator.

1.2.3. The accelerator modules

The electrons are accelerated by alternating electric fields stored in resonant RF cavities. The cavities used at the FLASH accelerator are superconducting nine cell cavities developed for the TESLA[1] collider project [RSTW01]. The cavities are made from

[1] Teraelectronvolt Energy Superconducting Linear Accelerator

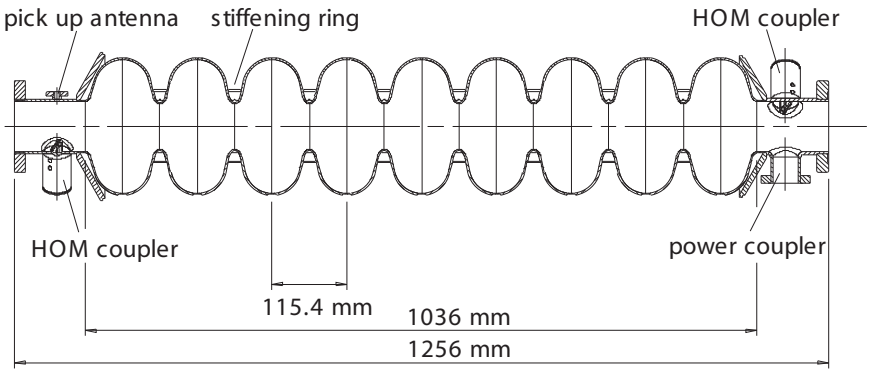

Figure 1.3.: Cross section of a superconducting RF cavity installed in the FLASH linac[Aun00]. The power coupler is connected by a wave guide to the klystron. Higher-order mode (HOM) couplers remove resonant fields of higher order that are induced by the electron bunches. A pick-up antenna is used to measure the field.

pure niobium and are operated at 2 K using superfluid helium cooling.

The cavities (Fig. 1.3) are excited at 1.3 GHz at their TEM_{010} mode, where the electric field is parallel to the axis. The length of the resonating cells $L = \frac{1}{2}\frac{c}{f}$ is be chosen such that a relativistic particle with speed $v \approx c$ needs half a period of the resonating frequency to pass from cell to cell. An electron entering a cell at the zero crossing of the electric field is accelerated along the full length of the cell and leaves the cell when the electric field strength changes its sign. In multi-cell cavities excited at their π-mode, neighboring cells have a phase offset of π. This means that a standing wave pattern emerges in the multi-cell cavities, where the sign of the electric field alternates from one cell to the next. Thus an electron entering the first cell at the zero crossing of the electric field is accelerated along the full length of the cavity. When it enters the next cell it is accelerated again, since the phase advance of the standing wave pattern is π between cells. The RF phase setting, where the electron has the maximum possible energy gain, is usually referred to as *on-crest acceleration*, for all other phases the electron gains less energy (*off-crest acceleration*) or even loses energy (*deceleration*).

The FLASH linac consists of six accelerating modules containing eight cavities each. The accelerating gradients vary between 12 MV/m and 25 MV/m, for electron energies between 380 MeV to 1 GeV. The photoinjector and the modules are powered by three 5 MW klystrons and one 10 MW klystron. The first 5 MW klystron drives the gun, the second one module ACC1, the third one drives modules ACC2 and ACC3 and the 10 MW klystron drives the modules ACC4-ACC6. The amplitude and phase of the accelerating fields in the cavities are controlled by adjusting amplitude and phase of the individual klystrons. As the phase setting for the RF in ACC1 is significantly different from the other accelerating modules, it is powered by a separate klystron. Each

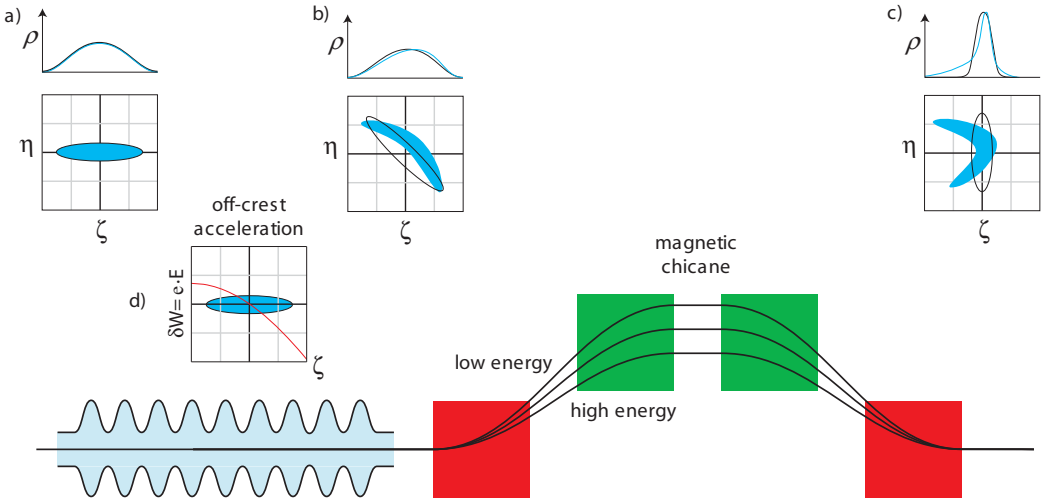

Figure 1.4.: Schematic drawing of a bunch compressor. The off-crest acceleration introduces a correlated energy spread. The phase space is sheared by the magnetic chicane. Symbols: δW: energy gain of a particle, η: particle energy relative to reference particle, ζ: relative longitudinal position inside the bunch, ρ: longitudinal charge density, E: electric field.
a) The particle distribution as a function of ζ and as a function of W and ζ before the acceleration. b) The particle distribution after off-crest acceleration. c) The particle distribution behind the magnetic chicane. The peak current is increased. The black ellipse shows linear compression, the blue shape the effects of non-linear compression. d) The energy gain in the accelerating cavity as a function of relative longitudinal position.
Adapted from [Isc03].

nine-cell cavity in the modules is equipped with a pick-up antenna to measure its field. The complex field amplitudes from all eight cavities an ACC1 are added vectorially in a digital signal processor. The vector sum is used to regulate phase and amplitude of module ACC1 and the module groups ACC2-3 and ACC4-6.

1.2.4. Bunch compression

The SASE-FEL process requires electron bunches with high peak currents of several kA. These currents cannot be directly produced in the injector gun, because the resulting repulsive space change forces would be huge and disrupt the bunch. To reach these high peak currents the 4 ps long electron bunches from the injector gun with peak currents of about 100 A are longitudinally compressed after further acceleration at energies of 125 MeV and 380 MeV. At these highly relativistic energies the attractive magnetic forces largely compensate the repulsive electric space charge forces. For the compression magnetic chicanes are used in which electrons with different energies have different path lengths so that an electron bunch with an energy distribution correlated with the longitudinal position can be compressed in length.

Shifting the phase of the first accelerating module away from the on-crest phase

leads to a stronger acceleration of the electrons in the tail of the bunch than the electrons in the head: an energy chirp is imposed on the bunch. In the following magnetic chicane the higher energetic electrons in the tail of the bunch are deflected less by the dipole magnets and travel on a shorter trajectory through the chicane, allowing them to catch up with the leading electrons (Fig. 1.4).

Since the bunch length covers a non-negligible part of the RF wavelength – 4 ps corresponds to about 2° of an 1.3 GHz oscillation – and the accelerating field has a sinusoidal time dependency, the energy chirp is not linear. This leads to a nonlinear compression and results in a longitudinal charge distribution, which is not Gaussian any more but has a short leading spike followed by a longer tail. The nonlinearity can be reduced somewhat by using two bunch compressors. If the energy chirp is introduced in two stages (once with a long bunch before the first bunch compressor and once between the first and second bunch compressor) the introduced nonlinearities will be weaker for the second chirping section, as the bunch has already been compressed by the first bunch compressor. Also other distorting effects like coherent synchrotron radiation are reduced by distributing the compression among two bunch compressors at different energies.

At FLASH the energy chirp is imposed on the bunch by an acceleration at about 8° off crest in the first accelerating module. The bunch with an energy of 125 MeV is then partially compressed in a C-type magnetic chicane and further accelerated to 380 MeV by two modules operated either on-crest or slightly off off-crest to introduce further energy chirp. The second bunch compressor is a S-type magnetic chicane further compressing the bunch to its final shape with a leading spike of about 100 fs length with a peak current of several kA.

This is also one of the most critical parts of the machine with regard to timing jitter. Any variation in the energy chirp is directly converted into timing jitter which is why the amplitude and phase stability of the RF fields inside the cavities is extremely critical. In a single-stage bunch compression scheme, the timing jitter introduced by the bunch compressors can be expressed in the form [SAL+05]:

$$\sigma_t^2 \approx \left(\frac{R_{56}}{c}\frac{\sigma_a}{A}\right)^2 + \left(\frac{C-1}{C}\right)^2 \left(\frac{\sigma_\phi}{\omega_{rf}}\right)^2 + \left(\frac{1}{C}\right)^2 \sigma_{in}^2 \tag{1.1}$$

Here, R_{56} is the dispersion of the bunch compressor (about 180 mm for FLASH and 100 mm for the XFEL), C is the the compression factor (between 20 and 100), ω_{RF} is the angular frequency of the accelerating RF, σ_A/A and σ_ϕ/ω_{rf} is the relative amplitude and phase stability of the RF in the accelerating cavities responsible for introducing the chirp onto the electron bunch and σ_{in} is the timing jitter introduced by fluctuations of the arrival time of the injector laser pulse at the photocathode.

As an example, a superconducting linear accelerator with a radio frequency of 1.3 GHz and a vector-sum based RF regulation is assumed (compression factor and R_{56} as stated above). The vector sum regulation - summing the vectors of the RF of many cavities and only keeping the sum vector stable - helps in terms of required stability for amplitude and phase of the RF in the cavities, as uncorrelated errors in amplitude and phase are reduced by $\sqrt{N}$, where N is the number of cavities in the vector sum. Furthermore, there is a correlation between amplitude and phase stability (1 degree of phase stability corresponds to 1.8 % amplitude stability). Assuming as a goal for the arrival time stability a value of 50 fs, the most critical number is the amplitude stability (between 3 and 5 ps/%). The impact of amplitude fluctuations on the arrival is of the same order as that of phase fluctuations (2 ps/degree). The RF stability needs to be on the order of $5 \cdot 10^{-5}$ for amplitude and 0.02 ° for the phase. It turns out, that incoming timing jitter actually gets reduced after the bunch compressor by a factor of 20, which is the bunch compression ratio. This is a significant advantage of the bunch compression scheme. It is however only true, if no energy feedback systems are present. The incoming timing jitter caused by the photoinjector laser leads to a different mean energy of the electron bunch. This is measured and corrected by changing the phase of the acceleration modules. This counteracts the reduction in timing jitter by the compression.

1.2.5. The diagnostic and collimation section

The last acceleration module is followed by a section equipped with several experiments for bunch diagnostics to measure the longitudinal charge distribution, coherent transition radiation (CTR), slice emittance and the bunch arrival time. These experiments include the transverse deflecting structure (TDS), the CTR beam line, the electro-optical beam phase monitor, the timing electro-optical experiment (TEO) and electro-optic diagnostics using temporal and spatial decoding (EOS) [GBS07].

A small dispersive section with collimators protects the undulator magnets from radiation damage. Copper apertures in front of the dispersive section remove most of the beam halo, while apertures inside the dispersive section remove electron dark current which has a different energy than the bunch.

1.2.6. The undulator section

The undulator system consists of six magnets each 4.5 m long. The undulator magnets create a sinusoidal field in vertical direction on the beam axis with a period of 27.3 mm and a peak induction of 0.46 T, leading to a horizontal oscillation of the electron beam (see figure 1.5).

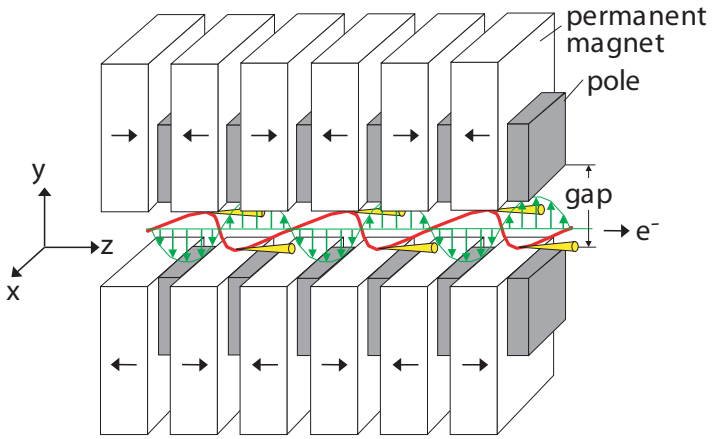

Figure 1.5.: Arrangement of the magnets in the undulator that creates a sinusoidal field on the beam axis [FP99]. The electron beam oscillation is not to scale.

Between the segments quadrupole magnets are installed to focus the beam as well as diagnostic tools, such as beam position monitors (BPM) and wire scanners to measure position and transverse shape of the electron beam. Achieving a perfect overlap of the electron beam with the radiation field generated inside the undulator is mandatory for the FEL process. Therefore, the utmost care has been taken in aligning all the elements. An excellent field quality has been achieved in the undulator modules so that the expected rms deviations of the electrons from the ideal orbit should be less than 10 μm [Ayv06].

Following the undulators a dipole magnet bends the electron beam to an underground beam dump while the FEL radiation continues through a section with photon diagnostic to the experimental hall with the user beam lines.

2. Theoretical Basis of Fiber Lasers

2.1. Propagation of ultra-short pulses in optical fibers

Much of ultrafast and nonlinear optics is based on an understanding and a quantitative description of the propagation of laser light in a dispersive optical medium. In this chapter, the basic wave equation will be derived, followed by the theory of pulse propagation in nonlinear dispersive media. Furthermore, the properties of optical fibers with regard to short-pulse propagation will be discussed, i.e. group velocity dispersion, nonlinear effects, fiber modes. This chapter is primarily based on [Agr01b, Agr01a], further details can be found there.

2.1.1. The wave equation

Like all electromagnetic phenomena, the propagation of pulses in optical fiber is governed by Maxwell's equations

$$\begin{aligned} \text{(i)} \quad \nabla \cdot \boldsymbol{D} &= \rho, \\ \text{(ii)} \quad \nabla \cdot \boldsymbol{B} &= 0, \\ \text{(iii)} \quad \nabla \times \boldsymbol{E} &= -\frac{\partial \boldsymbol{B}}{\partial t}, \\ \text{(iv)} \quad \nabla \times \boldsymbol{H} &= \boldsymbol{j} + \frac{\partial \boldsymbol{D}}{\partial t}, \end{aligned} \tag{2.1}$$

where $\boldsymbol{E}$ and $\boldsymbol{H}$ are the electric and magnetic field vectors, respectively and $\boldsymbol{D}$ and $\boldsymbol{B}$ are the corresponding electric and magnetic flux densities. These coupled equations describe the time evolution of the electric and magnetic fields. As there are no free charges in optical fibers, current density $\boldsymbol{j}$ and free charges ρ vanish. The relation between flux densities and electric and magnetic fields are generally given by

$$\boldsymbol{D} = \epsilon_0 \boldsymbol{E} + \boldsymbol{P} \quad \text{and} \quad \boldsymbol{B} = \mu_0 \boldsymbol{H} + \boldsymbol{M}, \tag{2.2}$$

where for an optical medium the induced magnetic polarization $\boldsymbol{M}$ is zero. It is possible to eliminate $\boldsymbol{B}$ and extract an equation for the electric field only. Using equation (iv) and 2.2, one obtains,

$$\nabla \times \boldsymbol{B} = \mu_0 \epsilon_0 \frac{\partial \boldsymbol{E}}{\partial t} + \mu_0 \frac{\partial \boldsymbol{P}}{\partial t} \tag{2.3}$$

Taking the curl of both sides of equation (iii) and using the mathematical identity $\nabla \times (\nabla \times \boldsymbol{E}) = \nabla(\nabla \cdot \boldsymbol{E}) - \nabla^2 \boldsymbol{E}$ yields

$$\nabla(\nabla \cdot \boldsymbol{E}) - \nabla^2 \boldsymbol{E} = -\frac{\partial}{\partial t} (\nabla \times \boldsymbol{B}) . \tag{2.4}$$

Using equation 2.3, one obtains an equation containing $\boldsymbol{E}$ only:

$$\nabla(\nabla \cdot \boldsymbol{E}) - \nabla^2 \boldsymbol{E} = -\mu_0 \epsilon_0 \frac{\partial^2 \boldsymbol{E}}{\partial t^2} - \mu_0 \frac{\partial^2 P}{\partial t^2} \tag{2.5}$$

Since there are no free charge carriers and the material is homogeneous, we have $\nabla \cdot \boldsymbol{E} = 0$ and using $\epsilon_0 \mu_0 = 1/c^2$, the equation above reduces to the wave equation for isolating, polarizable, nonmagnetic materials

$$\nabla^2 \boldsymbol{E} - \frac{1}{c^2} \frac{\partial^2 \boldsymbol{E}}{\partial t^2} = \mu_0 \frac{\partial^2 \boldsymbol{P}}{\partial t^2} \tag{2.6}$$

2.1.2. Derivation of the nonlinear Schrödinger equation

A few assumptions need to be made to further evaluate 2.6:

- The polarization response of the material is assumed to be instantaneous, i.e. $\boldsymbol{P}$ is only determined by the present conditions, there is no delayed response or memory effect in the system. This is valid for a nonlinear response that is electronic in nature, since the reconfiguration time of the electron cloud is on the order of 0.1 fs and hence significantly smaller than the period of the optical light wave. The contribution of molecular vibrations to the nonlinear part of the polarization (the Raman effect) is neglected for the time being and will be included later in this section.
- The nonlinearity in $\boldsymbol{P}$ is assumed to be small enough to be treated perturbatively.
- The optical field maintains its polarization along the fiber length, such that a scalar approach is sufficient.

The assumption of an instantaneous response allows to expand the induced polarization in a series of powers of the instantaneous electric field:

$$\hat{\boldsymbol{P}}(\boldsymbol{r},t) = \epsilon_0(\underbrace{\chi^{(1)}\hat{\boldsymbol{E}}(\boldsymbol{r},t)}_{\hat{\boldsymbol{P}}_L} + \underbrace{\chi^{(2)}\hat{\boldsymbol{E}}^2(\boldsymbol{r},t) + \chi^{(3)}\hat{\boldsymbol{E}}^3(\boldsymbol{r},t) + \ldots}_{\hat{\boldsymbol{P}}_{NL}}) = \hat{\boldsymbol{P}}_L + \hat{\boldsymbol{P}}_{NL} \tag{2.7}$$

It should be noted that the electric field has a time structure that has a rapidly and slowly varying component. The fast timescale corresponds to the optical cycle, which is on the order of $\lambda/c \approx 3\,\mathrm{fs}$. The slow timescale corresponds to the width of the pulse, which is typically on the order of 100 fs or longer. This leads to the following formulation for the electric field and polarization respectively where the field is written as a product of a slowly varying amplitude and a plane wave:

$$\begin{aligned}
\hat{\boldsymbol{E}}(\boldsymbol{r},t) &= \frac{1}{2}\boldsymbol{u}_x\left[E(\boldsymbol{r},t)\exp(i\beta_0 z - i\omega_0 t)) + c.c.\right] && (2.8)\\
&= \frac{1}{2}\boldsymbol{u}_x\left[F(x,y)A(z,t)\exp(i\beta_0 z - i\omega_0 t)) + c.c.\right] && (2.9)\\
\hat{\boldsymbol{P}}_L(\boldsymbol{r},t) &= \frac{1}{2}\boldsymbol{u}_x\left[P_L(\boldsymbol{r},t)\exp(i\beta_0 z - i\omega_0 t)) + c.c.\right] && (2.10)\\
\hat{\boldsymbol{P}}_{NL}(\boldsymbol{r},t) &= \frac{1}{2}\boldsymbol{u}_x\left[P_{NL}(\boldsymbol{r},t)\exp(i\beta_0 z - i\omega_0 t)) + c.c.\right]
\end{aligned}$$

It is understood, that only the real part of above equations is physically relevant, and hence the complex conjugate will not be explicitly stated anymore. Here, $\boldsymbol{u}_x$ is the unit vector perpendicular to the direction of propagation, which can be dropped due to the assumption that the polarization is preserved during the propagation through the fiber. $E(\boldsymbol{r},t)$ and $P_{L/NL}(\boldsymbol{r},t)$ are the slowly varying envelopes of the electric field and linear/nonlinear polarization respectively. For the later derivations, it is practical to separate the dependencies on x and y (modal pattern) from that on z and t (propagation). This makes sense, as the transverse mode structure in the fiber is to first order independent of propagation length and time. The quickly varying parts in both time and longitudinal position z are expressed as a plane wave which propagates in the z-direction and is of definite frequency ω_0 and associated wave number $\beta_0 = n\omega_0/c$.

With the assumptions from equation 2.7, the nonlinear polarization can be approximated by [Agr01b]

$$P_{NL}(\boldsymbol{r},t) = \epsilon_0\epsilon_{NL}(\boldsymbol{r},t)E(\boldsymbol{r},t) \quad \text{with} \quad \epsilon_{NL}(\boldsymbol{r},t) = \frac{3}{4}\chi^{(3)}|E(\boldsymbol{r},t)|^2 \tag{2.11}$$

ϵ_{NL} is slowly varying both spatially and temporally compared to the optical wavelength λ and period ω. To obtain a solution of the wave equation for the slowly varying amplitude $E(\boldsymbol{r},t)$, it is useful to apply a Fourier transform to equation 2.6 (keeping in

mind ($\frac{\partial}{\partial t} \rightarrow i\omega$)). Whenever a Fourier or reverse Fourier transform is applied in this thesis, the following form is used:

$$\tilde{E}(\boldsymbol{r}, \omega) = \int_{-\infty}^{\infty} E(\boldsymbol{r}, t) \exp[i\omega t] dt \tag{2.12}$$

or

$$E(\boldsymbol{r}, t) = \frac{1}{2\pi} \int_{-\infty}^{\infty} \tilde{E}(\boldsymbol{r}, \omega) \exp[-i\omega t] d\omega \tag{2.13}$$

respectively. Since ϵ_{NL} is usually intensity dependent, it is generally not possible to apply a Fourier transform. However, since a perturbation approach is used in which ϵ_{NL} is a small perturbation, it can be treated as locally constant:

$$\left(\nabla^2 + \epsilon(\boldsymbol{r}, \omega)\frac{\omega^2}{c^2}\right)\tilde{E}(\boldsymbol{r}, \omega) = 0. \tag{2.14}$$

with the dielectric function given by

$$\epsilon(\omega) = 1 + \epsilon_L + \epsilon_{NL} = 1 + \tilde{\chi}^{(1)} + \frac{3}{4}\tilde{\chi}^{(3)}(\omega). \tag{2.15}$$

Equation 2.14 can be solved by making an Ansatz of the form

$$\tilde{E}(\boldsymbol{r}, \omega - \omega_0) = F(x, y)\tilde{A}(z, \omega - \omega_0) \exp(ik_0 z) \tag{2.16}$$

which is the Fourier transform of equation 2.9. Here, $\tilde{A}(z, \omega)$ is a slowly varying function of z and $F(x, y)$ is the modal distribution of the pulse in the fiber. Some calculation (see e.g. [Agr01b]) leads to two equations for $F(x, y)$ and $\tilde{A}(z, \omega)$:

$$\frac{\partial^2 F}{\partial x^2} + \frac{\partial^2 F}{\partial y^2} + [\epsilon(\omega)\frac{\omega^2}{c^2} - \beta^2(\omega)]F = 0 \tag{2.17}$$

$$2i\beta_0 \frac{\partial \tilde{A}}{\partial z} + (\beta^2(\omega) - \beta_0^2)\tilde{A} = 0 \tag{2.18}$$

Owing to the assumption that $\tilde{A}$ is a slowly varying function of z, its second derivative with respect to z is neglected in both equations. The wave number $\beta(\omega)$ is determined by solving the eigenvalue equation for the fiber modes. The solution will not be discussed here, for details see [Agr01b]. One can approximate the dielectric function by

$$\epsilon(\omega) = (n(\omega) + \Delta n)^2 \approx n^2 + 2n\Delta n \tag{2.19}$$

where Δn is a small perturbation given by the nonlinearity of the refractive index and the absorption $\tilde{\alpha}$ and gain $\tilde{g}$ in the fiber

$$\Delta n = n_2|E^2| + \frac{i\tilde{\alpha}(\omega) - \tilde{g}(\omega)}{2k_0}. \tag{2.20}$$

The solution for the modal distribution $F(x, y)$ is unchanged compared to the case without the perturbation, but the eigenvalue solutions are altered to

$$\tilde{\beta}(\omega) = \beta(\omega) + \Delta\beta \quad \text{with} \quad \Delta\beta = \frac{k_0 \int\int_{-\infty}^{\infty} \Delta n(x, y)|F(x, y)|^2 dxdy}{\int\int_{-\infty}^{\infty} |F(x, y)|^2 dxdy}. \tag{2.21}$$

This is similar to the approach used in first-order perturbation theory in quantum mechanics, which takes the unperturbed eigenfunctions and computes corrected eigenvalues. Only single-mode fibers are considered here, so the only solution of interest for equation 2.17 is the fundamental fiber mode HE11 given by [Agr01b]

$$F(x, y) = J_0(\kappa\rho), \quad \rho = \sqrt{x^2 + y^2} \leq a \tag{2.22}$$

inside the core and

$$F(x, y) = \sqrt{a/\rho} J_0(\kappa\rho) \exp[-\gamma(\rho - a)], \quad \rho \geq a \tag{2.23}$$

outside the core. This modal distribution is difficult to work with and is for practical purposes approximated by the Gaussian distribution

$$F(x, y) = \exp[-(x^2 + y^2)/w^2] \tag{2.24}$$

where w is the width parameter obtained by fitting the exact distribution to a Gaussian form.

Rewriting equation 2.18 and approximating $\beta^2(\omega) - \beta_0^2 \approx 2\beta_0(\beta(\omega) - \beta_0)$ yields

$$\frac{\partial \tilde{A}}{\partial z} = i[\beta(\omega) + \Delta\beta - \beta_0]\tilde{A}. \tag{2.25}$$

For a final step, one takes the inverse Fourier transform of above equation to arrive at a time-domain representation of the slowly varying envelope function $A(z, t)$. Since generally an exact functional form for $\beta(\omega)$ is not known, it is helpful to expand it in a

Taylor series about the carrier frequency ω_0

$$\beta(\omega) = \beta_0 + (\omega-\omega_0)\left.\frac{d\beta}{d\omega}\right|_{\omega=\omega_0} + \frac{1}{2}(\omega-\omega_0)^2\left.\frac{d^2\beta}{d\omega^2}\right|_{\omega=\omega_0} + \ldots \equiv \beta_0 + \beta_1(\omega-\omega_0) + \frac{\beta_2}{2}(\omega-\omega_0)^2 \tag{2.26}$$

The cubic and higher terms are negligible if the pulse duration in the ps-range. For femtosecond pulses however, third-order dispersion has to be taken into account. Substituting equation 2.26 in equation 2.25 and taking the inverse Fourier transform 2.13 results in

$$\frac{\partial A}{\partial z} = -\beta_1\frac{\partial A}{\partial t} - \frac{i\beta_2}{2}\frac{\partial^2 A}{\partial t^2} + i\Delta\beta A \tag{2.27}$$

Fiber losses and nonlinear effects are accounted for by the term $\Delta\beta$ and can be evaluated using equation 2.20, leading to

$$\frac{\partial A}{\partial z} + \beta_1\frac{\partial A}{\partial t} + \frac{i\beta_2}{2}\frac{\partial^2 A}{\partial t^2} + \frac{\alpha}{2}A = i\gamma|A|^2 A \quad \text{with} \quad \gamma = \frac{n_2\omega_0}{cS_{eff}} \tag{2.28}$$

where γ is called the nonlinear parameter and S_{eff} the effective area of an optical fiber. A precise evaluation requires the use of the modal distribution F(x,y). If the Gaussian approximation for the fundamental mode is used, $S_{eff} = \pi w^2$. For the interesting regime around a wavelength of 1.5 μm, it ranges from around 20-100 μm^2.

One last transformation brings equation 2.28 into its commonly known form. One makes a transformation into a reference frame moving at the group velocity $v_g = 1/\beta_1$ of the pulse envelope

$$\frac{\partial A}{\partial z} + \frac{i\beta_2}{2}\frac{\partial^2 A}{\partial T^2} + \frac{\alpha}{2}A = i\gamma|A|^2 A, \tag{2.29}$$

where $T = t - z/v_g \equiv t - \beta_1 z$. This equation is called the nonlinear Schrödinger equation and is most commonly used to describe the propagation of ps-range pulses through optical fibers, taking into account fiber losses through α, chromatic dispersion through β_2 and fiber nonlinearities through γ.

For practical purposes, it is often very convenient to introduce characteristic length scales on which certain effects act, for instance dispersion and nonlinearities. This makes it possible to compare the relative strengths of effects vs. the total propagation distance. It is then possible to immediately get an idea which effects will play a role and which might be neglected. For the above equation, the characteristic scales are the propagation length L, the dispersive length L_D, defined as

$$L_D = \frac{T_0^2}{\beta_2} \tag{2.30}$$

and the nonlinear length L_{NL} as

$$L_{NL} = \frac{1}{\gamma P_0} \tag{2.31}$$

Here, T_0 is the initial pulse length and P_0 is the pulse peak power. Rewriting equation 2.29 leads to

$$\frac{\partial a}{\partial z} + \frac{i}{2}\frac{L}{L_D}\frac{\partial^2 a}{\partial \tau^2} + \frac{\alpha}{2}a = i\frac{L}{L_{NL}}|a|^2 a, \tag{2.32}$$

where the absolute square of the field now gives power instead of intensity, through the transformation $a(z,\tau) = A(z,t)/\sqrt{S_{eff}}$.

Unfortunately, some of the simplifications and assumptions used in the derivation of the NLSE are not valid for ultra-short pulses (100 fs regime). The bandwidth needed to support such short pulses is so large that effects due to third-order dispersion cannot be neglected anymore. Furthermore the assumption that the fiber nonlinearity responds instantaneously compared to the pulse duration is no longer justified. The contribution to $\chi^{(3)}$ from molecular vibrations (the Raman effect) occurs over a time scale of around 60 fs. The next section will deal with the extension of the NLSE to include these effects.

2.1.3. Higher order nonlinear effects

For pulses with sufficient optical bandwidth (>0.1 THz), the Raman effect can amplify low-frequency components by energy transfer form the high-frequency components and lead to a red-shift of the optical spectrum of the pulse, the so-called self frequency shift. To include this effect, one needs to take a new look at the nonlinear polarization in equation 2.6. It is still allowed to neglect any $\chi^{(2)}$ related effects as they require phase-matching. One assumes a form of

$$P_{NL}(\boldsymbol{r},t) = \epsilon_0 \chi^{(3)} E(\boldsymbol{r},t) \int_{-\infty}^{t} R(t-t_1)|E(\boldsymbol{r},t_1)|^2 dt_1 \tag{2.33}$$

which bundles the nonlinear behavior in a response function $\chi^{(3)}R(t-t_1)$ where R is defined similarly to a time-delayed delta function such that $\int_{-\infty}^{\infty} R(t)dt = 1$. In its simplest form this would correspond to $R(t-t_1) = \delta(t-(t_1+\Delta t))$. The integration extends to a finite upper boundary t to preserve causality. The perturbation approach from section 2.1.2 is still valid and a somewhat lengthy algebra finally leads to the expression (for details see [Agr01b])

$$\frac{\partial A}{\partial z} + \beta_1\frac{\partial A}{\partial t} + \frac{i\beta_2}{2}\frac{\partial^2 A}{\partial t^2} - \frac{\beta_3}{6}\frac{\partial^3 A}{\partial t^3} + \frac{\alpha}{2}A = i\gamma\left(1 + \frac{i}{\omega_0}\frac{\partial}{\partial t}\right)\left(A(z,t)\int_{-\infty}^{\infty} R(t')|A(z,t-t')|^2 dt\prime\right) \tag{2.34}$$

If one sticks to the regime of pulse durations, where the slowly varying envelope approximation is still valid (τ >>10 fs) it is possible to simplify equation 2.29 using a Taylor expansion of the form

$$|A(z,t-t')|^2 \approx |A(z,t)|^2 - t'\frac{\partial}{\partial t}|A(z,t)|^2, \tag{2.35}$$

One arrives finally at the following equation:

$$\frac{\partial A}{\partial z} + \frac{\alpha}{2}A + \frac{i\beta_2}{2}\frac{\partial^2 A}{\partial T^2} - \frac{\beta_3}{6}\frac{\partial^3 A}{\partial T^3} = i\gamma\left(|A|^2 A + \frac{i}{\omega_0}\frac{\partial}{\partial T}(|A|^2 A) - T_R A\frac{\partial |A|^2}{\partial T}\right) \tag{2.36}$$

In arriving at above equation, a reference frame moving with the group velocity is used, similar to 2.29 and T_R is defined as the first momentum of the nonlinear response function $T_R = \int_{-\infty}^{\infty} tR(t)dt$. This form of the NLSE now also contains the third-oder

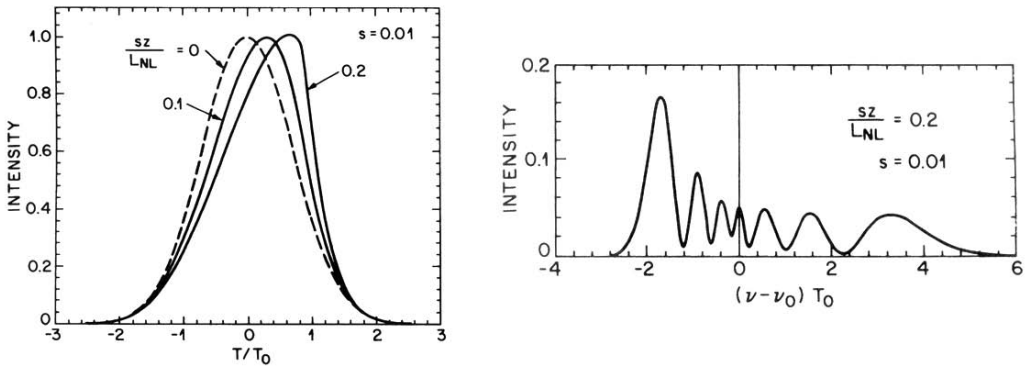

Figure 2.1.: Left: Self steepening for a Gaussian pulse (GVD effects neglected); Right: Spectrum of a Gaussian Pulse after propagation through a length of optical fiber. Self steepening is responsible for the asymmetry of the spectrum, which is broadened by self phase modulation (from [Agr01a])

dispersion (term proportional to β_3), the effect of self-steepening and shock formation (term proportional to ω_0^{-1}) and finally the effect of self-steepening caused by the delayed Raman response. Self-steepening results from the intensity dependence of the group velocity. This means that the intense center of a pulse gets shifted toward longer wavelengths (see left of Figure 2.1) and that an asymmetry appears in the spectrum of ultrashort pulses broadened by self-phase modulation (see right of Figure 2.1). A numerical value for first order momentum of T_R =3 fs has experimentally been obtained for the spectral region around 1550 nm.

2.1.4. Solution of the nonlinear Schrödinger equation

For negative β_2, the NLSE has a specific solution that does not change along the fiber length. Such a phenomenon is called a solitary wave solution. It was first described in 1834 by Scott Russell, who observed water waves propagating with undistorted phase over several kilometers through a canal.

The physical origin for optical solitons is a balance of dispersion and nonlinearity. If one rewrites equation 2.29, this becomes clear:

$$\frac{\partial A}{\partial z} = i\gamma|A|^2A - \frac{i\beta_2}{2}\frac{\partial^2 A}{\partial T^2} \quad \text{with} \quad \gamma = \frac{n_2\omega_0}{cS_{eff}} \tag{2.37}$$

This assumes no fiber losses, so $\alpha = 0$. So if the sign of β_2 and $\frac{\partial^2 A}{\partial T^2}$is negative, there can be a combination of pulse duration (the parameter responsible for the magnitude of β_2) and pulse energy (the parameter responsible for the magnitude of γ), such that both terms cancel and $\frac{\partial A}{\partial z} = 0$. This means that, neglecting fiber losses and higher order nonlinear effects, the envelope of the pulse does not change while propagating through a fiber. Through the effective area in the nonlinear parameter γ and the magnitude of β_2, the combination of pulse energy and duration is specific for each individual fiber type. As a rule of thumb, the so-called soliton energy is 1 nJ fiber for a pulse duration of 100 fs in SMF28 fiber. The solution is characterized by a very characteristic secans hyperbolicus shape:

$$|A(t)| = \sqrt{\frac{|\beta_2|}{\gamma T_0^2}}\operatorname{sech}\left(\frac{T}{T_0}\right) = \sqrt{\frac{|\beta_2|}{\gamma T_0^2}}\frac{1}{\cosh\left(\frac{T}{T_0}\right)} \tag{2.38}$$

This solution is called a first order soliton. Assuming a lossless fiber, this solution propagates indefinitely without changing its pulse duration.

2.2. Amplification in rare-earth doped fibers

2.2.1. Pumping and gain coefficient

Incident light of the correct wavelength can be amplified in optical fibers through stimulated emission. This is realized by optically pumping the amplifier fiber to obtain population inversion. Depending on the energy level of the dopants (usually rare earths like erbium, ytterbium or neodymium), the lasing scheme can be classified as three level or four level scheme (see figure 2.2). In either case, the dopants absorb pump photons and reach an excitation stage and then relax rapidly into a lower-energy excited state. The lifetime of this intermediate state is usually long (around 10 ms for

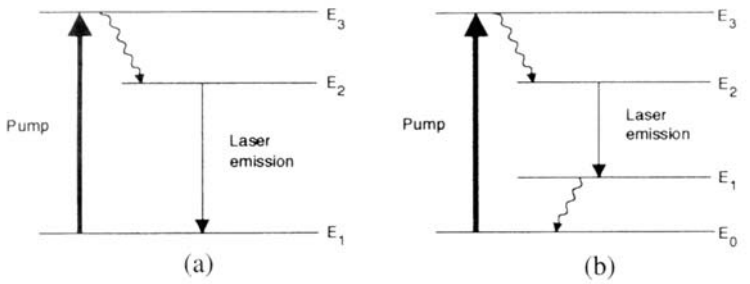

Figure 2.2.: Illustration of three and four level lasing schemes

erbium and 1 ms for ytterbium), and the stored energy is used to amplify incident light through stimulated emission. The difference between the three and four level lasing schemes is the level to which the dopant relaxes after stimulated emission. In the case of a three level lasing scheme, it is directly the ground state, whereas in the case of a four level lasing scheme it is another intermediate state. Erbium-doped fiber lasers and amplifiers are three-level lasers/amplifiers.

Pumping creates the necessary population inversion and hence provides the optical gain. Using the appropriate rate equations (see e.g. [ME88]) for a homogeneously broadened gain medium, one can write

$$g(\omega) = \frac{g_0}{1 + (\omega - \omega_a)^2 T_2^2 + P/P_s}, \tag{2.39}$$

where g_0 is the peak gain value, ω the frequency of the incident signal, ω_a the atomic transition frequency and P is the optical power of the signal being amplified. The saturation power P_s is mainly influenced by parameters such as the fluorescence time T_1 (in the range of 1 μs to 10 ms for commonly used dopants) and the transition cross section σ. The parameter T_2 is the dipole relaxation time and is usually on the order of 0.1 ps.

If one neglects the saturation effect for the moment, the equation shows that the gain reduction for frequencies off the transition frequency is governed by a Lorentzian gain profile as to be expected from a homogeneously broadened system. The gain bandwidth $\Delta\nu$ is defined as the full width at half maximum (FWHM) of the gain spectrum $g(\omega)$, given for a Lorentzian spectrum as

$$\Delta\nu_g = \frac{\Delta\omega_g}{2\pi} = \frac{1}{\pi T_2}. \tag{2.40}$$

However, the gain spectrum of a fiber laser is considerably affected by the amorphous nature of the silica and the presence of other co-dopants such as aluminum or germanium. Figure 2.3 shows the gain spectrum of a fiber with different co-dopants.

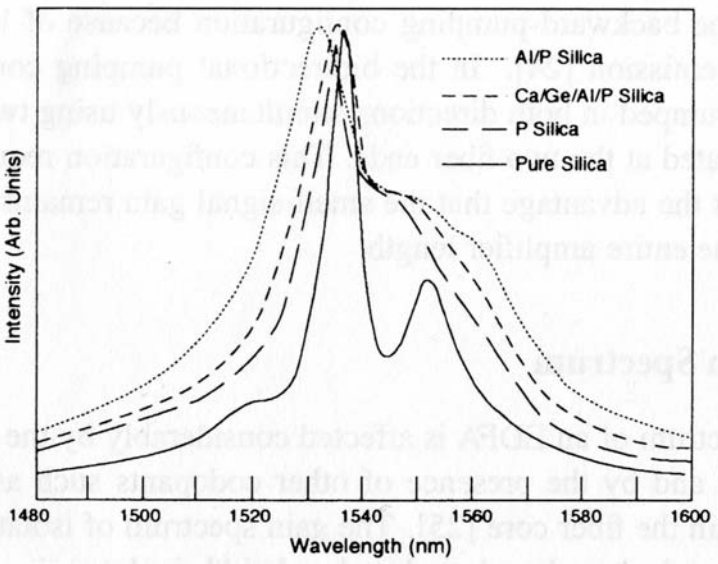

Figure 2.3.: Gain spectra of various erbium-doped fibers with different core composition (from [Agr01a])

It can be clearly seen, that the Lorentzian approximation is not sufficient.

2.2.2. Gain-induced dispersive and nonlinear effects

In this subsection, the implications of gain provided by dopants for the nonlinear Schrödinger equation will be described.

The lifetime of the first upper state is significantly shorter than the lifetime of the level from which stimulated emission takes place. Thus the lasing process can be approximated by a two-level system. The dynamics of a two level system are described by the Maxwell-Bloch equations [ME88]. The starting point is the wave equation 2.6. The induced polarization $\boldsymbol{P}(\boldsymbol{r})$ has to be altered to include a third term $\boldsymbol{P}_d(\boldsymbol{r})$ representing the contributions of the dopants. Using the slowly varying envelope approximation similar to 2.10, one obtains

$$\hat{\boldsymbol{P}}_d(\boldsymbol{r},t) = \frac{1}{2}\boldsymbol{u}_x\left[P_d(\boldsymbol{r},t)\exp(i\beta_0 z - i\omega t) + c.c.\right] \tag{2.41}$$

The slowly varying part obeys the Bloch equations ([ME88]) which relate the population inversion density $W = N_2 - N_1$ to the polarization and electric field:

$$\frac{\partial P(\boldsymbol{r},t)}{\partial t} = -\frac{P(\boldsymbol{r},t)}{T_2} - i(\omega_a - \omega_0)P(\boldsymbol{r},t) - \frac{i\mu^2}{\hbar}E(\boldsymbol{r},t)W \tag{2.42}$$

$$\frac{\partial W}{\partial t} = \frac{W_0 - W}{T_1} + \frac{1}{\hbar}\mathrm{Im}(E^*(\boldsymbol{r},t)\cdot P(\boldsymbol{r},t)). \tag{2.43}$$

Here, μ is the magnetic dipole moment, ω_a is the atomic transition frequency, and $E(\boldsymbol{r}, t)$ is the slowly varying amplitude defined as in equation 2.10.
Following the same derivation described in section 2.1.2, the nonlinear Schrödinger equation 2.28 is modified to the following form:

$$\frac{\partial A}{\partial z} + \beta_1 \frac{\partial A}{\partial t} + \frac{i\beta_2}{2}\frac{\partial^2 A}{\partial t^2} + \frac{\alpha}{2}A = i\gamma|A|^2 A + \frac{i\omega_0}{2\epsilon_0 c}\langle P_d(\boldsymbol{r}, t)\rangle \tag{2.44}$$

The bracket angles denote an averaging over the mode profile $|F(x, y)|^2$. The three equations 2.42, 2.43 and 2.44 need to be solved for pulses of a duration equal to the dipole relaxation time (0.1 ps). The analysis can be simplified considerably for longer pulses, where the dopants response to the induced polarization can be considered adiabatic (for details see reference [ME88]). Dispersive effects can be included by defining the dopant susceptibility as follows

$$\tilde{P}(\boldsymbol{r}, \omega) = \epsilon_0 \chi_d(\boldsymbol{r}, \omega)\tilde{E}(\boldsymbol{r}, \omega). \tag{2.45}$$

The susceptibility can be found (see again [ME88]) as

$$\chi_d(\boldsymbol{r}, \omega) = \frac{\sigma_s W(\boldsymbol{r}) n_0 c/\omega_0}{(\omega - \omega_a)T_2 + i}. \tag{2.46}$$

Most of the derivation of the propagation equation in section 2.1.2 remains valid, provided the dielectric constant is modified to take χ_d into account. This leads to a change for equation 2.20:

$$\Delta n = n_2|E|^2 + \frac{\chi_d}{2n}. \tag{2.47}$$

The major complication of things is that now $\Delta\beta$ in equation 2.21 becomes frequency dependent owing to χ_d. So when transforming the optical field back into time domain, not only β but also $\Delta\beta$ must be expanded into a Taylor series. The resulting equation can be found after some lengthy derivations (see reference [Agr91]):

$$\frac{\partial A}{\partial z} + \beta_1^{eff}\frac{\partial A}{\partial t} + \frac{i}{2}\beta_2^{eff}\frac{\partial^2 A}{\partial t^2} + \frac{\alpha}{2}A = i\gamma|A|^2 A + \frac{g_0}{2}\frac{1 + i\delta}{1 + \delta^2}A, \tag{2.48}$$

with

$$\beta_1^{eff} = \beta_1 + \frac{g_0 T_2}{2}\left[\frac{1 - \delta^2 + 2i\delta}{(1 + \delta^2)^2}\right], \tag{2.49}$$

$$\beta_2^{eff} = \beta_2 + g_0 T_2\left[\frac{\delta(\delta^2 - 3) + i(1 - 3\delta^2)}{(1 + \delta^2)^3}\right] \tag{2.50}$$

and the detuning parameter $\delta = (\omega_0 - \omega_a)T_2$ and the gain given by

$$g_0(z,t) = \frac{\sigma_s \int\int_{-\infty}^{\infty} W(\boldsymbol{r},t)|F(x,y)|^2 dxdy}{\int\int_{-\infty}^{\infty} |F(x,y)|^2 dxdy}, . \tag{2.51}$$

The spatial averaging is due to the use of equation 2.47 in equation 2.21. Looking at equation 2.48, it is clear that gain not only influences the group velocity of the pulse (keeping in mind that $v_g = \beta_1^{-1}$), but also the chromatic dispersion through the effective β_2. The magnitude of the change in β_1 is usually negligible, since the second term is on the order of 10^{-4} compared to β_1, however not so for β_2^{eff} since especially near the zero-dispersion wavelength of the optical fiber used the two terms become comparable. Even for the special case of $\delta = 0$, β_2^{eff} does not reduce to β_2, in fact it comes down to

$$\beta_2^{eff} = \beta_2 + ig_0 T_2^2, \tag{2.52}$$

which is now a complex parameter caused by the gain provided by the dopants. The physical origin of this so called "'gain dispersion"', is due to the finite gain bandwidth of doped fibers. The actual form of equation 2.52 is due to the parabolic gain approximation used in the derivations in reference [Agr91].

The integration of equation 2.51 is usually very difficult since the inversion profile depends on the spatial coordinates and the mode profile because of gain saturation. However, in practice only a small part of the fiber core is actually doped. If both mode and dopant intensity are nearly uniform over the doped region, one can assume W to be constant there and zero outside. Then one can readily integrate equation 2.51 leading to

$$g_0(z,t) = \Gamma_s \sigma_s W(z,t), \tag{2.53}$$

where Γ_s is the fraction of the mode power in the doped region. Using this result and equation 2.43, one can find the following equation for the gain dynamics:

$$\frac{\partial g_0}{\partial t} = \frac{g_{ss} - g_0}{T_1} - \frac{g_0 |A|^2}{T_1 P_s^{sat}} \tag{2.54}$$

Here, $g_{ss} = \Gamma_s \sigma_s W_0$ is the small signal gain. Taking into consideration that the fluorescence time T_1 is long compared to the pulse width and hence spontaneous emission and changes in pump power do not occur over the timescale of the pulse duration, one can integrate equation 2.54, which leads to

$$g_0(z,t) \approx g_{ss} \exp\left(-\frac{1}{E_s}\int_{-\infty}^{t} |A(z,t')|^2 dt'\right), \tag{2.55}$$

where E_s is the saturation energy which is on the order of 1 μJ. This energy level is not reached in the lasers and fiber amplifiers in the optical synchronization system, so gain saturation is negligible over the pulse duration. However for a pulse train, saturation effects can occur over timescales longer than T_1. In this case, the saturation is determined by the average power in the amplifier system $g_0 = g_{ss}(1 + P_{av}/P_s^{sat})^{-1}$

In summary, the pulse propagation in an optical fiber is governed by a generalized nonlinear Schrödinger equation 2.28 without any gain and with coefficients β_1^{eff} and β_2^{eff} if dopants are present in the fiber. These effective coefficients are not only complex but also vary along the fiber length. In a specific case where the detuning parameter is zero, the nonlinear Schrödinger equation can be written as

$$\frac{\partial A}{\partial z} + \frac{i}{2}(\beta_2 + ig_0T_2^2)\frac{\partial^2 A}{\partial T^2} = i\gamma|A|^2A + \frac{g_0 - \alpha}{2}A, \tag{2.56}$$

where $T = t - \beta_1^{eff}z$ is the reduced time, similar to the derivations in 2.1.2. The T_2 term takes into account the decrease in gain for spectral components of the pulse far from the gain peak. This equation is sometimes called the "Master Equation of Modelocking" [Hau91]

2.3. Mode-locking

Ultra-short pulses with a duration of a few-ps or less can only be achieved by mode-locking the laser. For this purpose, one has to establish a rigid phase relation between the many longitudinal modes which can exist in a laser cavity of a certain length. In this chapter, the principle of mode-locking will be introduced with special emphasis on passive mode-locking using an artificial saturable absorber, as this is the method of choice for the erbium-doped fiber lasers used in this thesis.

2.3.1. Superposition of longitudinal modes

An electromagnetic pulse propagating in a laser resonator can be described by a superposition of plane waves with different wavelengths. The possible wavelengths of the longitudinal modes in a resonator are given by the condition

$$n \cdot \lambda_n = 2 \cdot L, \tag{2.57}$$

where λ_n is the wavelength of the longitudinal mode and L the resonator length. In principle, a large number of modes of different frequency can exist at the same time. These modes will be independent in phase and amplitude. Thus the total electric field

in the resonator is given by the sum of the field of all excited modes:

$$E(z,t) = \sum_n E_n(z,t) = \sum_n E_{0,n} e^{ik_n z - i\omega_n t}, \quad \text{with} \quad E_{0,n} = |E_{0,n}| e^{i\phi_n} \tag{2.58}$$

where $E_{0,n}$ is the complex amplitude of the n-th mode and ϕ_n its phase. Assuming an equal amplitude for all modes, the intensity is given by

$$I(z,t) \propto E(z,t)E^*(z,t) = |E_0|^2 \sum_{n=1}^{N} \sum_{m=1}^{N} e^{i(\phi_n - \phi_m)} (m-n)\Omega(\frac{z}{c} - t). \tag{2.59}$$

with

$$\Omega = \omega_{n+1} - \omega_n = \frac{\pi c}{L} \tag{2.60}$$

being the frequency difference between two neighboring modes. If all modes have a fixed phase relation, equation 2.59 yields:

$$I(z,t) \propto |E_0|^2 \, e^{i\delta\phi} \sum_{n=1}^{N} \sum_{m=1}^{N} e^{i(m-n)\Omega(\frac{z}{c} - t).} \tag{2.61}$$

The second exponential function in equation 2.61 becomes equal to 1 for all terms of the sum if the condition

$$\frac{\Omega}{c}(z - ct) = 2\pi \cdot j \quad \Leftrightarrow \quad z - ct = 2L \cdot j, \quad j = 0, 1, 2, ... \tag{2.62}$$

is fulfilled. The maximum of equation 2.61 under this condition is

$$I_{max} = N^2 \, |E_0|^2 \equiv N^2 I_0 \tag{2.63}$$

One can derive the spatial and temporal distances of consecutive pulses as a function of the intensity I_{max} from equation 2.62, which yields:

$$\Delta z = 2L, \quad \Delta t = \frac{2L}{c} \equiv T \tag{2.64}$$

That means the intensity maxima repeat with the revolution time T of the laser cavity and there is one maximum inside the resonator at any given time. Through a fixed phase relation between the many modes in the resonator, regular pulses with a peak intensity I_{max} will develop, proportional to the square of the number of involved modes (see figure 2.4). To calculate the FWHM of the pulses (see [HP98]), one can assume that at a fixed time $t = 0$ the superposition of N modes is similar to the interference of

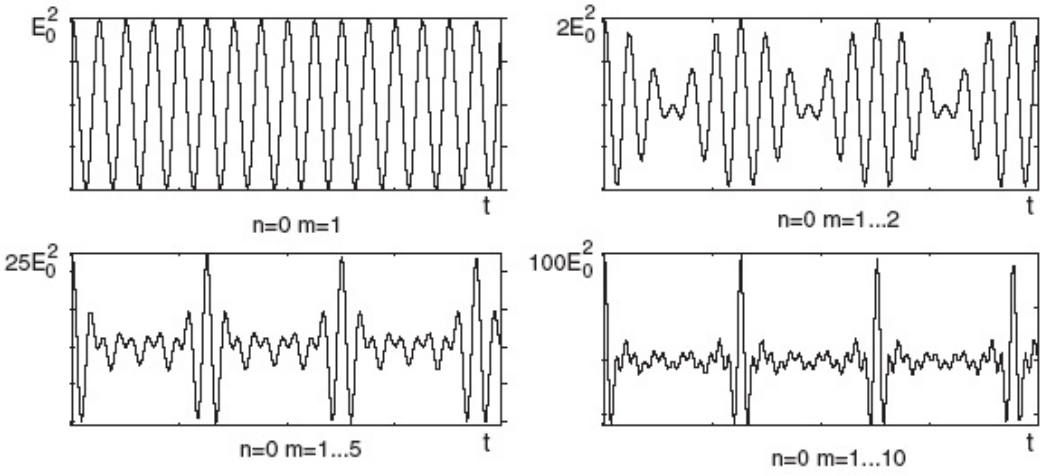

Figure 2.4.: Superposition of different number of longitudinal modes with a fixed phase difference. The intensity of these pulses scales quadratically with the number of involved modes.

N planar waves. Using the geometric series, one arrives at

$$I(t) = I_0 \frac{\sin^2(\frac{N\Omega}{2}t)}{\sin^2(\frac{\Omega}{2}t)}, \quad \Omega = \frac{\pi c}{L} \tag{2.65}$$

Using equation 2.65, one can derive the FWHM of the pulses:

$$I(\Delta T) = \frac{1}{2} I_{max} \quad \rightarrow \quad \Delta T = \frac{1}{N}\frac{2L}{c} = \frac{1}{N}T \tag{2.66}$$

So the pulse width decreases with the number of superposed modes and is proportional to the revolution time of the laser cavity.

A rigid phase relation between superposing modes can be achieved by a modulation of the gain of the resonator (or the losses respectively) with the difference frequency Ω of adjacent modes. All mechanisms to achieve a mode-lock rely on that principle. Through the loss modulation, the electromagnetic field in the resonator acquires an additional time dependence:

$$\begin{aligned} E_n(z,t) &= (E_{0,n} + E_n^{mod}\cos\Omega t)e^{ik_n z - \omega_n t} \\ &= \left[E_{0,n}e^{-i\omega_n t} + \frac{1}{2}E_n^{mod}\left(e^{-i\Omega t} + e^{i\Omega t}\right)e^{-i\omega_n t}\right]e^{ik_n z} \\ &= \left[E_{0,n}e^{-i\omega_n t} + \frac{1}{2}E_n^{mod}\left(e^{-i\omega_{n+1} t} + e^{-i\omega_{n-1} t}\right)\right]e^{ik_n z} \end{aligned} \tag{2.67}$$

Equation 2.67 shows that the time dependence induces sidebands in every mode whose

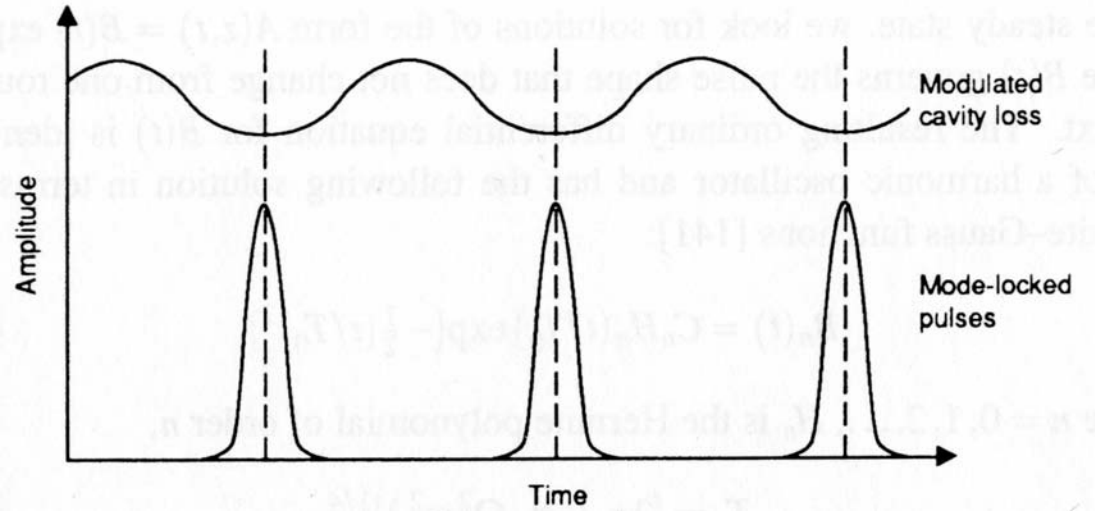

Figure 2.5.: Schematic Illustration of active mode locking through modulation of cavity losses (from [Agr01a])

frequencies coincide with the one of the neighboring modes. As this principle is valid for the total bandwidth, a phase synchronization between all longitudinal modes is reached. There are various possibilities to achieve this time dependence of the electromagnetic field. They can be categorized by the method of how the gain modulation is accomplished. If an actively driven device, for instance a switch or amplitude modulator is used, one speaks of active mode-locking, if a passive device (a saturable absorber for instance) is used one speaks of passive mode-locking.

2.3.2. Active mode-locking

This very common form of mode-locking requires an actively driven element in the laser cavity, either modulating the amplitude (AM mode-locking) or the phase (FM mode-locking) of the propagating light. To ensure phase synchronization, the amplitude/phase must be modulated with a frequency equal to or a harmonic of the mode spacing. Active mode-locking can be understood in both time and frequency domain. An amplitude modulation of a sinusoidal signal creates modulation sidebands as is well known through for example AM radio transmission. If the modulation frequency is equal to the mode spacing, the modulation sidebands overlap with neighboring modes leading to phase synchronization. In time domain, the picture is that the modulator creates cavity losses. As the laser emits more light during loss minima, this intensity difference will accumulate during successive round trips leading to a mode-locked behavior after reaching a steady state (see Figure 2.5). The cavity loss introduced by a

modulator can be written as

$$\alpha = \alpha_c + \alpha_m[1 - \cos(\omega_m t)], \tag{2.68}$$

where α_c are the regular cavity losses and α_m is the additional loss introduced the modulator with a frequency ω_m

2.3.3. Passive mode-locking

Beside the ability to model dispersion, gain, losses, nonlinearities, etc. in fibers, one important component is still missing to model mode-locked lasers. This is the nonlinear component used to make mode-locked lasing more favorable than cw lasing. For a laser to favour lasing in a mode with short pulses, an element or a combination of elements have to be present in the cavity, which introduce a higher loss at low power, so that a short pulse with higher peak power experiences a stronger net gain.

2.3.3.1. Semiconductor saturable absorber

One possibility is to use a SESAM (Semiconductor Saturable Absorber Mirror). A SESAM consists of a Bragg-mirror on a semiconductor wafer like GaAs, incorporating materials with an intensity dependent absorption. The saturable absorber layer consists of a semiconductor material with a direct band gap slightly lower than the photon energy (for a commercial product see e.g. [bat]). Often GaAs/AlAs is used for the Bragg mirrors and InGaAs quantum wells for the saturable absorber material. During the absorption electron-hole pairs are created in the film. As the number of photons increases, more electrons are excited, but as only a finite number of electron-hole pairs can be created, the absorption saturates. The electron-hole pairs recombine non-radiatively, and after a certain period of time they are ready to absorb photons again. Key parameters of the SESAM when designing mode-locked lasers are the recovery time of the SESAM, the modulation depth, the bandwidth, the saturation intensity and the non-saturable losses.

Generally the Bragg stack can be chosen to be either anti-resonant or resonant. SESAMs based on resonant Bragg stacks can have quite large modulation depths, but with the limited bandwidth of the resonant structure. Anti-resonant SESAMs can have quite large bandwidths (e.g. >100 nm), but at the expense of a smaller modulation depth. A larger modulation depth can be obtained from an anti-resonant design at the expense of higher intrinsic losses. In solid state lasers where the single pass gain is low, the unsaturable losses of the SESAM must also remain low, but in fiber lasers where the single pass gain is much higher, unsaturable losses are less important.

The recovery time should ideally be as small as possible. Recovery times on the order of the pulse duration will cause asymmetric spectra if the pulse is chirped when it interacts with the SESAM, and hence strongly affect the pulse dynamics inside the cavity. Even larger recovery times can limit the obtainable pulse duration from the laser. Because the relaxation time due to the spontaneous photon emission in a semiconductor is about 1 ns [bat], some measures have to be taken to shorten it drastically. Two technologies are used to introduce lattice defects in the absorber layer for fast non-radiative relaxation of the carriers: low-temperature molecular beam epitaxy (LT-MBE) and ion implantation. The relaxation time can be controlled by adjusting the growth temperature in case of LT-MBE and the ion dose in case of ion implantation. SESAMs have been known to exhibit dual recovery times [MGK01] with the shortest time in the picosecond or sub-picosecond range. A bi-temporal recovery time is ideal for mode-locked lasers, because the short recovery time enables short pulses and the longer recovery time is needed to initiate mode-locking. For a more extensive overview of SESAMs see e.g. [UKdA93, BK95] and for an extensive theoretical and analytical analysis of mode-locking with saturable absorbers see e.g. [FXKK98, HPMG$^+$99].

For fast saturable absorbers with recovery times much faster than the pulse length, the reflection can be modeled by:

$$q(t) = \frac{q_0}{1 + \frac{|A|^2}{P_{SA}}} \tag{2.69}$$

where q_0 is the non-saturated but in principal saturable loss. P_{SA} is the saturation power, E_{SA} the saturation energy, and τ_{SA} the recovery time. For SESAMs where the recovery time is of the order of the pulse length or more, a more appropriate model of the SESAM is [FXKK98, Hau00]:

$$\frac{\partial q(t)}{\partial t} = -\frac{q - q_0}{\tau_{SA}} - q\frac{|A(t)|^2}{E_{SA}} \tag{2.70}$$

In the limit $\tau_{SA} \to 0$ equation 2.70 approaches equation 2.69. The differential equation 2.70 can be numerically integrated to give $q(t)$, and from $q(t)$ the reflection from the SESAM can be calculated as:

$$R(t) = 1 - q(t) - l_0 \tag{2.71}$$

where l_0 is the intrinsic insertion loss. Reflection of the slowly varying electric field can then be calculated as $A(t)\sqrt{R(t)}$. The saturation energy can be calculated as the product of the saturation fluence and the effective area on the SESAM. The saturation energy can therefore be decreased by focusing tighter on to the SESAM.

A general tendency of lasers mode-locked with saturable absorbers of finite recov-

ery times is that the laser may tend to Q-switch mode-lock (i.e. emit a mode-locked pulse train which is highly amplitude modulated on a nanosecond time scale and hence resemble a nanosecond pulse with a mode-locked pulse train underneath the pulse envelope) [HPMG+99]. The tendency to Q-switch mode-lock is increased if the modulation depth is high. To avoid Q-switched mode-locking, the spot size on the SESAM can either be decreased, or the intra cavity average power increased (by either decreasing the output coupling or by increasing the pump power). However, the limit is set by the damage threshold of the SESAM. If the peak intensity of the pulse is increased above the damage threshold of the SESAM (typically 300 $^{MW}/_{cm^2}$), the SESAM may be permanently damaged, and a small spot burned on the surface.

2.3.3.2. Nonlinear polarization evolution

Fiber lasers can also be mode-locked by making use of the intensity dependent changes in the state of polarization when the orthogonally polarized components of a single pulse propagate inside an optical fiber. The polarization of the intense center of the pulse is rotated further than the less intense wings. Consider a fiber laser built in a ring configuration as depicted in figure 2.6.

After the polarizing beam splitter, the circulating pulse is linearly polarized. The quarter wave plate sets the polarization to be slightly elliptical, such that the Kerr effect in the fiber section has a notable effect on the polarization of the pulse. After the fiber section, the polarization of the pulse center will be different from the polarization of the wings. The combination of half- and quaterwave plate sets the polarization such, that the center of the pulse passes through the polarizing beam splitter and the wings are reflected out of the cavity. The net effect of the waveplates, fiber and polarizing beam splitter is a shortening of the pulse after each round trip, with the polarizing beam splitter effectively acting as a saturable absorber.

The reason why the polarization of the pulse at the beginning of the fiber section has to be elliptical is shown in the following. The main contributors to the intensity dependence of the polarization evolution are self-phase and cross-phase modulation. Assuming the two eigenmodes are circularly polarized with the x- and y-axis indicating the handedness, with intensity levels I_x and I_y, the total phase delays Φ_x and Φ_y along the axis can be obtained by adding the linear phase delays $\beta_x 2L$ and $\beta_y 2L$ as well as cross- and self-phase modulation term [Hof91]

$$\Phi_x = \left[\beta_x + \gamma I_x + \gamma \frac{2}{3} I_y\right] 2L \tag{2.72}$$

$$\Phi_y = \left[\beta_y + \gamma I_y + \gamma \frac{2}{3} I_x\right] 2L \tag{2.73}$$

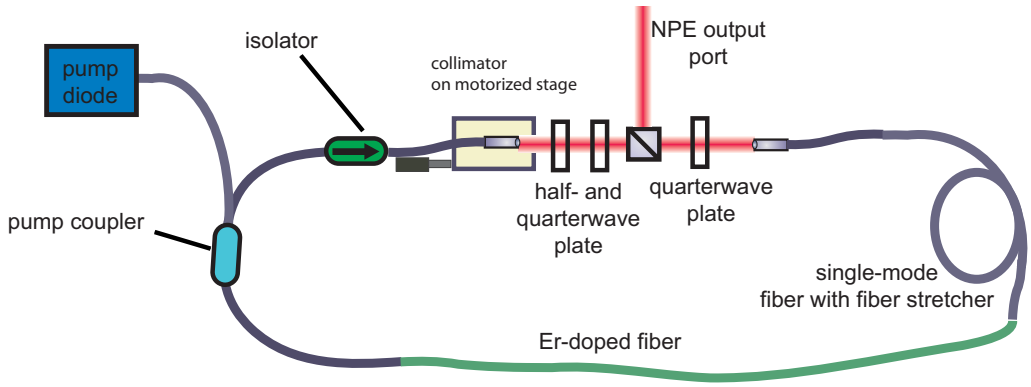

Figure 2.6.: Schematic of a fiber ring laser cavity

where L in the fiber length. The difference of the two yields the net phase shift between the two states:

$$\Delta\Phi = \Phi_x - \Phi_y = \left[(\beta_x - \beta_y) + \gamma(I_x - I_y) + \frac{2}{3}\gamma(I_y - I_x)\right] 2L \tag{2.74}$$

It can readily be seen that linear input polarization does not lead to any intensity dependent phase shift, so the polarization of the pulse has to be elliptical when entering the fiber section of the laser cavity. This is accomplished by the quarterwave plate after the polarizing beam splitter cube.

3. Laser System

Strong arguments made it obvious, that only mode-locked fiber lasers would have the potential to serve as master oscillators for the optical synchronization system. Firstly, erbium-doped fiber lasers operate at the telecommunication wavelength of 1550 nm, for which components are widely available and many optimized fibers exist. Secondly, no solid-state based laser system offers the reliability needed for perpetual operation in an accelerator environment, at least not without tremendous effort. Out of the various available geometries (linear cavity, Figure-8 laser, ring geometry) [Dul91, Loh93, TN93], the ring geometry had already proven itself as superior in terms of long-term stability. This is to a great extent due to the absence of mirrors and minimal free-space sections in fiber ring lasers.

Ultra-short pulses (100 fs duration) are necessary to operate optical cross correlators at high resolution. Hence, actively mode-locked lasers were no viable option, as the pulse duration at low repetition rates is far too high. The most promising approach was a passively mode-locked laser based on nonlinear polarization evolution.

3.1. Soliton versus stretched-pulse fiber lasers

The first fiber laser system was chosen to be a operating at a repetition rate of 40.2 MHz, which was later changed to 54.16 MHz. To maximize the output pulse energy a "stretched-pulse" configuration was chosen for the first tests, which at these repetition rates has an energy advantage over soliton lasers by about a factor of ten. In this section, the difference between soliton and stretched-pulse operation of fiber lasers will be discussed. The main difference lies in the dispersion layout of the laser cavity. If only anomalous dispersion is present, the stable solution to the nonlinear Schrödinger equation is a soliton, as discussed in section 2.1.4. One stability limit for mode-locking is given by the amount of nonlinear phase shift the pulse accumulates during one round trip. This depends on the peak power of the pulse and the fiber length. A soliton becomes unstable if it accumulates a phase shift of 2π or more per round trip. For a repetition rate of 50 MHz (corresponding to a fiber length of 4 meters), this limits the intra-cavity peak power to roughly 1 kW, which corresponds to a pulse duration of 250 fs and pulse energy of 250 pJ. At an approximate output coupling of 50%, this

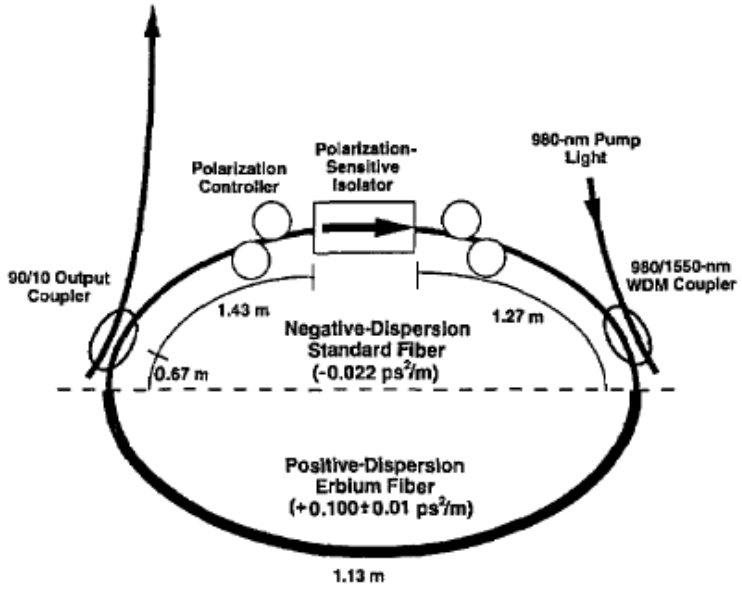

Figure 3.1.: Schematic of a stretched-pulse fiber laser (from[TN93])

would mean only a very small output power from the laser is available.

In an approach first found by Tamura et. al. in 1993 [TN93], alternating pieces of normal and anomalous dispersion fibers were combined, see figure 3.1. The result of this is a breathing of the pulse duration during one round trip, making the pulse short in the middle of the normal and anomalous pieces of the fiber cavity. This results in an effective decrease in peak power, since the pulse is only short for a small portion of the fiber cavity. As nonlinear effects are peak power dependent, the nonlinear phase shift accumulated per round trip is considerably decreased compared to the case of a soliton. This results in an increase of pulse energy that the laser can sustain before becoming instable, and thus a higher output power. A further increase in output power can be achieved, by constructing the laser such that the total net dispersion is not zero but slightly positive. Hence the pulse will not reach the transform limit inside the cavity, and will always have a positive chirp. This will further increase the maximum energy of the pulse inside the cavity while still remaining single pulsing. However, more pump power is required to achieve a high enough peak power in order to have mode-locking sustained. Output pulse energies in excess of 1 nJ have been obtained at a repetition rate of 40.2 MHz and 54 MHz.

For higher repetition frequencies, due to the overall shorter fiber length in the cavity, output pulse energies on the order or 0.25 nJ [Che06] to 0.5 nJ [Löh07] can also be generated from soliton lasers. Higher repetition frequencies generally have the advantage, that finding temporal overlap between two pulses is easier due to the closer

pulse spacing. This is a considerable advantage for optical cross correlators, if it is not possible to introduce delay by adding more fiber. Another argument for choosing higher repetition frequencies is the smaller pulse energy per average power. This is beneficial for the cross correlators, but inconvenient for processes requiring high peak power (e.g. frequency doubling) as it requires higher amplification.

For above reasons, a 216 MHz soliton laser was finally chosen to serve as master oscillator for FLASH. However, all initial noise investigations and experiments conducted during this thesis used a lower repetition rate laser in the stretched-pulsed regime. It was later verified that a soliton laser essentially has the same phase noise properties and even slightly better amplitude stability than the stretched-pulse laser [FL07].

3.2. Setup of a stretched-pulsed/soliton fiber laser

The setup of both stretched-pulse and soliton fiber laser will be described in detail in this section. A schematic overview is given in figures 3.2 and 3.3, figure 3.4 shows a picture of a running stretched-pulse laser. The construction for both lasers is similar in terms of components with the exception of the gain fiber.
The lasers are pumped by 980 nm single-mode laser diodes, which are stabilized by a fiber Bragg grating. The pump diodes are inexpensive and commercially readily available due to the demand of the telecom market. The coupling into the laser ring cavity is done with a wavelength-division multiplexer. This device consists of two parallel pieces of fiber, whose cores are fused together by an electric arc. By carefully choosing the final distance of the cores, it is possible to obtain a wavelength dependent transmission from one piece of fiber into the other. A wavelength division multiplexer

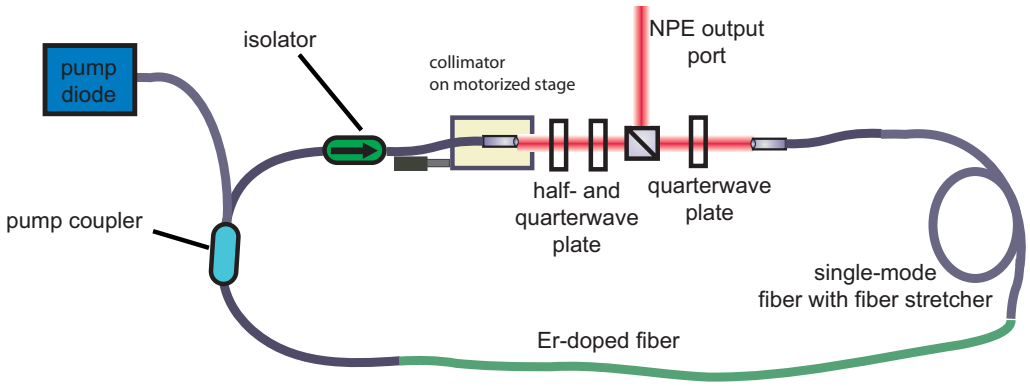

Figure 3.2.: Schematic setup a a stretched-pulse fiber laser

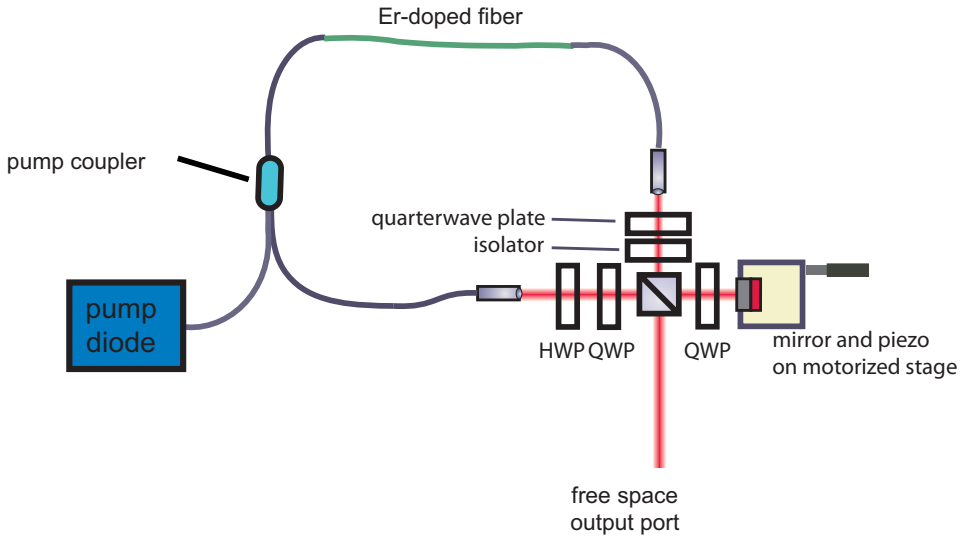

Figure 3.3.: Schematic setup of a 200 MHz soliton fiber laser

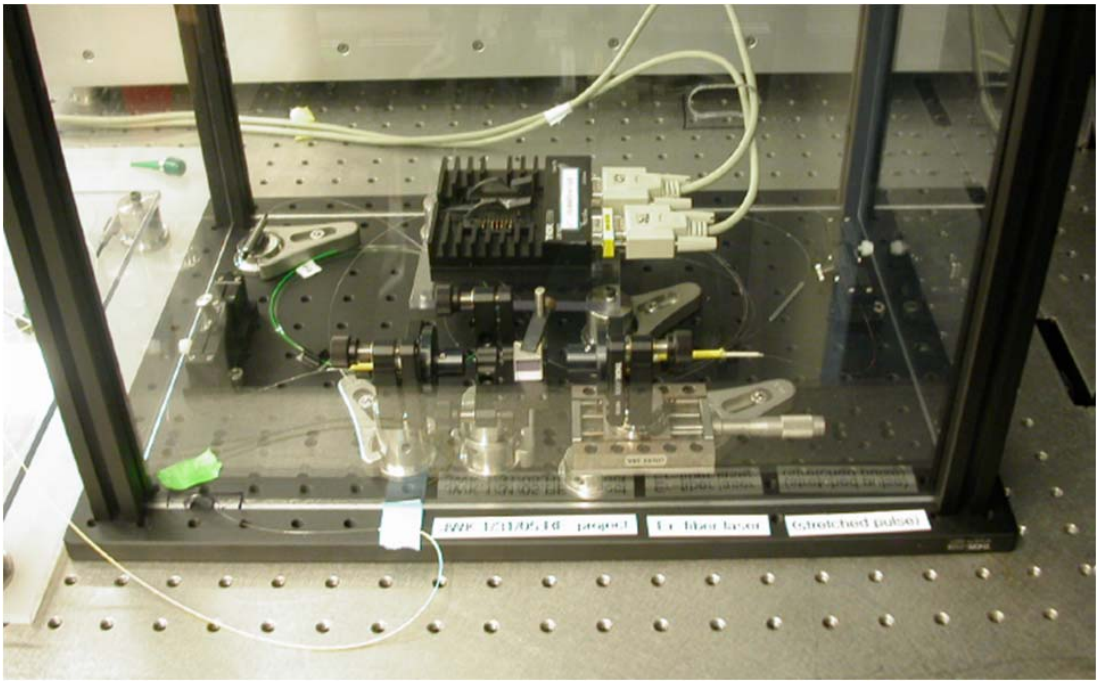

Figure 3.4.: Photo of an erbium-doped fiber laser. The polarization change is done using manual in-line polarization rotators instead of waveplates.

is obtained if the transmission for one wavelength (for instance the pump wavelength of 980 nm) from fiber piece A into B is 100%, and the transmission from B into A for another wavelength (for instance the signal wavelength of 1550 nm) is zero. A standard coupler can be obtained if the coupling ratio for a single wavelength is fixed.

The gain fiber is a highly doped erbium fiber (concentration of $6 \cdot 10^{25} m^{-3}$). The type of gain fiber differs for the stretched-pulse and soliton versions of the laser, since the positive dispersion needed for stretched-pulse operation is provided by the dispersion of the gain fiber.

An isolator is needed to ensure unidirectional operation. As the lasing process and mode-locking start from noise, it is a lot easier to achieve mode-locking if the amplified spontaneous emission from one side of the pumped gain fiber is absorbed in the isolator. For the stretched-pulse version, the isolator is implemented as an in-line isolator paired with a 10 percent output coupler which can be used for monitor purposes.

Since the repetition frequency of the laser needs to precisely match a subharmonic of the accelerator RF (1.3 GHz), an adjustable free space section between two collimators has to be introduced. It contains the waveplates and the polarizing beam splitter required for mode-locking. One of the collimators is mounted on a motorized translation stage which can be used to coarsely adjust the repetition rate. The fine tuning is done with an in-line fiber stretcher which serves as actuator for the phase-locked loop to the accelerator RF. To achieve the stretching, the fiber is glued to a piezo-electric crystal which stretches and compresses the fiber when a voltage is applied. Care has to be taken to only elongate and not bend the fiber to prevent stress-induced birefringence. This would disturb the mode-locking and lead to instabilities. The fiber length variation that has to be compensated to keep the PLL closed is too long to be handled by the fiber stretcher alone. Should the voltage applied to the piezo reach the upper or lower limit, the motorized translation stage incorporated in the free-space section is used to keep the repetition frequency within the range of the piezo actuator.

The free space section has to be designed differently in case of the 216 MHz soliton laser. Due small total fiber length, it is not possible to use an in-line fiber isolator or a fiber stretcher. The setup chosen is depicted in figure 3.3. The free-space section consists of a quaterwave plate, a halfwave plate and a polarizing beam splitter cube, just as for the stretched-pulse laser. The light passing through the beam cube traverses through a quarterwave plate and is reflected off a mirror mounted on a piezo. This serves as actuator for the PLL. The light passes through the quarterwave plate again which is set such, that the total polarization rotation is 90 degrees. So when the light passes through the beam cube again, it is reflected, passes the isolator and a quarterwave plate and enters a collimator.

An overview of the dispersion properties of the fiber segments for both soliton and stretched-pulse lasers is given in tables 3.1 and 3.2. The total net dispersion of the

stretched-pulse laser is at the upper limit of the stability range. This laser is pumped with an optical power of up to 400 mW and emits a total output power (free space output and coupler) of 1.2 nJ.

section	fiber type	length (cm)	dispersion ($\frac{fs^2}{mm}$)	total dispersion
collimator 1	Flexcor1060	23	-9	-2070
fiber stretcher	SMF28	151	-23	-34730
pump coupler	Lucent980	40	3	1200
gain fiber	Lucent custom made	87	78	67860
isolator	SMF28	40	-23	-9200
collimator 2	Flexcor1060	23	-9	-2070
free space section		12.5	0	0
total		359.5		21350

Table 3.1.: Length of fiber segments and dispersion properties for a stretched-pulse fiber laser with a repetition rate of 54 MHz

section	fiber type	length (cm)	dispersion ($\frac{fs^2}{mm}$)	total dispersion
collimator 1	SMF28	4	-23	-920
pump coupler	Lucent980	16	3	480
gain fiber	Liekki ER80-8/125	53	-23	-12190
collimator 2	SMF28	4	-23	-920
free space section		23	0	0
total		100		-13550

Table 3.2.: Length of fiber segments and dispersion properties for a soliton fiber laser with a repetition rate of 216 MHz

4. Laser Characterization

The amplitude and phase noise properties of the laser master oscillators are crucial for the performance of the optical synchronization system. Since the phase fluctuations at high offset-frequencies cannot be compensated by phase-locking the laser to another oscillator, the absolute phase noise of the laser has to be small in that frequency region. The design specifications for the laser master oscillator called for an integrated phase noise of 10 fs from 1 kHz to the Nyquist frequency (half the repetition frequency of the laser). In this chapter, the phase noise characterization techniques will be briefly introduced and the measurements will be presented.

4.1. Optical properties

To ensure proper operation of the laser, the optical spectrum, the electric pulse train from a photodiode and the autocorrelation of the pulse need to be monitored. If too much energy is present in the cavity, the laser will react by going into multiple-pulsing. This can either mean two pulses circulating in the cavity, spaced at half the repetition period (period doubling), or two coupled pulses a few picoseconds apart. Either case will show up in the autocorrelation trace or on an oscilloscope trace. Figures 4.1, 4.2 and 4.3 show typical measurements obtained from a 54 MHz fiber laser in single pulse operation. The pulse duration assuming a Gaussian pulse shape derived from figure 4.3 yields 1.45 ps, which matches the expected pulse duration of 1.40 ps from simulations (see figure 4.4 and appendix A) very well.

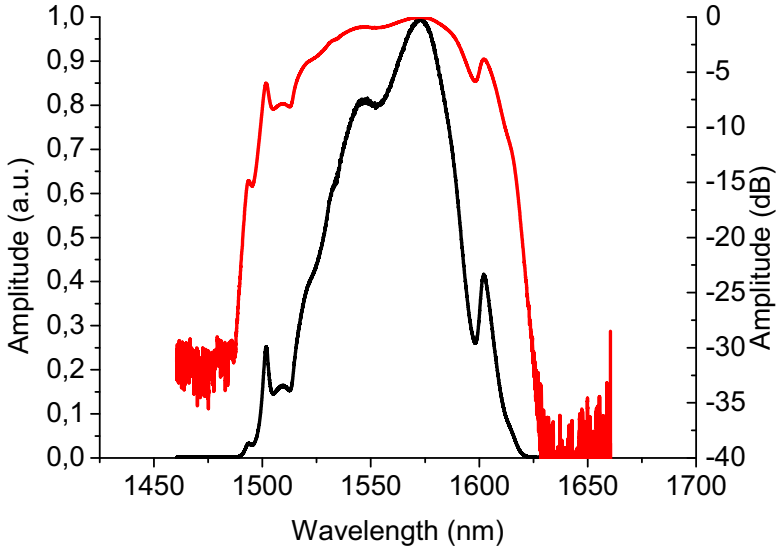

Figure 4.1.: Optical spectrum of a 54 MHz fiber laser (linear scale - black; logarithmic scale - red).

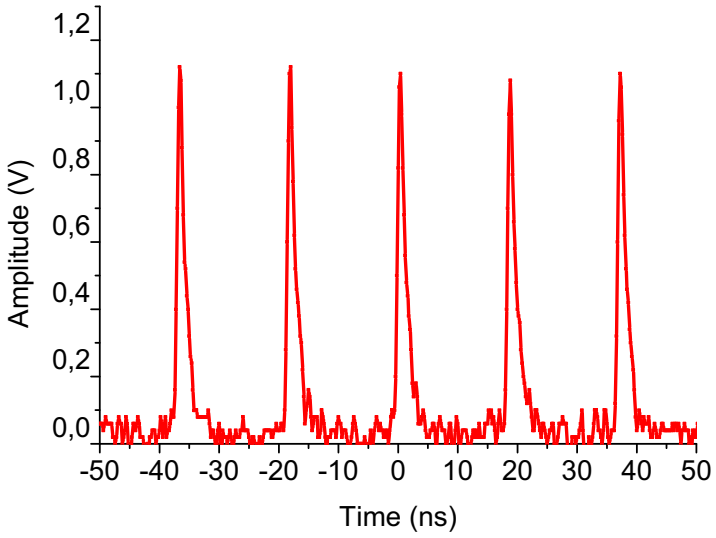

Figure 4.2.: Oscilloscope trace of the pulse train of a 54 MHz fiber laser.

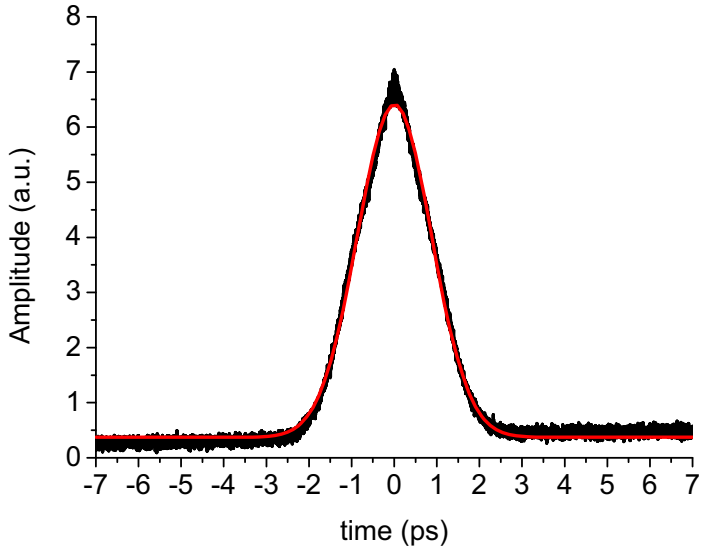

Figure 4.3.: Autocorrelation of the laser pulse train measured at the free space output port (gaussian fit - red)

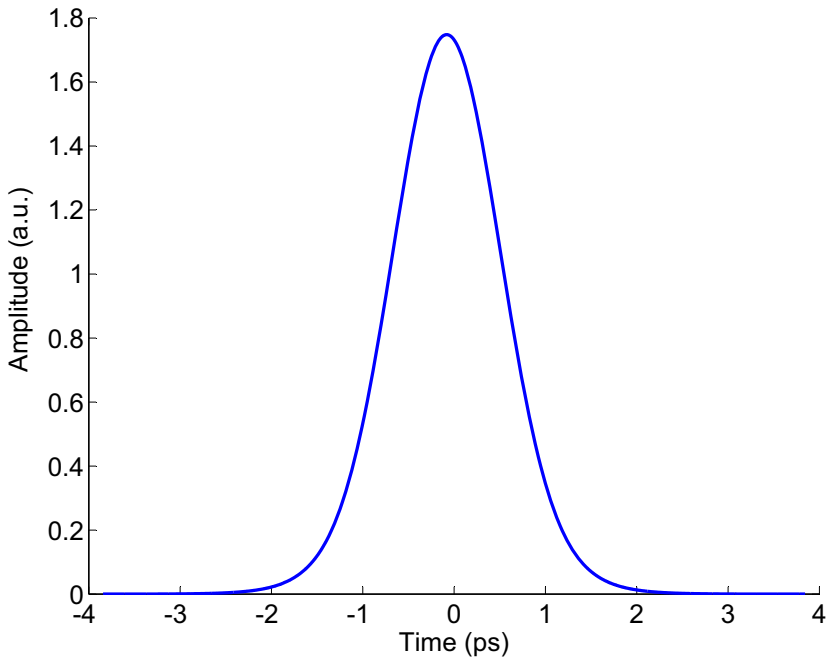

Figure 4.4.: Simulated pulse just before the free-space output port of the laser

4.2. Measuring amplitude and phase noise

The common method to measure amplitude and phase noise is using the electrical pulse train created by a train of optical pulses incident on a photo diode. The rise time and duration of the electrical pulses is dependent on the properties of the photodetector. We used a photodetector with a bandwidth of 10 GHz and a corresponding rise time of 35 ps. In frequency domain, a pulse train translates to a frequency comb, whose lines are spaced evenly at the repetition frequency of the laser.

The fluctuations of the electrical pulse train can be viewed as the sum of temporal fluctuations and amplitude noise. Amplitude noise is equally present in all comb lines, independent of the harmonic number of the repetition frequency. The temporal jitter is also equal for all comb lines, but the phase error increases linearly with frequency. Hence the measured jitter will be dominated by phase fluctuations, if one looks at a high harmonic of the repetition frequency. This method is commonly known as the von-der-Linde method [vdL86] and relies on a number of assumptions, like small amplitude fluctuations and the absence of correlation between intensity and phase fluctuations. The first measurements of timing jitter were conducted by using this method, but it turned out that no clear distinction between amplitude and phase noise could be made, since the phase noise of fiber lasers is extremely low.

4.2.1. Amplitude noise

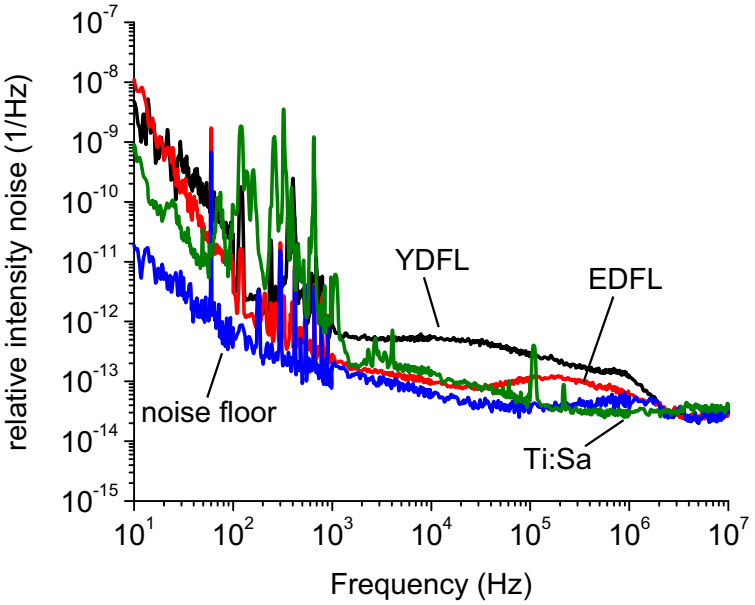

Figure 4.5.: Amplitude noise of various laser sources.

Since the amplitude noise is equal for all comb lines in the frequency spectrum, the natural choice for the measurement is the DC component. The photodetector output is filtered by a low-pass filter with a corner frequency at half the repetition frequency of the laser and the signal is suitably amplified to be measured by an FFT-Analyzer, e.g. a Vector Signal Analyzer. The typical measurement setup for amplitude and phase noise is shown in figure 4.12. The obtained spectrum has to be normalized to the amplitude of the comb line where the measurement was taken, in this case the amplitude at zero frequency.

Various lasers have been compared in terms of their relative intensity noise. The results are shown in figure 4.5. The integrated amplitude noise is nearly equal for the erbium-doped fiber laser and the ytterbium-doped fiber laser (0.03% rms and 0.04% rms respectively) for a bandwidth of 10 Hz to 10 MHz. For comparison, the amplitude noise of a Ti:Sa laser built in the lab of Prof. Kaertner at MIT has also been measured. Here, the integrated phase noise amounts to 0.17% rms, making it a factor of three worse than the fiber lasers investigated. The decrease in amplitude noise for all measurements in the frequency range above 1 MHz is due to a filtering effect in the amplifier used. The dominating factors in amplitude noise are accoustic and mechanical perturbations and residual amplitude noise of the diode-based pump lasers. The Ti:Sa laser was pumped by a VERDI diode-pumped laser, which has an even higher amplitude noise than the single mode diodes used for pumping the fiber lasers. The superior performance of the fiber lasers in terms of amplitude noise can be attributed to the extremely long upper state lifetime of the dopant (10 ms for erbium and 1 ms for ytterbium) compared to Ti:Sa (10 μs). The upper state lifetime of the dopant acts as a low-pass filter for amplitude noise from the pump laser. Since the cutoff frequency of the Ti:Sa gain medium is around 100 kHz, all the amplitude noise from the pump up to that frequency range is directly transfered to amplitude noise of the Ti:Sa laser. The spectra for the fiber lasers show a significantly cleaner behavior in that regime.

4.2.2. Phase noise

The phase noise was measured using an Agilent E5052A signal source analyzer, whose method of operation will be described in the following section. Phase noise can be measured by phase locking a local reference oscillator to the signal of the device to be tested with a low-bandwidth phase-locked-loop (PLL) and applying both the reference oscillator signal and the device signal to a mixer. The PLL keeps the phase difference between both signals at 90 degress, making the mixer output signal zero. The remaining fluctuations represent the phase difference between the two signals and hence the timing jitter between them. This voltage is then sampled by an ADC system with high dynamic range. A schematic overview explaining the technique is shown in Figure

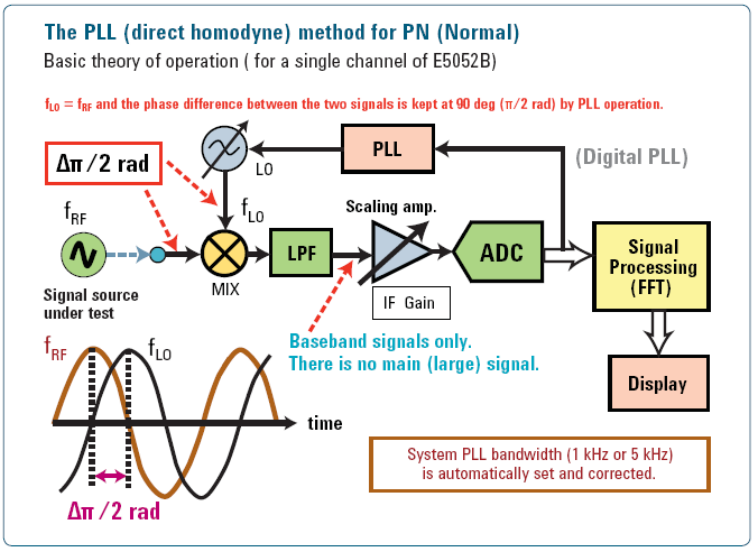

Figure 4.6.: Schematic of a phase noise measurement using a local reference oscillator and PLL (from [Agi])

4.6.

Let the signal to be measured be phase locked to the internal reference, so that both signals are in quadrature or have a 90 ° phase difference. Assume

$$V_{LO}(t) = A_{LO} \cdot \sin(\omega_c t + \Delta\phi_{LO}) \quad \text{and} \quad V_{dev}(t) = A_{dev} \cdot \cos(\omega_c t + \Delta\phi_{dev}) \tag{4.1}$$

where ω_c is the the common frequency for local reference and device under test, A_{LO}, A_{dev}, $\Delta\phi_{LO}$ and $\Delta\phi_{dev}$ are the amplitudes and the phase jitter of either signal. The output of the mixer multiplies the two waveforms, which yields

$$\begin{aligned} V_{mixer} = V_{LO}(t) \cdot V_{dev}(t) &= A_{LO}A_{dev} \cdot \sin(\omega_c t + \Delta\phi_{LO}) \cos(\omega_c t + \Delta\phi_{dev}) \\ &= \frac{1}{2} A_{LO}A_{dev}[\sin(2\omega_c t + \Delta\phi_{LO} + \Delta\phi_{dev}) + \sin(\Delta\phi_{LO} - \Delta\phi_{dev})]. \end{aligned}$$

The low-pass filter eliminates the sum frequency, which results in

$$V_{filtered} = \frac{1}{2} A_{LO}A_{dev} \sin(\Delta\phi_{LO} - \Delta\phi_{dev}). \tag{4.2}$$

Since the phase fluctuations are small, the approximation $\sin(\Delta\phi_{LO} - \Delta\phi_{dev}) \approx \Delta\phi_{LO} - \Delta\phi_{dev}$ can be made. So finally, the phase fluctuation difference between local oscillator and the test signal is measured. This leads to a basic requirement: The phase noise contribution of the local reference oscillator has to be small compared to the phase noise of the signal to be measured.

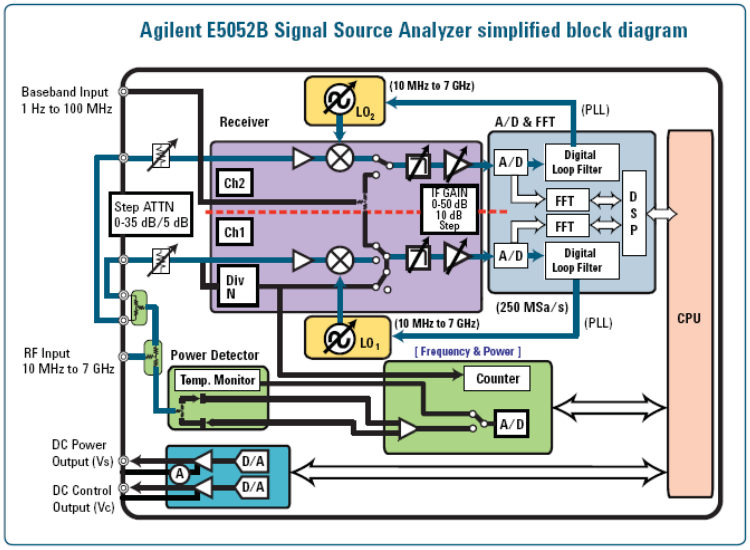

Figure 4.7.: Schematic overview of the E5052 Signal Source Analyzer(from [Agi]). LPF: low-pass filter, PN: phase noise, IF gain: gain of the DC phase fluctuations

The signal source analyzer (Agilent E5052A) features an additional possibility to reduce the contribution of the local reference oscillators' phase noise by using a correlation scheme, lowering the measurement noise floor by up to 20 dB. It is schematically shown in figure 4.7. The input signal is split and mixed with two identical reference oscillators. A digital signal processor then performs a correlation between the two signals, thus reducing the uncorrelated intrinsic phase noise of the reference oscillators by $\sqrt{N}$, where N is the number of measurements.

Another issue is that the effects of the PLL on the measured phase noise have to be corrected for. This is done internally by the Agilent Signal Source Analyzer.

4.2.3. Phase noise results

The measurement setup for both amplitude and phase noise is depicted in figure 4.12. The pulse train is photodetected, a harmonic at 1.3 GHz is filtered using a bandpass filter (1% bandwidth, 12^{th} order), and amplified to match the input specifications of the signal source analyzer. Results for both ytterbium-doped and erbium-doped fiber lasers operating at repetition rates of 40.2 MHz are shown in figures 4.8 and 4.9. The total timing itter can be obtained by integrating the power spectral density. The integrated jitter amounts to 40 fs rms for the ytterbium-doped system, where about half of this is located at frequencies around 1 kHz. From a few kHz to the Nyquist frequency, the timing jitter of both laser is almost equal. This is due to the decreasing effect of the ytterbium gain filtering. Since the upper state lifetime of erbium is a factor of 10

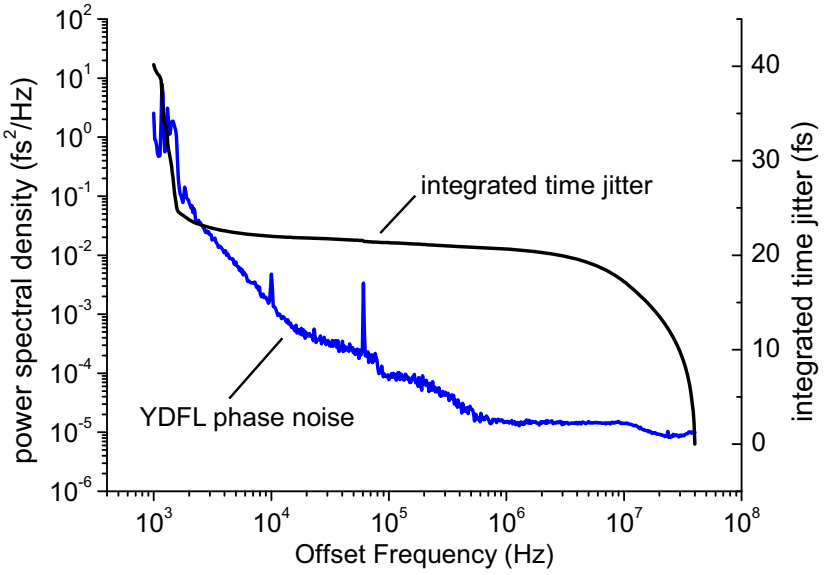

Figure 4.8.: Power spectral phase noise density and integrated time jitter of an ytterbium-doped fiber laser.

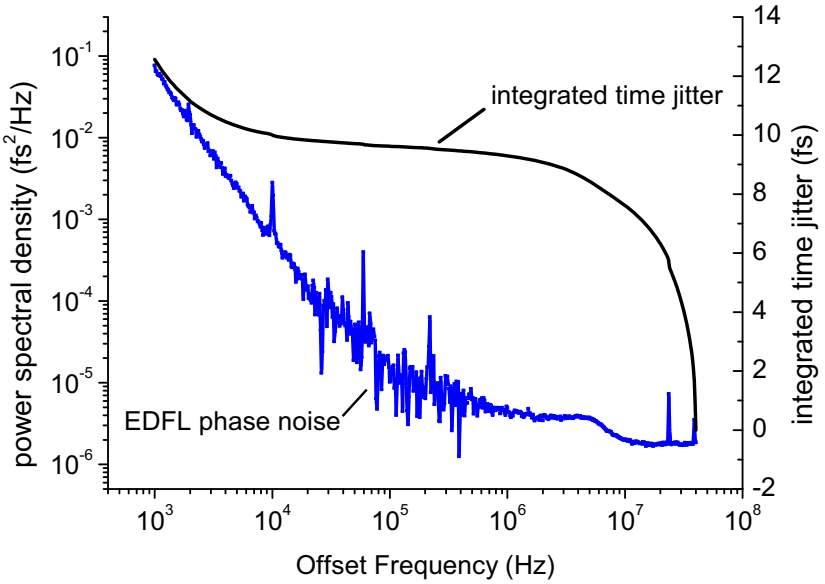

Figure 4.9.: Power spectral phase noise density and integrated time jitter of an erbium-doped fiber laser.

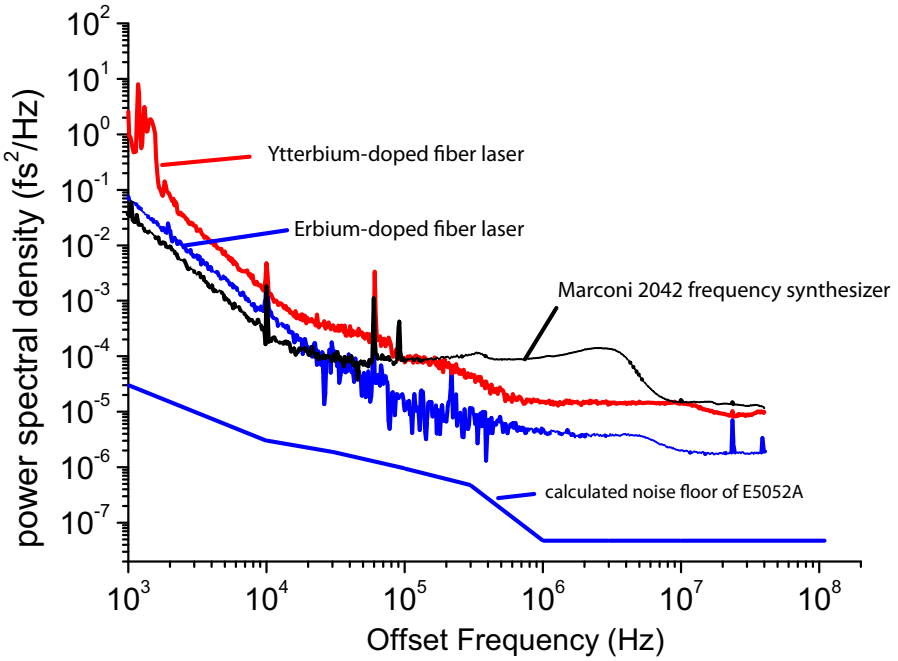

Figure 4.10.: Power spectral densities of erbium- and ytterbium-doped fiber lasers with a Marconi frequency synthesizer as a microwave reference and the calculated noise floor of the measurement system

longer (10 ms versus 1 ms for ytterbium), this effect is not seen in erbium-doped fiber lasers. Its phase noise amounts to 12 fs rms from 1 kHz to 20 MHz. In Figure 4.10, both traces are shown in comparison to a high-quality microwave oscillator (Marconi 2042). It can be seen, that the erbium-doped fiber laser has a significantly smaller phase noise at offset frequencies above 1 kHz than a high-quality frequency synthesizer.

The photodetection process limits the phase noise measurements presented here. In order to understand the reasons for that, the design and functionality of the photodetectors have to be looked at. This will be done in the following section.

4.2.4. Measurement limitations caused by photodetection

Photodetectors can be described in a simple model (see figure 4.13) by a regular diode with a capacitance which is formed by the P-I-N junction. To enhance bandwidth and output current, the diode is operated with a reverse bias voltage applied. The bandwidth is largely determined by the junction capacitance which in turn is dominated by the effective area of the diode. The smaller the area, the larger is the bandwidth. The junction capacitance together with the load resistance forms a low-pass filter, which also limits the bandwidth.

There are three main effects which limit the usefulness of photodetectors in high-

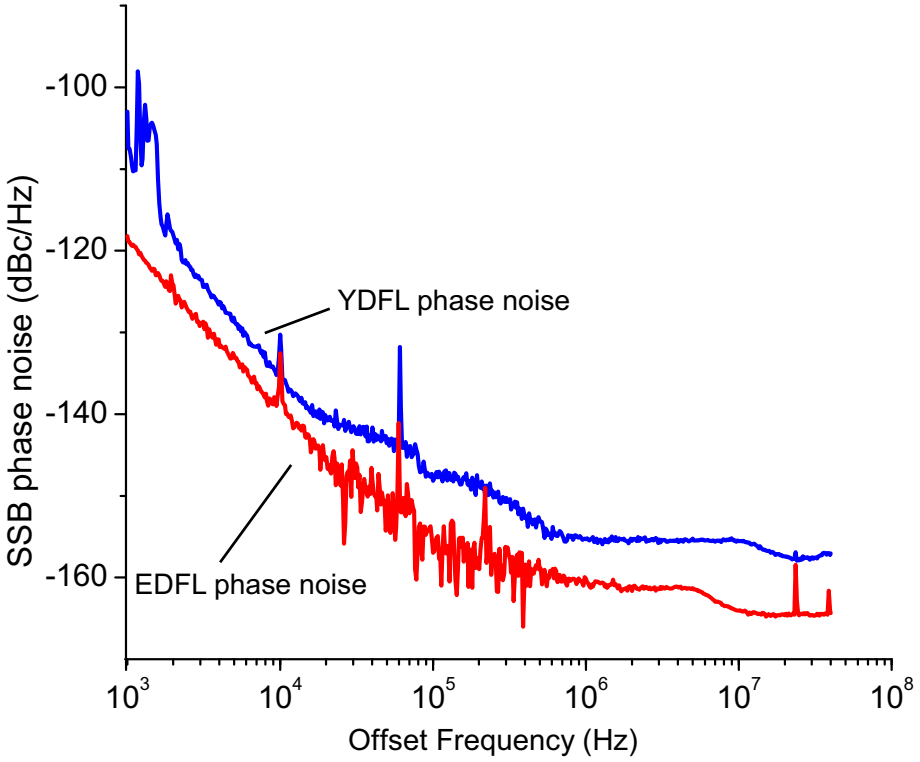

Figure 4.11.: Single sideband phase noise for the ytterbium- and erbium doped fiber laser

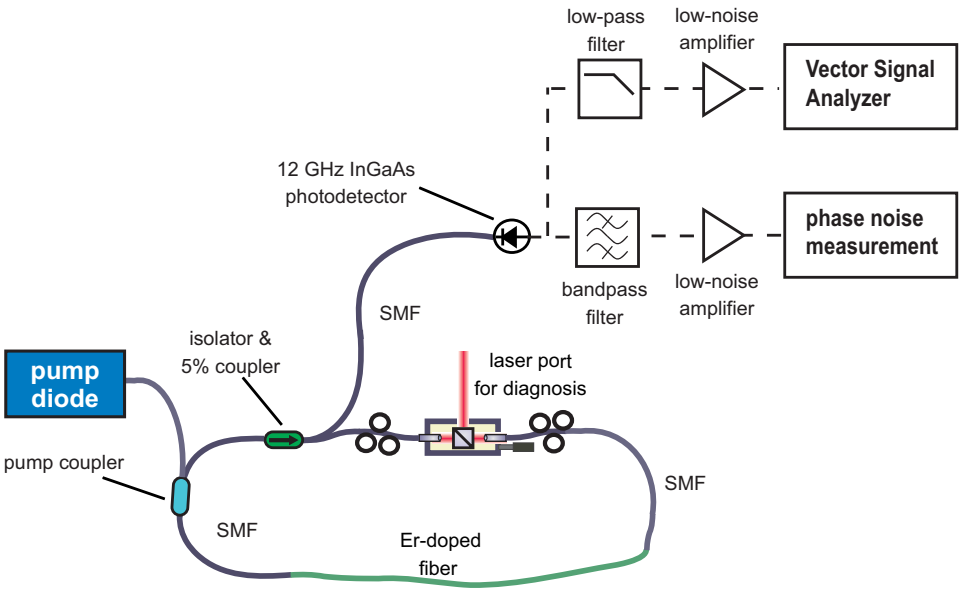

Figure 4.12.: Schematic overview of the measurement setup used for amplitude and phase noise measurements

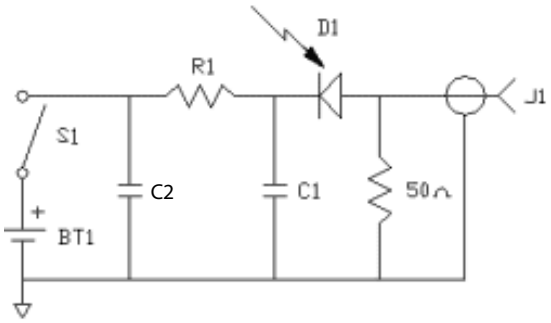

Figure 4.13.: Equivalent circuit of a photodiode. R_1, S_1 and C_2 are resistance, switch and noise suppression capacitance of the bias circuit, C_1 is the diode capacitance and the 50 Ohm resistor represents the load over which the voltage is measured

quality phase noise measurements.

- Thermal noise of the load resistance,
- Amplitude to phase noise conversion,
- Temperature dependence of the phase.

4.2.4.1. Thermal noise

The main limitation for the measurement of phase noise at high offset frequencies is the thermal noise of the load resistor across which the output voltage of the photodetector is measured. The total saturation current the photodiode can deliver is limited by the design of the PIN junction and the applied bias voltage. An InGaAs photodetector can deliver a maximum peak current of 30 mA for an incident pulse train with an average power of around 10 mW, which corresponds to a peak voltage of 1.5 V into a 50 Ohm load (for a typical oscilloscope trace see Figure 4.2). The total power is divided equally to all the comb lines, which results in a typical power level of -13 dBm (or 50 μW) per comb line. The thermal noise floor of the load resistor at room temperature in a 1 Hz bandwidth is -174 dBm (or $2.98 \cdot 10^{-21}$ W). This value has to be normalized to the power of the comb line that is measured. Note that since dB is a logarithmic unit, the normalization is achieved by subtraction. The resulting noise floor is expressed relative to the carrier (dBc=dB with reference to a carrier). So neglecting any signal losses or degradation of the signal to noise ratio in the amplifier, the noise floor is given by

$$S_{s/n} = -174dBm - (-13dBm) = -161dBc. \tag{4.3}$$

In our case this results in a noise floor of around -154 dBc for high offset frequencies for the erbium-doped fiber laser, which can be clearly seen in figure 4.11. The power

of the 1.3 GHz combline obtained from the ytterbium-doped fiber laser was at -20 dBm, accounting for the higher noise floor of -154 dBm. The decrease in phase noise at around 1 MHz is due to the beginning filtering effect of the RF bandpass filter.

4.2.4.2. Amplitude to phase noise conversion

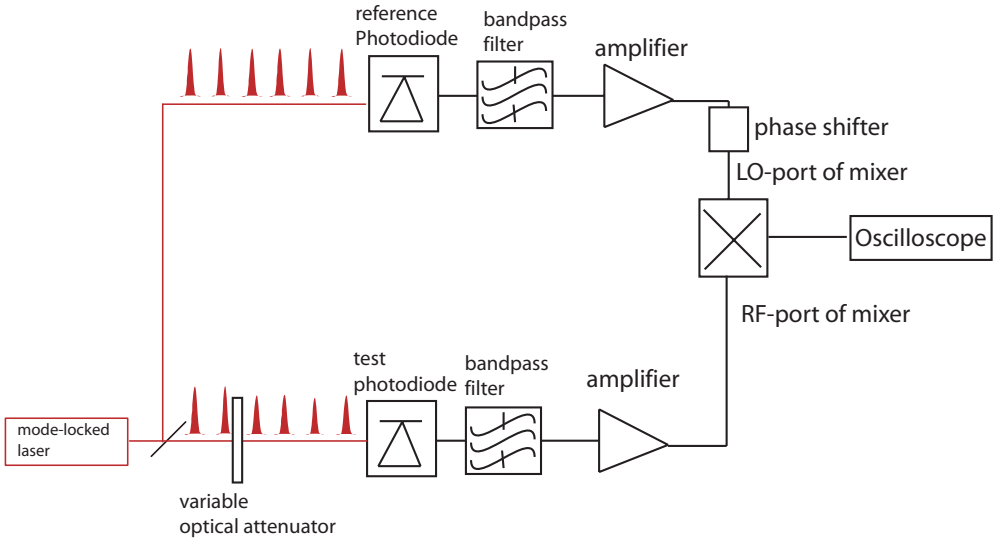

Figure 4.14.: Schematic overview of the amplitude to phase noise conversion measurements of photodiodes

One nonlinear process happening in photodetectors is the dependency on optical input power of the junction capacitance and hence the phase of the output signal. The amplitude to phase noise conversion was measured using the setup depicted in figure 4.14. The pulse train from a mode-locked erbium-doped fiber laser was split in two and each part was detected with a photodiode. The optical power was kept constant at the reference diode and varied using a variable optical attenuator for the test photodiode. A harmonic of the repetition rate of the fiber laser was selected using two bandpass filters (2 GHz), amplified and fed to a mixer. To be sure to measure only phase fluctuations, the signals were kept in quadrature using a manual phase shifter in the reference arm. The amplitude modulation to phase noise modulation conversion coefficient (AM-PM coefficient) varies with type of diode and with the bias voltage. The effect of this coefficient is a timing change of the emitted electrical pulse train depending on incident power fluctuations. The timing differences for two bias voltages of the same photodetector is depicted in figure 4.16. The linear fit yields AM-PM coefficients of $1.84 \pm 0.06 \frac{\text{ps}}{\text{mW}}$ for 6 V bias voltage and $1.56 \pm 0.06 \frac{\text{ps}}{\text{mW}}$ for 12 V bias voltage. Both measurements were performed with a commercial high-bandwidth

photodetector [ET3b]. The amplitude stability of fiber lasers (see figure 4.5) was measured to be 0.03% in a range from 10 Hz to 10 MHz, which yields a minimum temporal jitter due to AM-PM conversion of 5 fs in that frequency range for an input power of 10 mW. A comparison to another type of photodiode with significantly less bandwidth (1.5 GHz), as depicted in figure 4.15, shows the strong deviations between types of photodetectors for otherwise identical conditions. The AM-PM coefficient for the 1.5 GHz diode [ET3a] amounts to $4.8 \pm 0.1 \frac{\text{ps}}{\text{mW}}$. So a careful selection of the photodetector is essential.

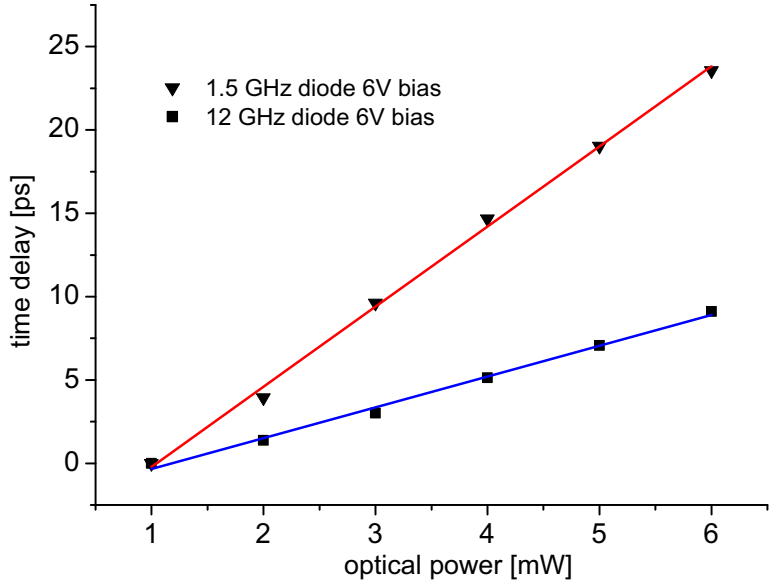

Figure 4.15.: Time delay vs optical power dependency of two photodetectors with 1.5 GHz and 12 GHz bandwidth. The AM-PM coefficient is the slope of this graph.

4.2.4.3. Temperature dependence of photodetectors

The phase of the electronic pulse train generated by the photodetector relative to the incident optical pulse train also depends on temperature. This is of no concern for short-term measurements, but has serious impact on the long-term stability of the photodiode signals. The phase shift per temperature has been measured to be between 326 fs and 366 fs per degree centigrade [Lor], which makes long-term stable signal extraction with 10 fs precision virtually impossible using photodetectors and bandpass filters. It is possible to stabilize the photodiode to a level of 0.1° centigrade, which would mean a drift of 32 fs to 36 fs.

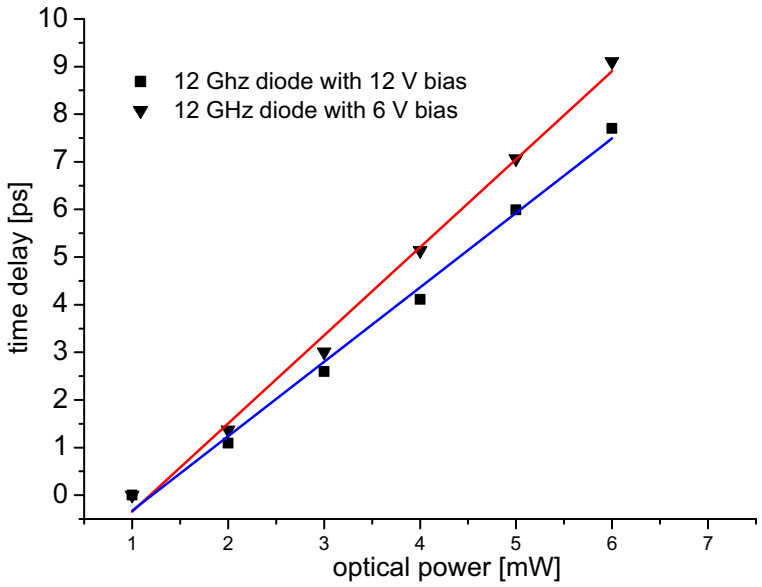

Figure 4.16.: AM-PM dependence of a 12 GHz photodetector for two different bias voltages.

AM-PM conversion alone would not be a significant problem, if one considers only the absolute phase noise performance required above a frequency of 1 kHz. However if photodiodes are used to provide RF signals to various end stations that should be long-term stable, the AM-PM conversion also becomes a significant issue. Since the AM-PM conversion varies from photodiode to photodiode and the amplitude of the laser pulses at various points in the facility is different, there will be timing variations between different end-stations.

In summary it can be said that the RF signal generation from an optical pulse train using photodiodes is limited to about 50 fs, due to temperature dependencies and AM-PM conversion. The whole concept of the optical synchronization system relies on the idea, that the transmission of the optical pulse train and subsequent recovery of RF signals at end stations is nearly drift and jitter free. Hence photodiodes are not suitable for RF signal recovery necessary, if 10 fs short-term and long-term stability are desired. Then, a Sagnac interferometer to phase lock an external RF oscillator to the optical pulse train is a viable option [KL06].

4.2.5. Amplitude and phase noise of fiber amplifiers

The optical synchronization system needs many fiber-based amplifiers to compensate the losses through transmission and output couplers. In an initial test, an ytterbium-

doped fiber laser and a commercial high-power amplifier were used to investigate the impact of amplification on the amplitude and phase noise of the laser pulse train. A fiber laser oscillator based on either erbium or ytterbium has been measured to show a comparable amplitude noise and timing jitter at high offset-frequencies (see figures 4.10 and 4.5). This is understandable if one considers that the noise at high offset-frequencies (>10 kHz) is unaffected by the different corner frequencies (100 Hz for erbium and 1 kHz for ytterbium) of the noise filtering of both materials.

Amplitude noise is commonly characterized as relative intensity noise and determines the signal-to-noise ratio in most experiments utilizing the laser pulse train. Even though the fiber link stabilization relies on a balanced detection scheme, which should automatically make it independent of amplitude noise, many other systems rely on low amplitude noise (e.g. the beam arrival time monitor [LHL+06]). Keeping the additional phase noise at high offset frequencies low is crucial for all subsystems, since there is no way to correct for this error.

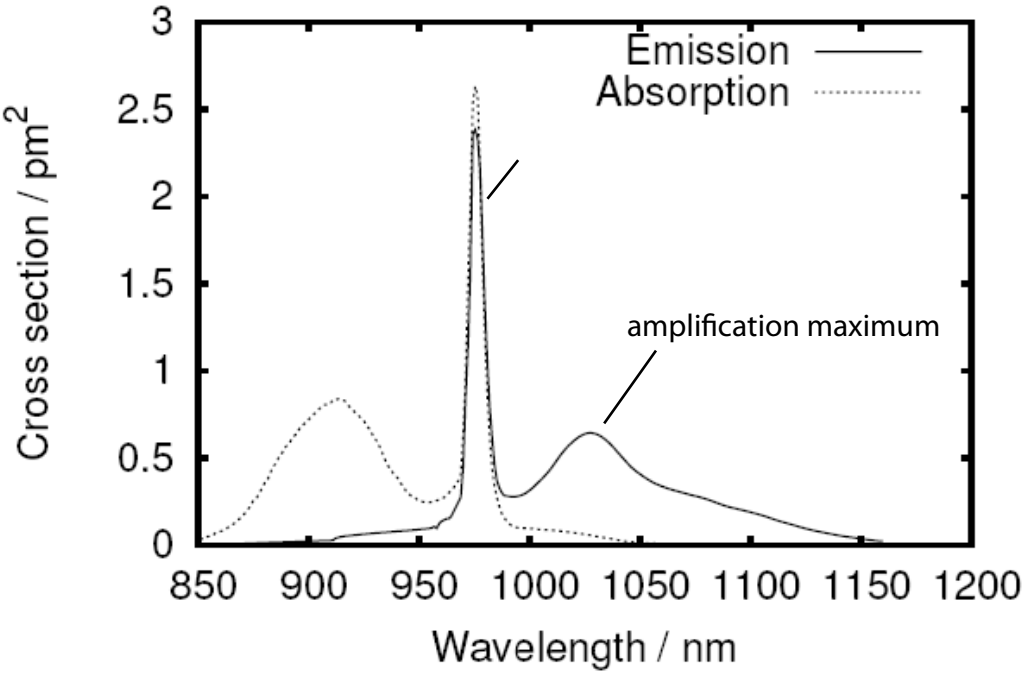

Figure 4.17.: Emission and absorption spectrum of ytterbium

The experimental setup for measuring the amplitude and phase noise for high-power amplification is shown in Figure 4.18. The fiber laser oscillator used has a central wavelength of 1030 nm±30 nm at a repetition rate of 36 MHz. The gain window of the commercial fiber amplifier is around 1060 nm±15 nm nm, so the output spectrum of the oscillator needs to be shifted into that region. This is achieved by using a Yb-

fiber with lower doping as gain fiber in the oscillator and an aperture placed inside the grating section, where the beam is spatially chirped, to filter the spectrum around 1060 nm. The gain profile of ytterbium is shown in figure 4.17. Since the amplification is exponential, it will narrow the spectrum to a wavelength range around 1030 nm if the amplification is too high. This effect is called gain narrowing. It can be suppressed by limiting the single-pass gain within the oscillator.

The seed pulses are coupled to the amplifier through a 9% fiber coupler, placed after the gain fiber in the oscillator. The fiber amplifier has three stages, a preamplifier, a second stage amplifies up to 500 mW, and a final stage for high-power amplification to several watts. Even though the synchronization system will not employ amplifiers at such high output powers, it is still interesting to see how the increasing nonlinearity during high-power amplification affects the noise properties.

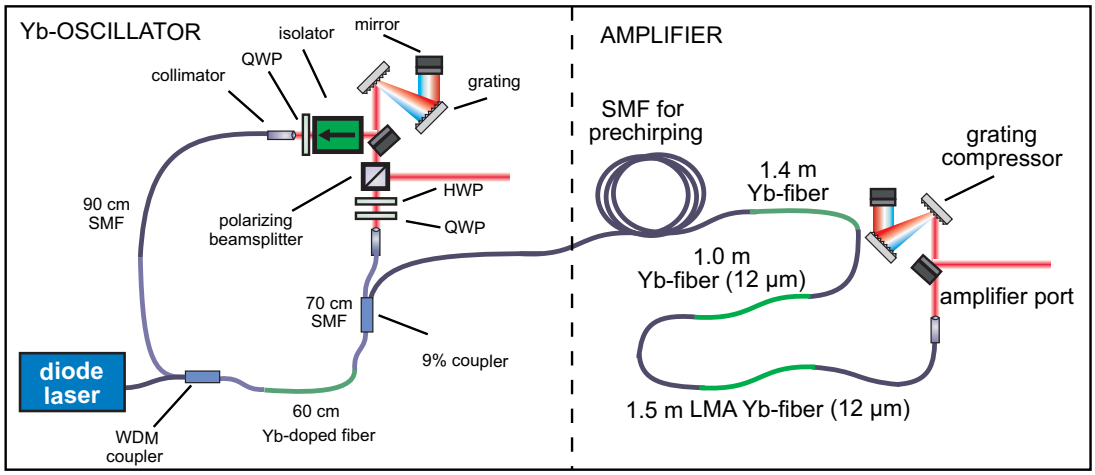

Figure 4.18.: Schematic of the experimental setup for amplitude and phase noise measurements at high power. SMF: single-mode fiber, LMA: large mode area, WDM: wavelength-division multiplexing, QWP: quarter-wave plate, HWP: half-wave plate.

The oscillator pulses are pre-chirped in a stretch of single-mode fiber to reduce the peak power during amplification. Self-phase modulation and other nonlinear effects will occur if the pulse peak power is too high during amplification, with negative impact on the recompressible pulse duration. To counteract these effect, the pulses are pre-chirped in a bulk grating compressor. Third-oder dispersion is added during the chirping and will in turn limit the compressibility of the pulses after amplification. The level of pre-chirping, where optimal compression after the amplification can be achieved, depends on the output pulse energy. A fiber length of 25 meters, chirping the pulses to 14 ps, was chosen for both low-power (1.4 W output power) and high-power experiment (10 W output power). The fiber length was increased to 50 meters for the high-power measurement (10 W output power) to reduce nonlinear effects dur-

ing amplification.

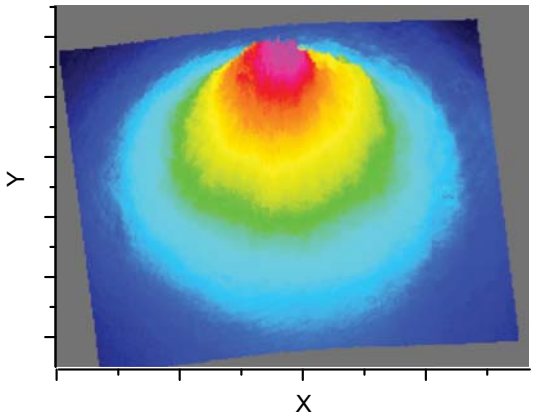

Figure 4.19.: Spatial profile of the amplified laser pulse at 5 W average output power.

At an average power of 1.8 W (which corresponds to a pulse energy of 20 nJ), pulses with minimal nonlinear distortion are obtained. After de-chirping the pulses in a grating compressor (600 lines/mm, angle of incidence 45°, a grating-to-grating separation of 44 cm), the pulse duration is inferred from an auto-correlation measurement to be 250 fs FWHM (a Gaussian pulse shape is assumed). Uncompensated third-order dispersion, mainly from the grating compressor, prevents further compression of the pulses. At higher powers, the nonlinear distortions on the pulses are more pronounced. Nevertheless, acceptable pulse quality can be retained up to 120 nJ. The pulse duration after de-chirping (with 35 cm of grating spacing) is increased to 320 fs and the pedestal becomes more pronounced (Figure 4.21). The nonlinear effects can be reduced with increased pre-stretching of the pulses. For a 50 m-long pre-chirp fiber, the pulses are 25 ps-long in the final stage of amplification. Twice as high pulse energies are obtained without excessive nonlinear distortion. However, uncompensated third order dispersion limits the compressed pulse duration to 500 fs.

The major advantage of single-mode fibers is that high-quality, single-mode beams are produced without special precautions for higher order mode suppression, which may not be long-term stable. The spatial profile of the pulses at an average power of 5 W is shown in figure 4.19. The beam shape remains unchanged independent of the power level and there is no discernable mechanical sensitivity (such as to bending of the fiber).

While fiber oscillators are among the quietest lasers, the effect of high-gain amplification (in this case 300 fold) on the noise level was unclear. The characterization of the relative intensity noise and measurements of the single-sideband phase noise of the amplified pulse train are presented in Figure 4.23 and 4.22 respectively. It can be seen that the amplification process only adds a moderate amount of amplitude noise:

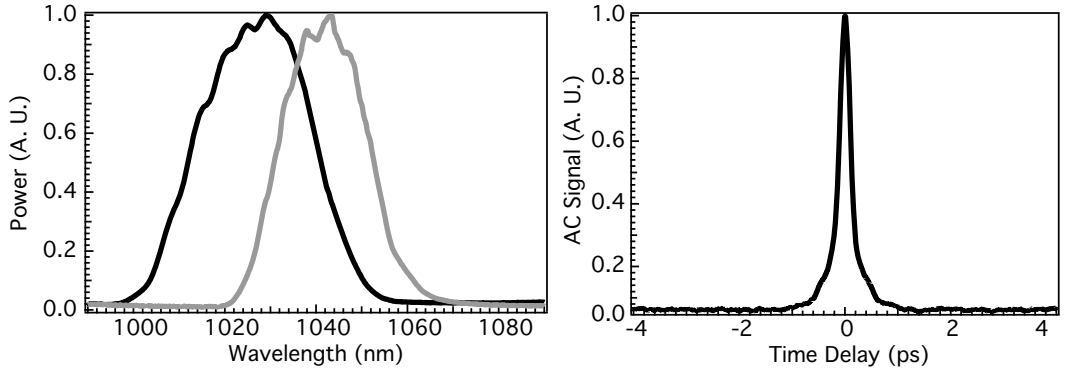

Figure 4.20.: Characterization of the pulses at 1.8 W of average power (20 nJ pulse energy): (a) Optical power spectrum of the amplified pulse (dark line) and the seed pulse (light line). (b) Intensity autocorrelation of the amplified pulse after external compression.

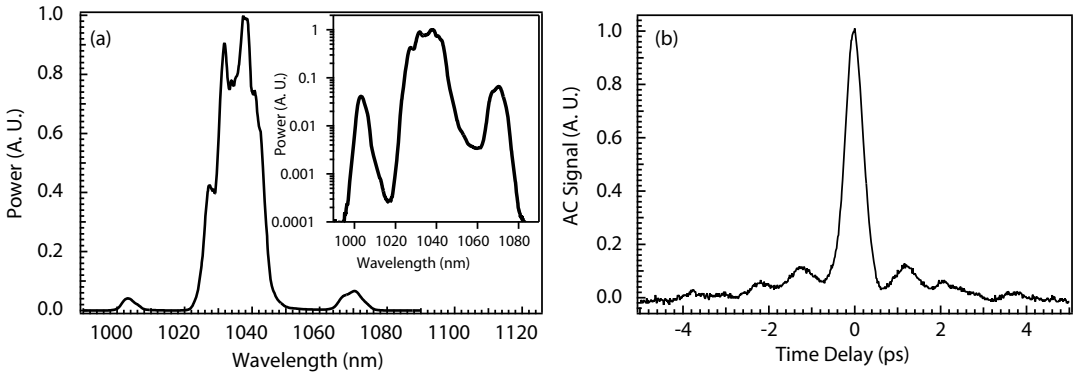

Figure 4.21.: Characterization of the pulses at 10 W of average power (120 nJ pulse energy): (a) Optical power spectrum of the amplified pulse. The inset shows the spectrum in log scale. (b) Intensity autocorrelation of the amplified pulse after external compression.

the integrated noise (from 10 Hz to 1 MHz) is 0.018% for the oscillator pulses and 0.033% for the amplified pulses, where major noise is only added in the 100 Hz to 10 kHz region. The phase noise measurements were preformed with an Agilent E5052 phase noise measurement setup. Different modes of the amplifier were investigated regarding their implications on the phase noise performance of the optical pulse train. If the amplifier is underpumped (green curve in figure 4.22), the high frequency noise is increased substancially, amounting to 70 fs rms. For an overpumped amplifier, amplified spontaneous emission and residual pump light also lead to a significant increase of the phase noise (blue curve in figure 4.22 with an integrated level of 115 fs). However for optimal settings of the amplifier power, virtually no increase could be measured (ref curve in figure 4.22) compared to the phase noise of the unamplified pulse train depicted in black. The integration yields 29 fs compared to 27 fs respectively.

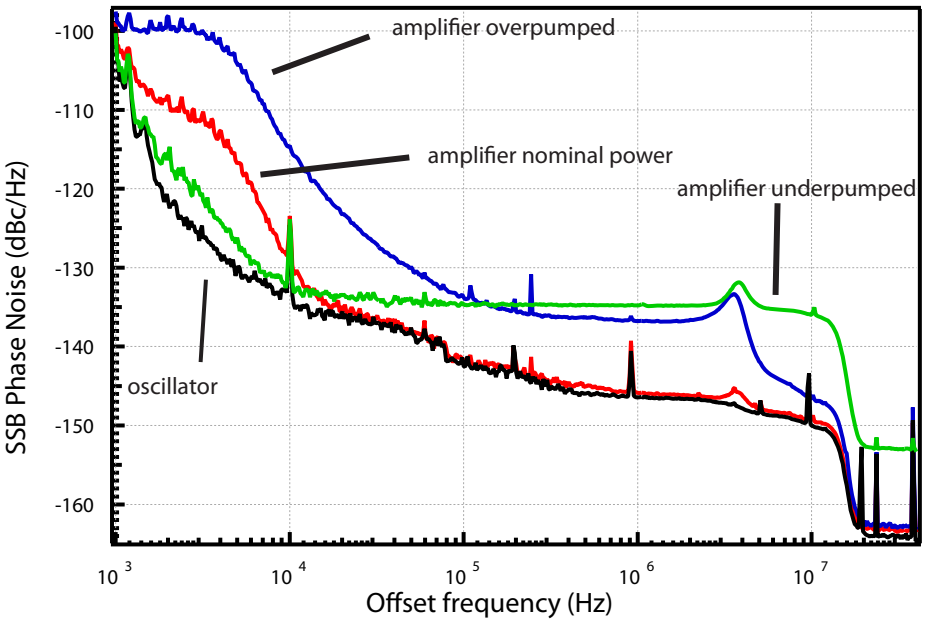

Figure 4.22.: Phase noise spectra obtained for various settings of the pump power of the amplifier.

These measurements indicate, that amplification of optical pulse trains to even a lot higher power than anticipated for the optical synchronization system can be done without significantly altering its amplitude and phase noise properties.

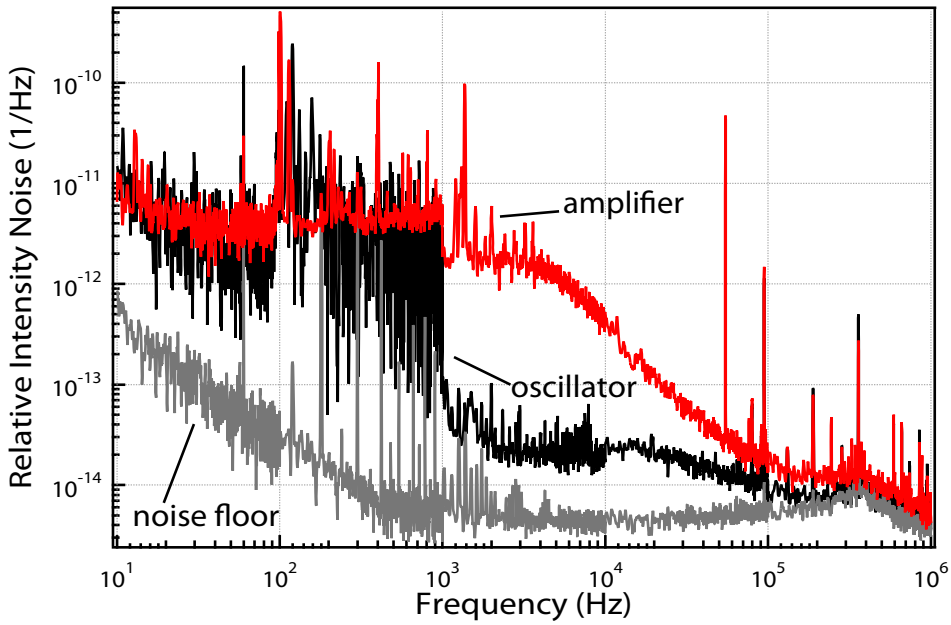

Figure 4.23.: Amplitude noise of the initial and amplified optical pulse train

5. First Tests of the System in an Accelerator Environment

A very important step in the development of a functioning prototype system is the test in a real-life environment. The MIT Bates Linear Accelerator Center facility provided that possibility. It was founded in 1967 with the mission to built a 400 MeV normal conducting electron linac running at an RF frequency of 2.856 GHz for electron scattering experiments. The linac in later years received a recirculator as an upgrade which made energies up to 1 GeV possible. The electron beam could then either be used for a liquid-hydrogen target scattering experiment (SAMPLE) or the electrons were accumulated in a storage ring to allow for collision experiments (BLAST) and use in other spectrometers (OOPS, OHIPS). A schematic overview of the facility is given in figure 5.1. The main feature of the accelerator was that it could provide polarized and unpolarized electrons with two gun systems.

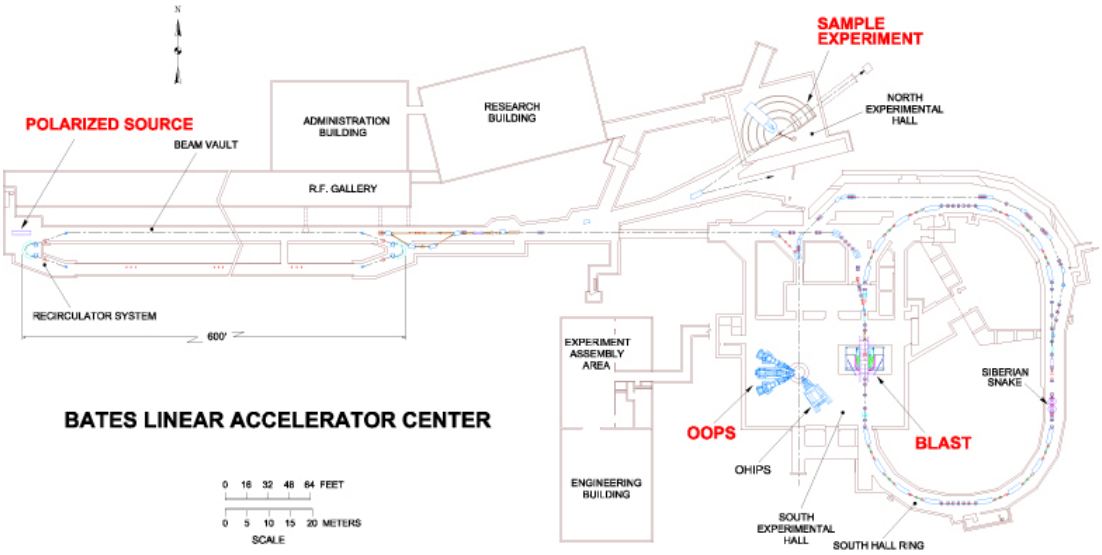

Figure 5.1.: Layout of the MIT Bates Linear Accelerator Center.

About 15 years ago, when optical fibers for signal transmission were first becoming widely used, the timing group designed and installed a fiber-based transmission line with sub-ns stability. Thus the facility proved to be an ideal testing facility for the

synchronization effort. The fiber employed at that time was the predecessor to SMF28 fiber which has become the standard in telecommunication for data transmission at 1.55 μm wavelength. The link extended along the complete facility from the injector to the very end, amounting to a total length in excess of 500 meters (see Fig. 5.2). Furthermore, there was no active temperature stabilization and the fiber was only passively thermally isolated in a separate conduit for about half of the link length. The fiber bundle was put on top of a cable tray for the rest of the distance. In addition to unfavorable temperature conditions, also all kinds of electromagnetic and audio noise was present to provide some challenges for the various feedback systems.

Figure 5.2.: Aerial photograph of the MIT Bates Linear Accelerator Center, with the red line indicating the position of the optical fiber.

The experiment consisted of three separate parts:

- Locking of the fiber laser to the 2.856 GHz master oscillator of the Bates Facility to reduce the close-in noise of the laser system,

- stabilizing the fiber length with an RF-based feedback to reduce the total residual timing jitter added by the transmission to a few femtoseconds,

- recovering an RF signal from the optical pulse train after 1 km of total travel through the fiber link with minimal added jitter.

5.1. Locking of the EDFL to the RF reference oscillator

A schematic of the experiment is shown in Figure 5.3. The EDFL runs at a repetition rate of 40.22 MHz, such that the 72nd harmonic is at the desired synchronization frequency of 2.856 GHz. The laser is locked to the reference using a phase-locked loop (PLL), generating an error signal by comparing the 72nd harmonic of the laser repetition rate to the reference oscillator frequency. This signal is fed back to a fiber stretcher, onto which 2 meters of the laser fiber are wound. By controlling the fiber length, the repetition rate is adjusted. The unity gain point of the PLL has to be chosen carefully to ensure that the final phase noise of the phase-locked fiber laser is dominated by the reference oscillator for low offset-frequencies and by the free-running fiber laser for high offset-frequencies and the integral phase noise is minimal. The fiber laser then *de facto* becomes the master oscillator of the facility. By locking to an RF reference for better low-frequency stability, one combines the good low-frequency properties of the RF oscillator and the excellent high-frequency properties of the free-running EDFL. Hence, a net improvement of the phase noise compared to the noise of each individual device is achieved.

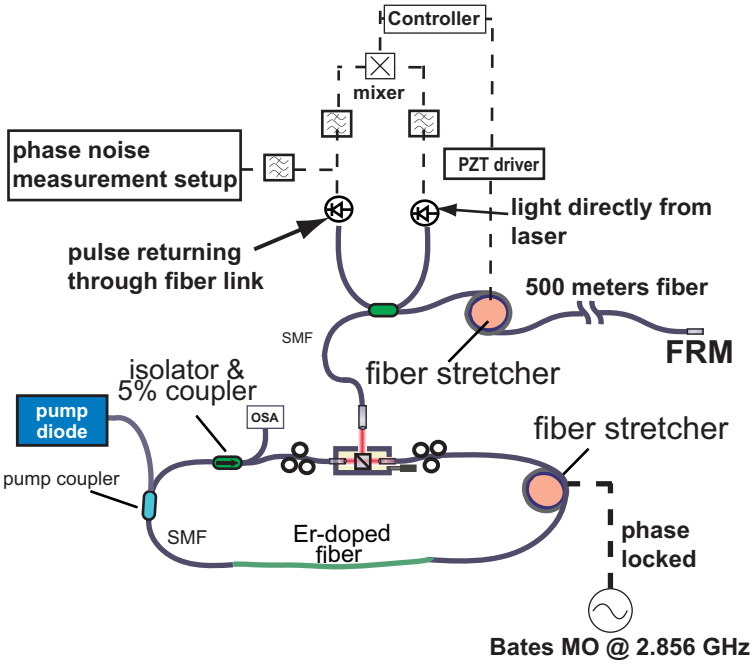

Figure 5.3.: Schematic setup of the synchronization system at MIT Bates Laboratory.

The experiment was conducted over a timespan of about 2 weeks. The fiber laser

was stable throughout this time and did not loose mode-lock or display any spectral changes. Considering the simplicity of the setup (see Fig. 5.4), this was also a promising indication that fiber lasers are stable enough to fulfill the reliability requirements of an accelerator.

Figure 5.4.: Photo of the fiber laser setup at the MIT Bates laboratory.

5.2. Stabilization of the fiber link

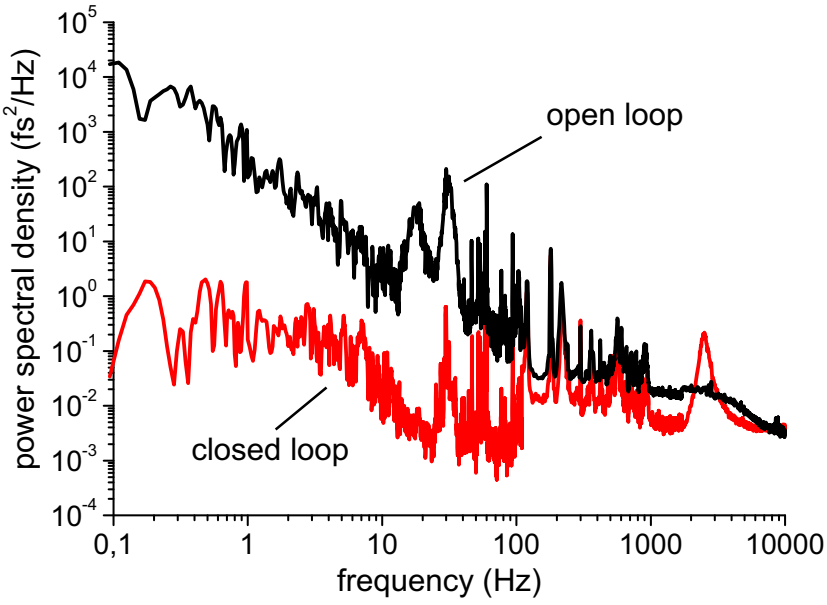

Figure 5.5.: Mixer output signal of the RF fiber link stabilization.

The refractive index of an optical fiber changes with temperature, with the consequence that the arrival time of a pulse propagating through the fiber varies accordingly. A typical value is between $1 \cdot 10^{-6}$/°C [Lee89] and $8 \cdot 10^{-6}$ /°C [CEF+05], which corresponds to a variation of between 3 ps and 25 ps for a link length of 1 km and a temperature change of 1 °C.

Stabilizing the fiber link using optical pulses has the inherent advantage of directly stabilizing the transit time through the fiber unlike schemes based on interferometric stabilization. Part of the light at the end of the link is reflected back into the same fiber using a Faraday rotator mirror. This mirror reflects the light with a 90 degree rotation of the polarization, counteracting the effects of residual birefringence in the fiber. In terms of polarization propagation, a single mode fiber can be regarded as an assortment of alternating half- and quarter-wave plates set at random angles. The index of refraction for both optical axis of the fiber is different, so the pulse has propagated through a fiber link with an average group velocity determined by the propagation length through either optical axis. A Faraday rotator mirror reflects the optical pulse train with a 90° shift in polarization. So the component that entered the Faraday rotator in the s-polarization is reflected in the p-polarization. When returning through the link, the effects of the polarization rotation in the fiber are thus compensated.

There are two possible feedback schemes that can be employed. An RF-based scheme is used for a coarse lock and an optical cross-correlation can be utilized for a fine lock. In the former scheme, part of the light directly from the laser and light returning through the fiber link are detected using two high-bandwidth photodiodes. Out of the resulting RF spectrum a harmonic is selected (due to the availability of filters, a frequency of 1 GHz was chosen) and combined in quadrature in a mixer. The resulting phase error signal is fed to an analog proportional-integral controller and finally to the fiber stretcher. The mixer output is monitored with a high-resolution signal analyzer to assess the performance of the lock.

The result for both open and closed loop scenarios stabilizing the MIT-Bates fiber link, is shown in Figure 5.5. By integrating the curves from 0.1 Hz and 5 kHz and taking the square root, one obtains the timing jitter. If the loop is open the jitter amounts to 66 fs, with the loop closed it is reduced to 12 fs. This measurement is an in-loop measurement, meaning that the mixer output signal used in the feedback was evaluated. This technique is not sensitive to noise and drifts in the high-frequency components (amplifiers, mixer, filter, etc.), whereas noise form the low-frequency part introduced by the regulation electronics is accounted for. A fully independent measurement would have required an out-of-loop phase detector. In any case, the high-frequency noise caused by high-frequency amplifiers is very small, if they are carefully selected.

The stabilization of the fiber link using RF techniques can of course not provide the long-term drift stability needed for the final system, however this experiment pro-

vided valuable experience. Firstly, the open-loop noise on the fiber link stabilization was significantly lower than initially expected, which simplifies the utilization of an optical cross-correlator significantly. The most important observation was, that no high-frequency jitter was added during the propagation of the pulse train through the fiber. The added noise was only present at frequencies below a few kHz which are well within the regulation bandwidth achievable with a PLL. An implementation of an optical cross-correlator scheme was not possible for this initial test, because a dispersion compensating fiber was not available at that time.

5.3. Recovering the RF signal after transmission

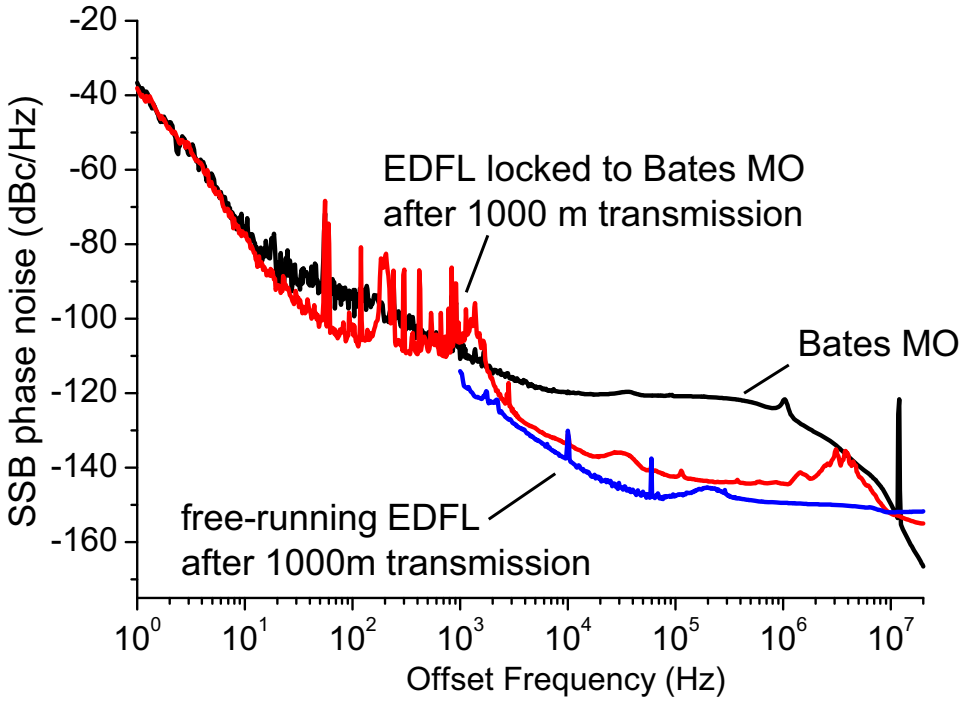

Figure 5.6.: Single sideband phase noise of the Bates Reference Oscillator (Bates MO), the EDFL locked to the reference after transmission through the link and the free running EDFL.

One crucial question for a timing distribution system is the delivery of RF signals to different end-stations with high stability to enable improved RF control for the accelerating cavities. After stabilizing the fiber link and locking the EDFL to a local RF oscillator, the phase noise of the recovered RF signal at the end of the fiber link is the relevant parameter. Figure 5.6 shows the phase noise of the RF master oscillator at the MIT-Bates Facility and of the EDFL locked to the RF source after returning through the fiber link (total travel distance of 1 km). It can be seen that the laser follows the RF

master oscillator extremely well for the lower frequency range. For offset-frequencies between 100 Hz and 10 kHz, there is technical noise added, such as ripple introduced by power supplies, visible as spurs at 60 Hz and harmonics thereof. This is mainly due to the current driver of the pump diode and can be eliminated by operating the pump diodes on battery power, or by better electrical isolation of the diode driver. At an offset-frequency of 1.5 kHz, the phase noise spectra of the free running laser and the RF reference oscillator meet. This is therefore the optimal unity gain frequency for the PLL. As can be seen in Figure 5.6, the locked EDFL phase noise spectrum is almost identical to the free running laser spectrum inside the locking bandwidth (blue line). The phase locking of the EDFL to the MIT-Bates master oscillator source adds around 30 fs timing jitter. This is reduced to a few femtoseconds, if one neglects the power ripple. The absolute phase noise is reduced, even taking the excess timing jitter due to the phase-lock into account, from 272 fs to 178 fs in a bandwidth of 10 Hz to 20 MHz. Including the residual noise of the fiber link stabilization, the complete system adds less than 50 fs of timing jitter in a bandwidth of 0.1 Hz to 20 MHz.

In summary, this test run turned out to be extremely successful and proved that the concept of an optical synchronization system is feasible. While a test of the long-term drift performance was not possible due to the RF-based stabilization of the fiber link, it became clear that there was no noise added at frequencies above a few kHz by the transmission of the optical pulse train. It can also be said, that even a simple stabilization scheme performed extremely well, almost meeting the desired residual timing jitter of 10 fs over a few seconds. The results of these investigations thus lay the foundation for the implementation of the optical synchronization system in FLASH or the XFEL.

6. The Optical Master Oscillator for FLASH

6.1. Setup of the infrastructure

The FLASH synchronization system requires a separate room in which the laser system, optical cross-correlators and the necessary electronics are situated. Defining the requirements and supervising the setup has been part of this thesis. The only viable position for such a room is next to the injector laser. This has the advantage of being close to the RF regulation systems and the injector laser, keeping the distance to two key systems of the machine small (red markings in figure 6.1). A schematic of the location of the new synchronization hutch is shown in figure 6.1. Special care was taken during construction in order to minimize EMI (electro-magnetic interference) and grounding problems. For this reason, a central ground copper plane mounted along the walls is foreseen inside the hutch (see figure 6.2). The grounds from all electrical components will be connected to that plane which in turn is connected to the central ground of the hall at a single point.

To minimize EMI from the outside area of the hall, the concept was to form a Faraday cage as far as possible. The exterior (yellow) metal plates are all connected to the metal frame and at one point the frame is connected to the interior ground of the hutch. Furthermore, the floor of the synchronization hutch is covered with a thin copper sheet which is also connected to the ground plane.

The FLASH hall has only one central concrete floor. Since also vibrating components are standing on that floor (pumps, klystrons, etc.), the decision was made to isolate the optical table. Four holes of around 30 cm diameter were drilled through the concrete floor at the position of the posts of the optical table. Before they were again filled with concrete, they were isolated against the rest of the floor.

The room features a separate air conditioning which has a design thermal stability for the surface of the optical table of better than ±0.5 °C.

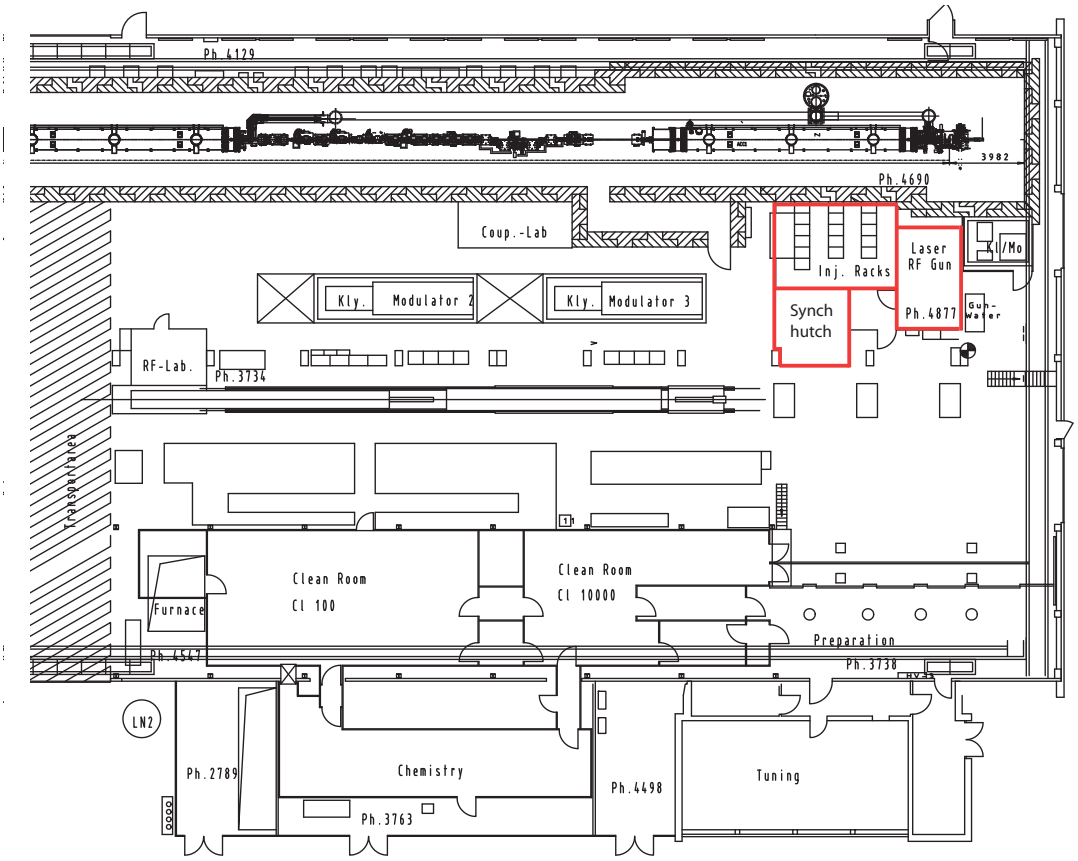

Figure 6.1.: Plan of the injector area in the FLASH hall

(a) View of the injector area with the synchronization hutch.

(b) Interior view during construction 1. The central ground plane for the room is a copper band attached to the wall.

(c) Interior view during construction 2. The floor is covered with a 300 µm thick copper sheet.

(d) Interior view during construction 3

Figure 6.2.: Images of the new synchronization hutch at different phases of construction.

6.2. Layout/integration into the accelerator environment

The laser master oscillator (LMO) system needs to operate continuously and without interruption, since the whole timing and synchronization system of the machine depends on it. Therefore it is necessary to employ a fully redundant scheme, with the possibility to switch from one laser to another without interrupting accelerator operation.

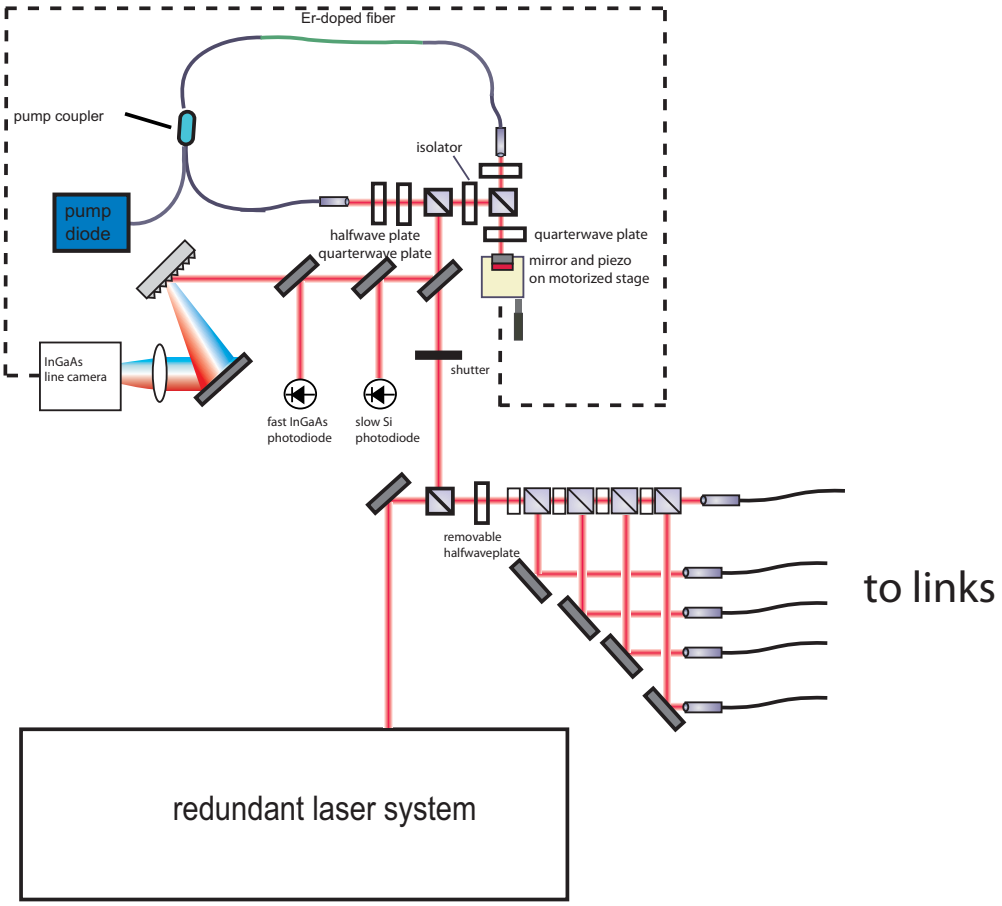

Figure 6.3.: Schematic of the proposed FLASH LMO system. Five of the 16 link output ports are shown.

A schematic of the setup of the LMO system is shown in figure 6.3. Two fiber lasers will run at a repetition frequency of 216 MHz, which is the 6th subharmonic of the accelerator RF frequency of 1.3 GHz. The lasers are built such, that they have all diagnostics embedded to ensure proper operation. The design of the laser enclosures

is presently underway, so the main design features will be described in this section. To test the digital feedback described later on in this section, fiber lasers running at a repetition frequency of 54 MHz were chosen, since the 216 MHz lasers are still under construction.

6.2.1. Laser diagnostics

Appropriate diagnostics to ensure control and proper operation of the laser are essential. The housing is made from a solid aluminum base-plate, where all optical components are mounted on. The baseplate is temperature stabilized and incorporated in a housing. Care is taken, that impact due to temperature fluctuations and microphonics is minimized. In the laser housing, three different diagnostics will be implemented. The characteristic parameters for the laser are the optical spectrum, the average power and the peak power. The optical spectrum, measured by using a dispersive grating and an InGaAs line array, is a clear indicator if mode-locking has been lost or a significant change in the operating point has occurred. The data from this array will be available in the accelerator control system. The average power is measured by an InGaAs photodetector, which at the same time generates the electrical frequencies needed to phase-lock the lasers to the accelerator RF. The peak power can be measured by making use of the two-photon absorption process in a silicon diode, which is sensitive in a wavelength range from 300 nm to 1000 nm. The average signal obtained is a direct measure for the peak power the pulses deliver. The principal is the same as for an autocorrelator based on two-photon absorption. Any change in the output peak power or pulse duration will be immediately visible. All the data will be evaluated in the control system and if one laser changes its optical output parameters, the shutters are changed such that the optical pulse train from the backup laser is transmitted to the fiber links and the faulty pulse train is blocked.

6.2.2. Combination and distribution

The free-space output of the two lasers are set to have orthogonal polarization, permitting the combination in a polarizing beam splitter cube. However, a removable halfwave plate has to be introduced in order to change the polarization of the backup laser, such that a laser beam of the correct polarization is transmitted to the links irrespective of the laser being used.

The single pulse train now enters a series of polarizing beam cubes each followed by a halfwave plate. This combination makes it possible to adjust the power of each reflected arm of the cubes which is fed to polarization maintaining fiber couplers. The total number of outputs will be 16 (see figure 6.3), which are then each amplified by

an fiber amplifier and fed to the optical cross correlators used to stabilizing the fiber links.

6.2.3. Synchronization to the accelerator RF

It has been discussed in section 4.2.2 that fiber lasers exhibit extremely low phase noise in the frequency band from 1 kHz to the Nyquist frequency (half the repetition frequency), but are susceptible to environmental noise for lower frequencies. RF oscillators can be built with extremely low-noise at low offset-frequencies by means of locking for instance a DRO (Dielectric resonator Oscillator) to a quartz oscillator at a frequency around 10 MHz. This combination will have the phase noise of the quartz oscillator at low offset-frequencies and the noise of the DRO at high offset-frequencies.

The same approach is chosen to improve the phase noise properties of the EDFL's. A custom made DRO oscillator at 1.3 GHz (Poseidon Scientific Instruments), which is stabilized by a low-drift PLL to a quartz oscillator, provides the reference frequency to which the laser is phase-locked. Thus the laser follows the lower noise microwave reference oscillator for frequencies up to the locking bandwidth the PLL and retains its intrinsic phase noise for higher offset-frequencies.

The DRO was designed such, that the phase noise meets that of the free running laser at an offset-frequency of around 1 kHz, which is within an easily achievable PLL bandwidth. The locking is done electronically with a PLL at microwave frequencies. A future upgrade will be using a Sagnac-type interferometer to optically lock the laser to the DRO. It will be briefly described here, for further reference see [KL06]. Figure 6.4 shows the schematic of the Sagnac interferometer. Part of the input pulse train is tapped off by photodiode 1. This signal is used to generate a reference signal at half the repetition rate $f_R/2$ of the fiber laser. The reference signal is then applied to both the phase modulator and the downconversion mixer. The rest of the input pulse train is sent into the Sagnac loop with an in-loop phase modulator. The output power from the Sagnac loop is expressed as $P_{out} = P_{in} sin^2(\Delta\phi/2)$, where $\Delta\phi$ is the phase difference between counter-propagating pulses in the loop. When there is no phase modulation, the loop output should be zero if the coupling ratio is exactly 50:50. The pulse train is phase modulated by the sum of the signal from the microwave input port at frequency Nf_R (N is an integer) and the reference signal at frequency $f_R/2$. The phase modulator is positioned in such a way that counter-propagating pulses at the phase modulator experience opposite phases due to the modulation by the reference signal. By this phase modulation, the output pulse train from the Sagnac loop is amplitude modulated at the frequency of $f_R/2$ as conceptually shown in Fig. 1. The pulse train detected at the fiber-loop output with photodiode 2 is bandpass filtered at $f_R/2$, mixed in phase with the reference signal and downconverted to base band. This phase error output is filtered

and controls the piezo of the fiber laser. When the phase-locked loop is in the locked state, the Sagnac-loop output pulse train is not modulated. Sub-10 fs relative timing jitter has been demonstrated using this technique. Details to the theoretical approach

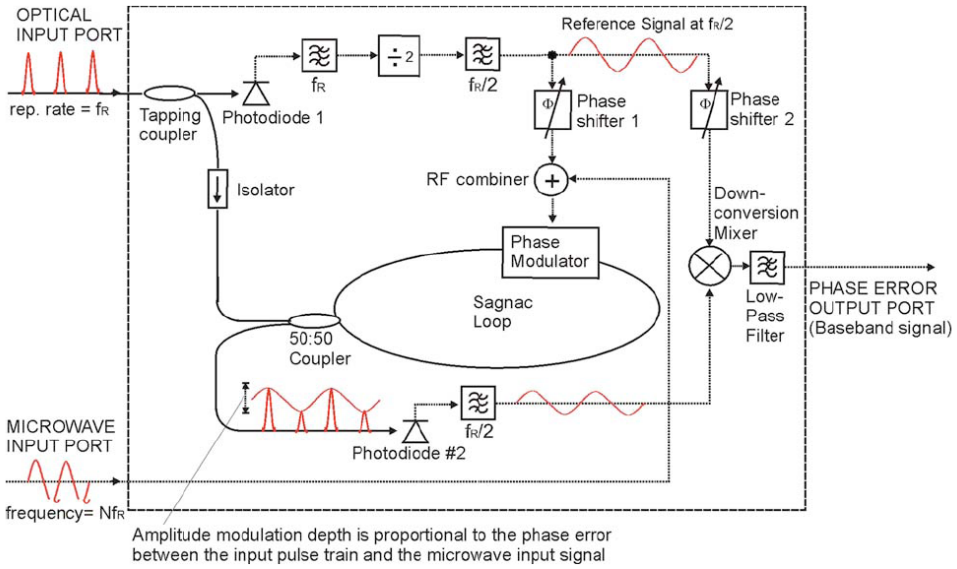

Figure 6.4.: Schematic of the balanced Sagnac interferometer. The solid and dotted lines indicate optical and electrical signal paths (from [KL06]).

to a PLL can be found elsewhere [Win04]. A simple PLL controller consists of a device one wishes to regulate, a sensor which measures the device output signal and a compensator which modifies the properties of the sensor signal to enable the control of the system (e.g. amplifiers and integrators). The idea of closed-loop controlling is

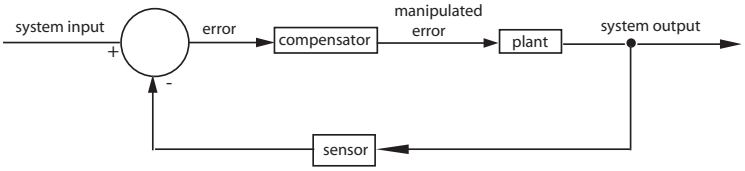

Figure 6.5.: Schematic of a single-loop control system

to generate an error signal, by comparing the output to a reference value and feeding this back to the input. If this is done in the form of negative feedback (e.g. positive deviation is subtracted from the input and vice versa), it is possible to keep the output signal at the desired reference.

6.2.3.1. The phase detector

The initial tests for the phase-locking were performed with 54 MHz stretched-pulse lasers instead of the 216 MHz lasers that will be used in the final system. For this purpose, the division ratio of the programmable divider (24 for 54 MHz instead of 6 for 216 MHz) has to be adjusted. The schematic of the phase detector unit used for the stabilization of the LMO System in depicted in figure 6.6. It uses one PLL operating at 9.0277 MHz (the 6th sub-multiple of the laser repetition frequency) and another one at 1.3 GHz (the main accelerator RF frequency). The reason for the dual-frequency setup of the PLL lies in the necessity to keep a fixed phase relation between both laser systems, even if one has to be restarted. To enable an ultra-low residual jitter performance, the highest possible comparison frequency is selected which is 1.3 GHz. This however leaves 24 possible positions (zero-crossings) where the PLL can catch. If the phase-lock of a failed fiber laser is reestablished, it cannot be guaranteed that the laser pulse position is identical to the one of the backup laser which is now seeding the synchronization system. The solution to this problem is the introduction of the second PLL into the system. It runs at a comparison frequency which is at $1/24$ of the LMO repetition frequency. This leaves only one zero-crossing where the PLL can catch per 24 revolutions of the laser pulse inside the cavity. The lower frequency PLL catches first and thus selects the phase of the laser pulse. Once the lock is established, the second PLL running at 1.3 GHz will take over. The electrical pulse train from one of the diagnostic photodiodes is split using a 16 dB directional coupler, where the smaller output is low-pass filtered to select the first first harmonic of the laser repetition rate and is fed to a digital divider which divides the signal frequency by 24 to reach 9.0227 MHz. This is compared to the central 9.022 MHz reference of the machine. The divider chip features a reset input to make sure that the counting always starts at a time given by a trigger synchronized to the electron bunch.

From the main part of the signal, the 6th harmonic of the laser repetition rate is selected using an appropriate bandpass filter and amplified to a level of around 5 dBm. The reference signal for the phase detector of the 1.3 GHz PLL is the 1.3 GHz microwave master oscillator signal. Both are fed to a analog double-balanced diode ring mixer.

The resulting error signals of both phase detectors are filtered by a 1.9 MHz low-pass filter and amplified using an ultra-low noise operational amplifier to match the input range of the ADC for the digital controller. The signal is now amplified by the loop filter, which can be either a digital or an analog proportional-integral controller. The proportional and integral part are in parallel, so the advantages of an integrator at low frequencies can be obtained without compromising the phase margin at higher frequencies. After being amplified to a higher voltage level, the signal is fed to the

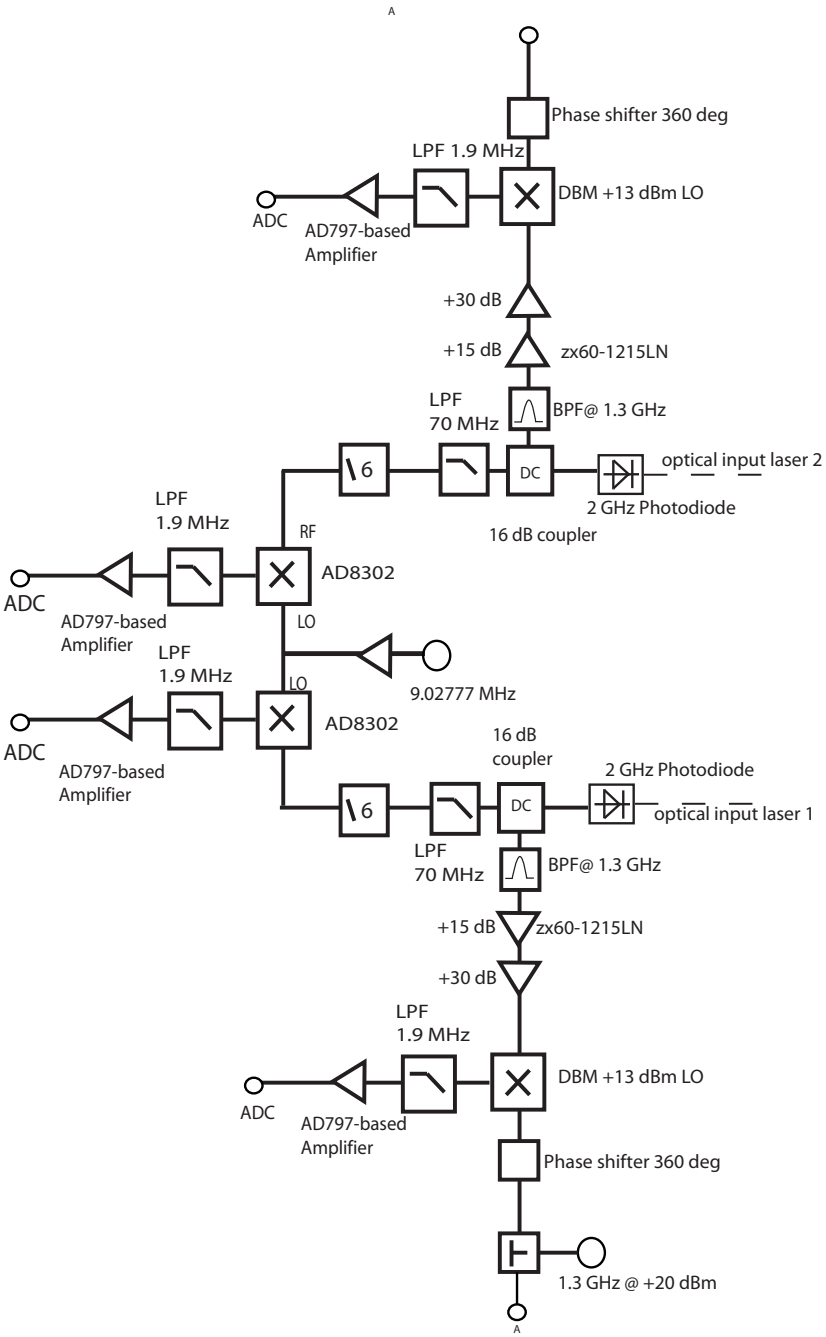

Figure 6.6.: Schematic of the Phase Detector Unit

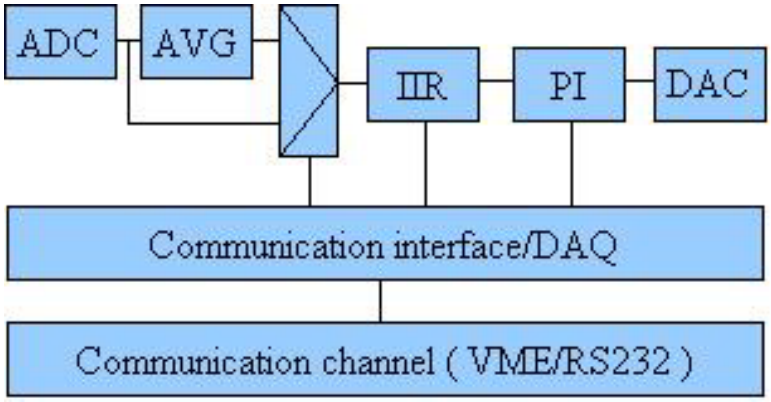

Figure 6.7.: Schematic of the digital controller architecture

piezo in the fiber laser cavity. This adjusts the repetition rate of the LMO.

6.2.3.2. The controller

There are two fundamental approaches which can be considered for the controller of this system. One choice is to use a conventional analog controller. It has been shown, that excellent synchronization performance can be achieved using such a system [Win05]. The drawback is the limited flexibility. It is very difficult to realize transfer functions that are of higher complexity than a simple PID-controller. Such advanced control functions permit for example the implementation of a notch-filter to counteract the effects of the resonance of the piezo crystal. This would then allow a higher gain in the PLL. Furthermore the switching of two PLLs is significantly easier using a digital controller which will be described in the next section.

6.2.3.3. Digital controller

The digital PI controller was implemented using an in-house developed FPGA-based (Field programmable gate array) controller board for the low-level RF control, called SIMCON 3.1 [Gie05]. The internal structure of the controller is shown on figure 6.7. The digital controller offers the same functionality as its analog pendant, namely a parallel PI-controller with an optional second order infinite impulse response low-pass filter.

The error signal from the double balanced mixer is sampled at a frequency of 60 MHz. Then the data is decimated to provide one valid sample every 1 μs. Optionally, averaging of 60 samples of the error signal can be used to reduce the ADC noise. The controller transfer function is applied to the resulting digital signal which is then converted with a DAC and fed back to the piezo via a piezo driver.

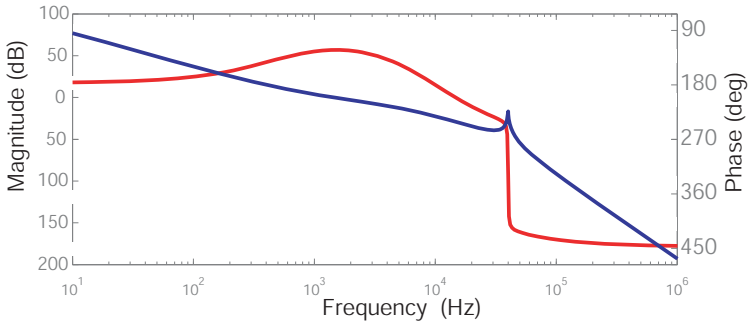

Figure 6.8.: Plot of the open loop transfer function (Bode plot) (magnitude - red, phase - blue)

For diagnostic purposes, a flexible data acquisition system was used. It saves 16 signals over 64 ms (64000 samples of each signal) to the external memory of the SIMCON controller. Two forms of communication were were implemented: a standard VME interface and a serial link.

6.2.3.4. Controller type and simulation

For full details on the theoretical description of a PLL and mathematical derivation of transfer functions, see reference [Win04]. In our case the feedback acts on the laser cavity length through the piezo actuator. The laser will in terms of phase act as an integrator with the transfer function $G_l = k_l/s$, where k_l is the gain of the piezo inside the laser cavity (in our case 0.35 $^{\mathrm{Hz}}/_{\mathrm{V}}$) and $s = i\omega$. Mechanical resonances (f_{res}) of the piezo have to be considered (~40 kHz), which can be modeled by a harmonic oscillator with a damping coefficient γ. This yields a transfer function of

$$G_{piezo} = \frac{(2 \cdot \pi \cdot f_{res})^2}{s^2 + 4\pi\gamma f_{res} \cdot s + (2\pi f_{res})^2} \tag{6.1}$$

which ultimately limits the achievable gain of the PLL. A linear response is assumed for the phase detector around the locking point, which is valid for analog mixers around the zero-crossing, i.e. $\Delta\phi = 0, \pi, 2\pi \ldots$. The controller consists of a PI-regulator ($G_{PI} = K_P + \frac{K_I}{s}$) and an optional low pass filter with a corner frequency of f_{lp} =10 kHz.

The open loop transfer function simulated with MATLAB is shown in figure 6.8. The unity gain bandwidth is at 1 kHz which is in good agreement with the experimental results. It can be seen from figure 6.10, that the phase noise spectra of the locked laser and the reference oscillator start deviating just above 3 kHz which is the point of unity gain.

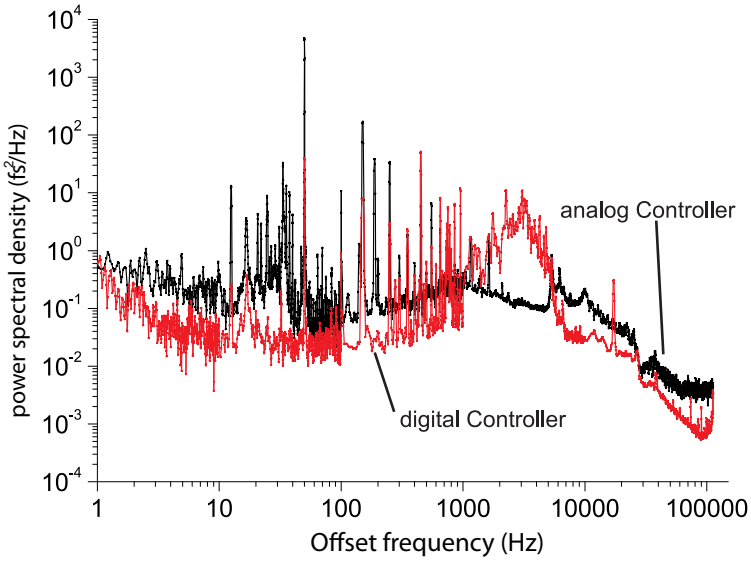

Figure 6.9.: Power spectral density of the closed-loop error signal for both analog (black) and digital (red) controllers.

6.2.3.5. Comparison of analog and digital feedbacks

The first step to compare the performance of the two feedback types was to lock one LMO to a 1.3 GHz reference with either system and evaluate the residual jitter. Figure 6.9 shows the power spectral density of the error signal when the system is locked with either the analog or the digital controller. The integration of these signal yields the respective residual jitter. It amounts to 74 fs for the analog controller and 107 fs for the digital controller, both in a bandwidth from 1 Hz to 112 kHz. The difference in performance of the two controllers is almost entirely due to the PLL peaking[1] of the digital controller. This is due to a slightly higher proportional gain in the digital controller compared to the analog one, which limits the phase margin of the system and leads to the jitter increase around 2 kHz. Reducing the proportional gain will yield a comparable result to the analog controller. It should be noted, that a significant part of the jitter in the digital controller is due to the 50 Hz ripple. The magnitude of this perturbation does not change with proportional and integral gain settings of the controller, making a crosstalk from the power supply to the DAC a likely candidate for the cause. It can possibly be improved in the next redesign of the digital controller board. An advantage of the digital controller is the possibility to average the ADC data. The sampling rate of the ADC is a lot higher than needed for the regulation (60 MHz), so an averaging procedure was employed bringing the effective sampling rate

[1] This is also known as ”waterbed”-effect, which means that for higher suppression at low frequencies, some noise will be created at higher frequencies.

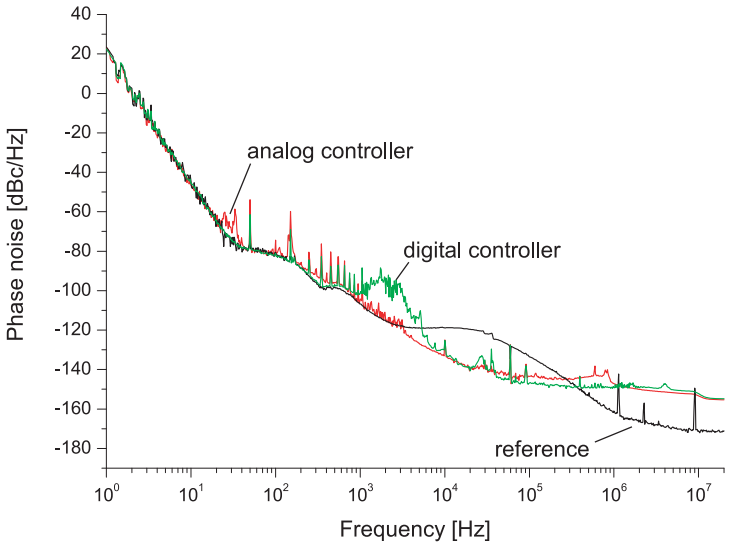

Figure 6.10.: Phase noise for the locked fiber laser with both analog (red) and digital (green) controllers and the reference (black).

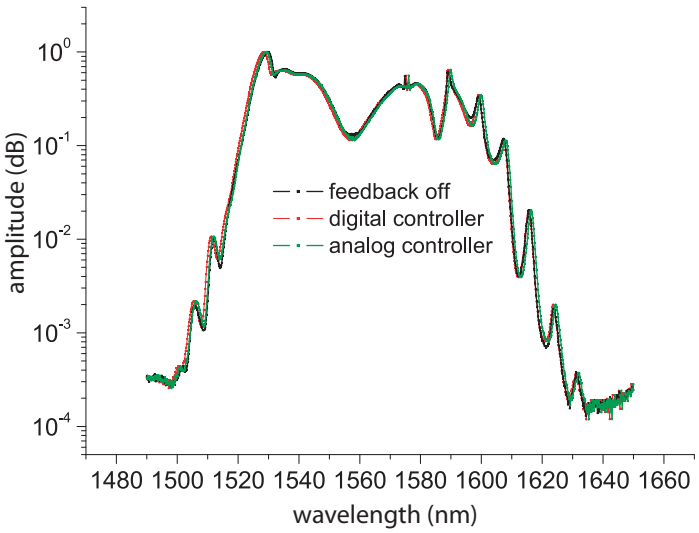

Figure 6.11.: Optical spectrum of the fiber laser without feedback (black), with digital controller (red) and analog controller (green)

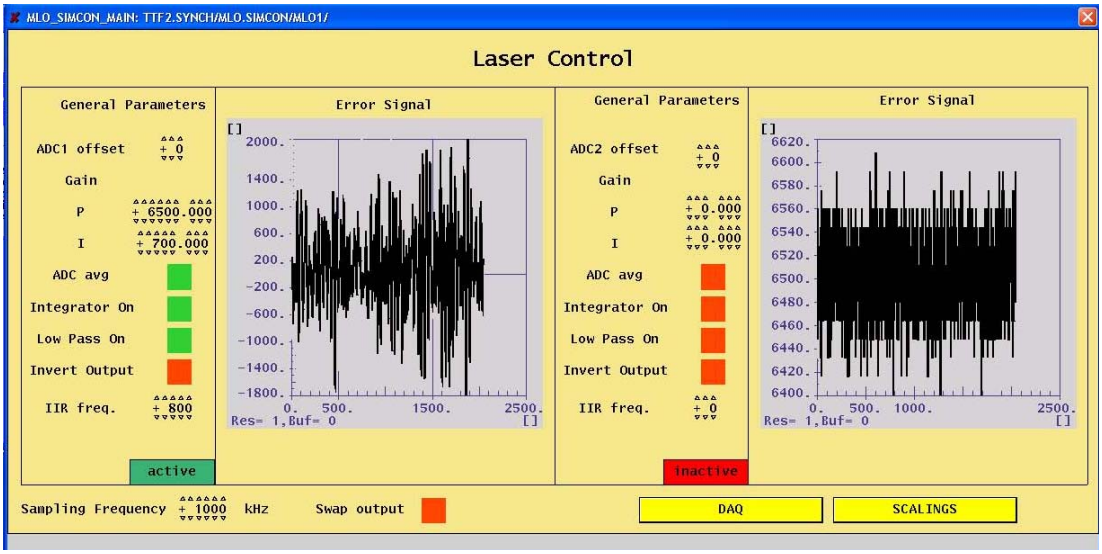

Figure 6.12.: Image of the control panel for the SIMCON controller. The left half is devoted to the 1.3 GHz PLL system, the right side to the 9.0277 MHz PLL

down to 1 MHz was employed. This reduces the uncorrelated noise of the ADC by a factor of almost 8.

An important requirement is that the activated PLL does not increase the phase noise at higher offset-frequencies. This is indeed not the case. The measured phase noise with and without feedbacks is depicted in figure 6.10. There is no significant increase in the high frequency phase noise when locking with either system.

A further important issue is the possible change of the optical spectrum of the laser pulses due to the phase locking. Figure 6.11 shows the optical spectrum of the fiber laser without any feedback and with either controller. No significant change was observed for either feedback option.

The benefits of using the digital loop filter are extensive. The signals are directly available in the control system and the PLL switching can be easily accomplished in the FPGA by setting the appropriate register . Furthermore, it is possible to implement the decision tree that determines if the lasers are still operating according to specifications. For this reason, the digital controller based on the SIMCON controller board has been chosen for the FLASH LMO system. The SIMCON controller board was implemented into the accelerator control system, a sample picture of the control panel is shown in figure 6.12. Both controller and laser operated for weeks without maintenance. As an example, the voltage applied to the piezo and in-loop timing jitter is shown over a 24 hour time period in figure 6.13. It can be seen that the timing jitter is usually around 60 fs rms, in spite of frequent operation of the translation stage (discontinuities in the black curve in figure 6.13). The number of translation stage

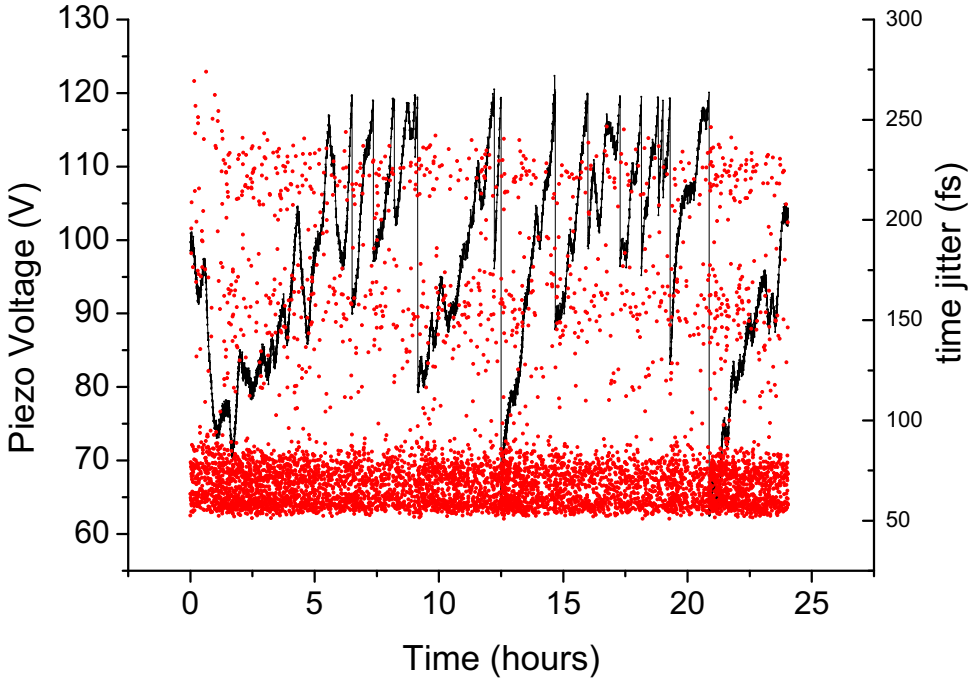

Figure 6.13.: Plots of the voltage applied to the piezo and in-loop timing jitter measured over a 24 hour period

movements will be further reduced by improved laser packaging (smaller sensitivity to microphonics and temperature fluctuations).

The timing jitter shows frequent jumps to a value of around 250 fs rms. A careful analysis has led to the discovery, that the 1.3 Ghz reference of the machine has a phase jump of almost 10 ps, 3 ms before an electron pulse train is emitted. The sampling of the in-loop error signal is not synchronized to the machine, so it statistically hits the area of the phase jump which leads to the 250 fs timing jitter peaks. The reasons for these instabilities of the RF reference are not yet fully resolved. They may be related to the strongly increased power demands (e.g. of klystron capacitor banks and of the RF gun) before an electron pulse train is emitted.

In summary, the main components of the FLASH laser master oscillator system have been designed and the construction of the packaging for both lasers and distribution is ongoing. The tests conducted for the phase-locking to the accelerator RF over many weeks show that a residual timing jitter of around 60 fs rms can be expected and the lasers were virtually maintenance free.

7. Conclusion and Outlook

An optical synchronization system has been built and tested, based on the distribution of ultra-short laser pulses. It promises to achieve 10 fs synchronization of various parts of the accelerator over short and long timescales. This is an essential prerequisite to utilize the full potential of the 10 fs to 100 fs FEL pulses produced by FEL-type X-ray sources or energy recovery linacs.

A crucial part of the system is the mode-locked laser which serves as the laser master oscillator for the system. It exhibits extremely low phase and amplitude noise at offset-frequencies outside the locking range of a phase-locked-loop (typically above 1 kHz). Furthermore the laser system operates with the high reliability required by an accelerator environment. A redundant erbium-doped fiber laser was designed and built operating at a wavelength of 1550 nm. It is passively mode-locked delivering optical pulses of 100 fs duration if transform limited. The phase noise was measured to be 10 fs in the range of 1 kHz to the Nyquist frequency, the amplitude noise was 0.03%. Such a laser is one of the most quiet lasers presently available. It was also verified that amplification to high pulse energies of 140 nJ does not add significant amounts of amplitude and phase noise.

A first test in a realistic accelerator environment was performed at the MIT Bates laboratory. A 500 meter long optical fiber was stabilized using an RF-based scheme. It was verified that there were no noise contributions above the frequency range of a few kHz. This was a very important conclusion, as noise at frequencies above a few ten kHz would be extremely difficult to reduce with a PLL. The noise level measured with the feedback closed was 12 fs for a frequency range of 0.1 Hz to 20 kHz. This proved that even a simple RF-based feedback can accomplish stabilizations to the 10 fs level on short timescales. Furthermore, the fiber laser was phase locked to the (local) RF master oscillator of the facility. The phase noise of the transmitted signal was measured with a photodetector and a commercial phase noise measuring system and no significant performance degradation was observed. This was the first proof of principle for an optical synchronization system. Presently, many facilities (FLASH, FERMI@Elettra, and the European XFFL) are planning such a system or are already implementing it. The work in this thesis has laid the foundation and made the initial tests for such optical synchronization systems.

Finally, the optical master oscillator for FLASH was designed and the initial infras-

tructure for the optical synchronization system at FLASH was set up.
The next steps are to implement the timing stabilization using optical cross correlators. This will enable long-term stabilization of the fiber link to the 10 fs level. Arrival time measurements at various points in the machine will finally have to verify, that the electron bunch stability benefits from the optical synchronization system. A further project is the locking of the various laser systems used in the machine to the new optical reference distribution. Appropriate cross correlators have been designed and tested [JWKS07]. With these projects complete, it will be possible to switch FLASH from the microwave to an optical synchonization system and allow unsurpassed timing stability for pump-probe experiments.

A. Simulation of Mode-locking by Nonlinear Polarization Evolution

In this appendix, a numerical model for fiber laser simulations is presented. It is based on the nonlinear Schrödinger equation 2.36 which was described in chapter 2. The model includes the effects of saturable gain, second and third order dispersion, linear losses and nonlinear effects such as gain dispersion in the amplification section, self-phase modulation and the Raman effect. The pulse is assumed to start from noise and is iterated over many round trips until a steady state solution is reached. The results obtained in this chapter are based on a code written by Prof. F. Oemer Ilday of Bilkent University, Ankara and a Java interface written by one of his students. It employs the split step Fourier method, which will be briefly explained in this section.

A.1. Split-step Fourier method

A convenient method for solving the nonlinear Schrödinger equation

$$\frac{\partial A}{\partial z} + \frac{\alpha}{2}A + \frac{i\beta_2}{2}\frac{\partial^2 A}{\partial T^2} - \frac{\beta_3}{6}\frac{\partial^3 A}{\partial T^3} + = i\gamma\left(|A|^2 A + \frac{i}{\omega_0}\frac{\partial}{\partial T}(|A|^2 A) - T_R A\frac{\partial |A|^2}{\partial T}\right) \tag{A.1}$$

is the split-step Fourier method. It is based on the assumption that dispersion and nonlinear effects act independently over a short piece of fiber. It is useful to write equation A.1 formally as

$$\frac{\partial A}{\partial z} = (\hat{D} + \hat{N})A, \tag{A.2}$$

where $\hat{D}$ is the differential operator accounting for dispersion and absorption in a linear medium and $\hat{N}$ is the nonlinear operator governing all nonlinear effects on pulse propagation. They are given by

$$\hat{D} = -\frac{\alpha}{2} - \frac{i\beta_2}{2}\frac{\partial^2}{\partial T^2} + \frac{\beta_3}{6}\frac{\partial^3}{\partial T^3} \tag{A.3}$$

and

$$\hat{N} = i\gamma\left(|A|^2 + \frac{i}{\omega_0}\frac{\partial}{\partial T}(|A|^2 A) - T_R A\frac{\partial |A|^2}{\partial T}\right) \tag{A.4}$$

Propagation over a small distance h is carried out in three steps. First, the pulse propagates over half the distance with only dispersive effects. Then, in the middle of the section, nonlinearity is included after which the pulse propagates again half the distance. Mathematically, this results in

$$A(z+h,T) \approx \exp\left(\frac{h}{2}\hat{D}\right)\exp\left(\int_z^{z+h}\hat{N}(z')dz'\right)\exp\left(\frac{h}{2}\hat{D}\right)A(z,T). \tag{A.5}$$

The exponential operators can be readily evaluated in the Fourier domain. For the dispersive operator $\exp\left(\frac{h}{2}\hat{D}\right)$, this yields

$$\exp\left(\frac{h}{2}\hat{D}\right)A(z,T) = FFT_T^{-1}\exp\left(\frac{h}{2}\hat{D}(i\omega)\right)F_T A(z,T) \tag{A.6}$$

where $\hat{D}(i\omega)$ is obtained by replacing the differential operator $\partial/\partial T$ by $i\omega$. As $\hat{D}(i\omega)$ is just a number in Fourier space, the evaluation of equation A.6 is fairly straightforward.

A.2. Simulator interface

The simulator interface was written in Java and allows to enter all parameters needed for the simulation. A screen shot is shown in figure A.1. Table A.1 summarizes the parameters needed for the numerics of the simulation.

Name of parameter	Function
tres	the number of points
Treal	actual length of the pulse corresponding to a number of points T0
T0	number of points corresponding to pulse length Treal
Roundtrip number	number of roundtrips before simulation ends
zres	number of discrete steps taken between every page
saveevery	number of roundtrips after which data is saved to file
Power	actual power value which corresponds to power 1 in normalized units
Central Wavelength	central wavelength used for simulation
Traman	parameter characterizing the strength of the Raman effect
Maxpage	the number of segments each fiber section is divided into

Table A.1.: Numerical parameters needed for the simulator

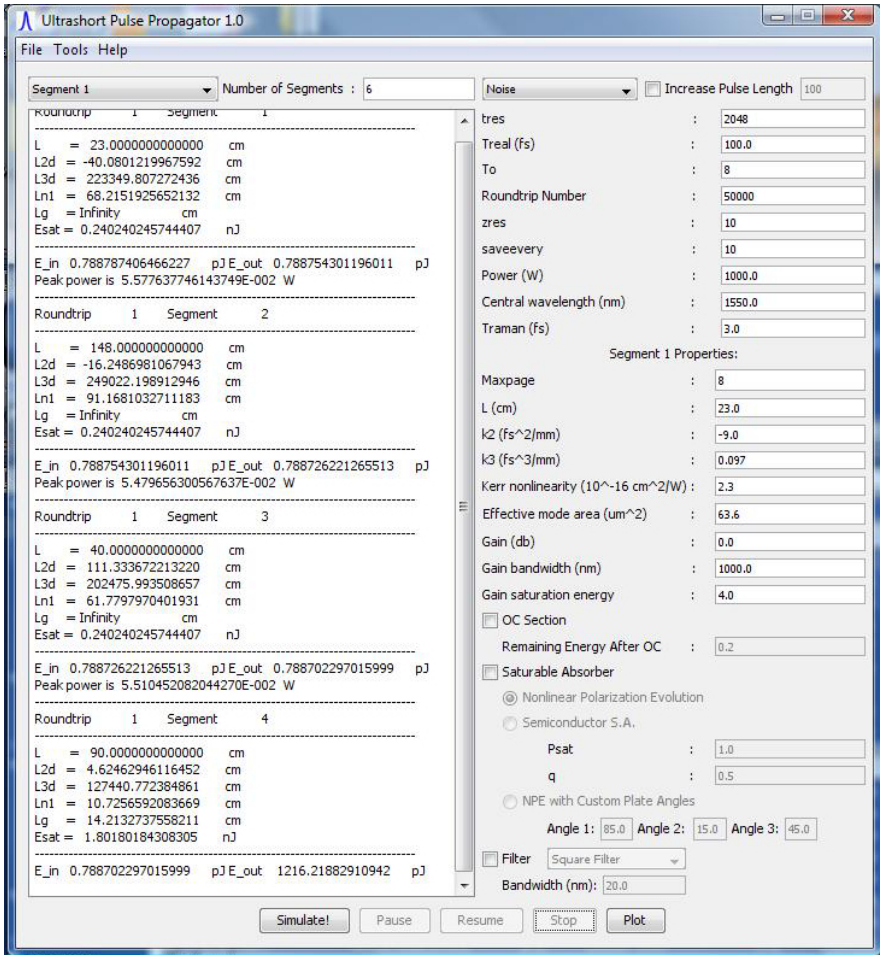

Figure A.1.: Screenshot of the Simulator Interface

A.2.1. Implementation of the saturable absorber

The saturable absorber is implemented at the end of a section, by converting the total nonlinear phase shift accumulated over the round trip into an amplitude modulation. For the semiconducter saturable absorber, it is modeled by

$$I_{SSA} = \frac{1-q}{1+\frac{I}{I_{sat}}}, \tag{A.7}$$

where q is the modulation depth and I_{sat} is the saturation power of the saturable absorber. For nonlinear polarization evolution, the model is

$$I_{NPESA} = (1-q)\cdot\cos^2\left(\frac{\pi}{2}\frac{I}{I_{sat}}\right) \tag{A.8}$$

A.2.2. Results for a stretched-pulse fiber laser

The parameters used for the stretched pulse fiber laser are summarized in table A.2. A 10 % output coupler is assumed at the isolator position. Second and third order dispersion have been calculated from the data available in the various datasheets. There is typically a 5 % uncertainty associated with the mode-field diameter, core diameter and numerical aperture. As dispersion depends linearly on core diameter and numerical aperture, the error is also on the order of 5 %.

section	fiber type	length (cm)	dispersion ($\frac{fs^2}{mm}$)	total dispersion
collimator 1	Flexcor1060	23	-9	-2070
fiber stretcher	SMF28	151	-23	-34730
pump coupler	Lucent980	40	3	1200
gain fiber	Lucent custom made	87	78	67860
isolator	SMF28	40	-23	-9200
collimator 2	Flexcor1060	23	-9	-2070
free space section		12.5	0	0
total		359.5		21350

Table A.2.: Length of fiber segments and dispersion properties for a stretched-pulse fiber laser with a repetition rate of 54 MHz

Figure A.3 shows the buildup of a stable solution over many round trips. It can be seen, that it takes about 100 roundtrips until one perturbation is sufficiently amplified. The solution then becomes stable rather quickly. All plots in figure A.3 are taken behind the point in the cavity, where the nonlinear polarization evolution takes effect. Figure A.4 shows the evolution of the optical spectrum during one round trip in the steady state solution. It can be seen, that the spectral shape does not change significantly until amplification starts in the gain fiber. With increasing peak power, self-phase modulation starts affecting the spectrum leading to its broadening. Since the pulse is chirped at the output port, the wings of the spectrum are reflected out and the center remains inside the laser cavity. The simulated spectra and pulse durations match nicely the effectively measured spectra and output pulse durations (see figures 4.1 and 4.3).

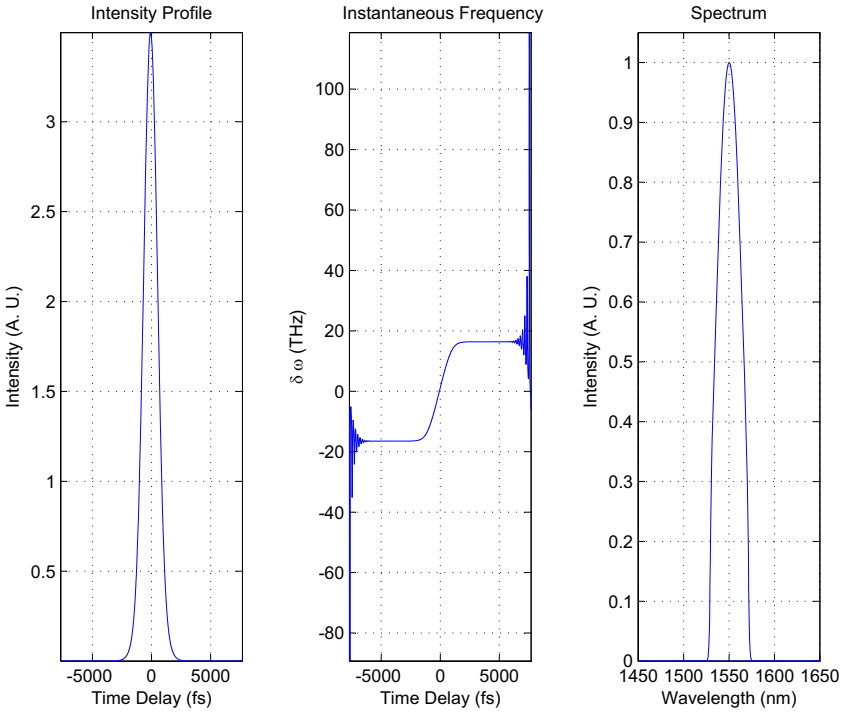

Figure A.2.: Temporal profile of the pulse (left), optical phase (middle and optical spectrum (right) in the free-space section of the cavity)

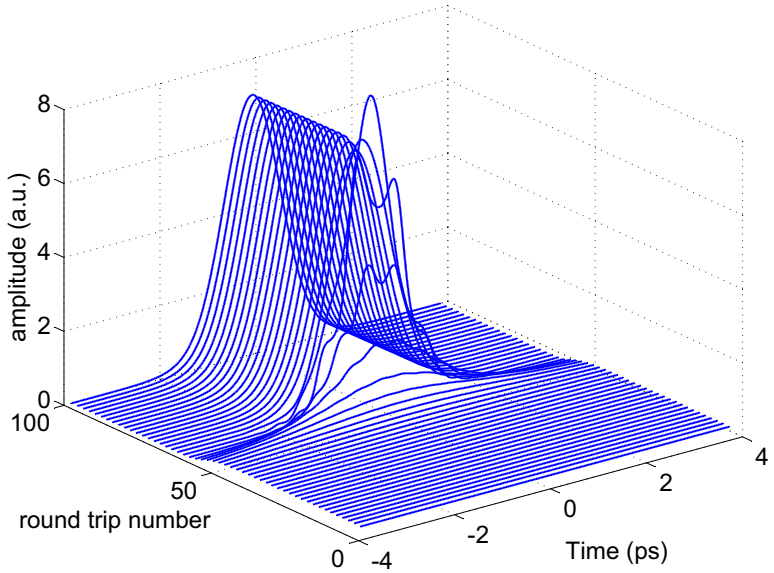

Figure A.3.: Buildup of the pulse inside the cavity over many roundtrips

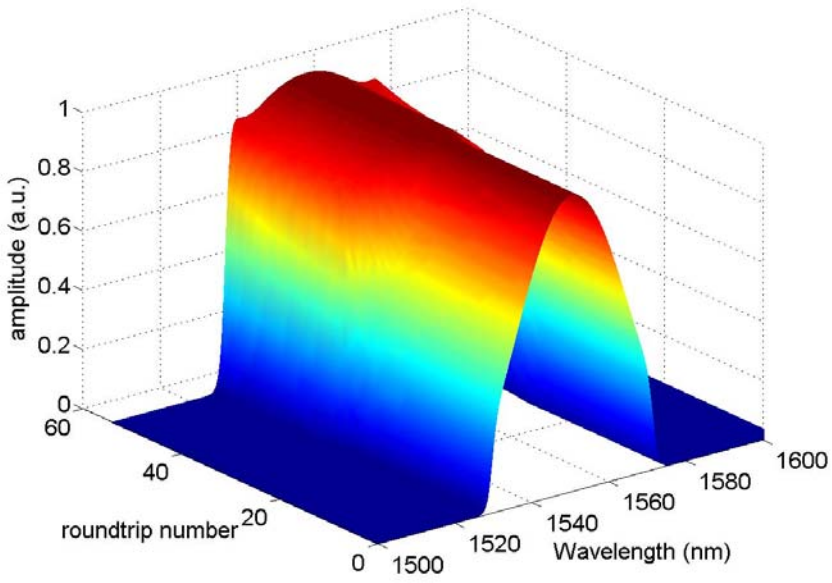

Figure A.4.: Evolution of the spectrum during one roundtrip

List of Figures

List of Tables

Bibliography

[Agi] Agilent Technologies: *Agilent E5052B Advanced Phase noise and transient measurement techniques*. http://cp.lietrature.agilent.com/litweb/pdf/5989-7273EN.pdf.

[Agr91] Agrawal, Govind P.: *Optical Pulse Propagation in doped fiber amplifiers*. Phys. Rev. A, 44:7493, 1991.

[Agr01a] Agrawal, Govind P.: *Applications of Nonlinear Fiber Optics, 1st Edition*. Academic Press San Diego, San Francisco, Noew York, Boston, London, Sydney, Tokyo, 2001.

[Agr01b] Agrawal, Govind P.: *Nonlinear Fiber Optics, 3rd Edition*. Academic Press San Diego, San Francisco, Noew York, Boston, London, Sydney, Tokyo, 2001.

[Alt06] Altarelli et. al., M. (editor): *The European X-Ray Free-Electron Laser Technical Design Report*. DESY, 2006.

[Aun00] Aune et al., B.: *The superconducting TESLA cavities*. PRST-AB, 3, September 2000.

[Ayv06] Ayvazyan et al., V.: *First operation of a free-electron laser generating GW power radiation at 32 nm wavelength*. Euro. Phys. J. D, 37:297–303, 2006.

[bat] *www.batop.de*.

[BK95] Brovelli, L. R. and U. Keller: *Design and operation of antiresonant Fabry-Perot saturable semiconductor absorbers for mode-locked solid-state lasers*. J. Opt. Soc. Am. B, 12:311–322, 1995.

[Bro07] Brochetta et. al., C. (editor): *Fermi@Elettra Conceptual Design Report*. Sincrotrone Trieste, 2007.

[CEF+05] Czuba, K., Frank Eints, Matthias Felber, Janus Dobrowolski and Stefan Simrock D: *First Generation of Optical Fiber Phase Reference Distribution System for TESLA*. Technical Report, DESY TESLA-REPORT 2005-08, 2005.

[Che06] Chen, J.; Sickler, J. W.; Ippen E. P.; Kaertner F. X.: *High repetition rate, low jitter, low intensity noise, fundamentally mode-locked 167 fs soliton Er-fiber laser*. Optics Letters, 32:1566–1568, 2006.

[DK05] Danailov, M. B.; Ilday, F. Ö. and F. X. Kärtner: *Integrated Design of Laser Systems for a FEL User Facility*. In *Proceedings of the FEL 2005, Stanford, USA*, 2005.

[Dul91] Duling, I. N.: *All-fiber ring soliton laser mode locked with a nonlinear mirror*. Optics Letters, 16:539–541, 1991.

[ET3a] *EOTECH Photodiode ET-3010, www.eotech.com*.

[ET3b] *EOTECH Photodiode ET-3500F, www.eotech.com*.

[FL07] F. Loehl, H. Schlarb, J. Chen F. X. Kärtner J.-W. Kim: *First prototype of an optical cross-correlation based fiber-link stabilization for the FLASH synchronization system*. In *Proceedings of the DIPAC 2007 Conference, Venice, Italy*, 2007.

[FP99] Faatz, B. and J. Pflüger: *Magnet Sorting for the TTF-FEL Undulator using Simulated Annealing*. Technical Report, DESY, 1999. TELSA-FEL 1999-01.

[FP02] Flöttmann, K. and Ph. Piot: *An upgraded Injector for the TTF FEL-User Facility*. In *Proceedings of the EPAC 2002*, Paris, France, 2002.

[FXKK98] F. X. Kärtner, J. A. der Au and U. Keller: *Mode-Locking with Slow and Fast Saturable Absorbers - What's the Difference?* IEEE J. Selected Top. in Quantum Electron., 4:159–168, 1998.

[GAB+08] Gahl, C., A. Azima, M. Beye, M. Deppe, K. Döbrich, U. Hasslinger, F. Hennies, A. Melnikov, M. Nagasono, A. Pietzsch, M. Wolf, W. Wurth and A. Föhlisch: *A femtosecond X-ray/optical cross-correlator*. Nature photonics, published online, 2008.

[GBS07] G. Berden, W. A. Gillespie, S. P. Jamison E.-A. Knabbe A. M. MacLeod A. F. G. van der Meer P. J. Phillips H. Schlarb B. Schmidt P. Schmüser

and B. Steffen: *Benchmarking of Electro-Optic Monitors for Femtosecond Electron Bunches*. Phys. Rev. Lett., 99:164801, 2007.

[Gie05] Giergusiewicz et. al., W.: *Low latency control board for LLRF system SIMCON 3.1*. In *Proc. of SPIE Vol. 5948*, 2005.

[Hau91] Haus, H. A.; Ippen, E. P.; Fujimoto J. G.: *Structures for additive pulse mode locking*. Journal of the Optical Society of America B, 8:2068–2078, 1991.

[Hau00] Haus, H. A.: *Mode-Locking of Lasers*. IEEE J. Selected Top. in Quantum Electron., 6:1173?1185, 2000.

[Hof91] Hofer, M, Fermann M. E. Haberl F. Ober M. H. Schmidt A. J.: *Mode-Locking with cross-phase and self-phase modulation*. Optics Letters, 16:502–504, 1991.

[HP98] Herziger, Gerd and Reinhart Poprawe: *Lasertechnik I*. Fraunhofer Institut fuer Lasertechnik, Aachen, 1998. Vorlesungsscript.

[HPMG+99] Hönninger, C., R. Paschotta, F. Morier-Genoud, M. Moser and U. Keller: *Q-switching stability limits of continuous-wave passive mode locking*. J. Opt. Soc. Am. B, 16:46–56, 1999.

[Isc03] Ischebeck, R.: *Transverse Coherence of a VUV Free Electron Laser*. PhD thesis, Hamburg University, 2003. DESY-THESIS-2003-033.

[JWKS07] J.-W. Kim, J. Chen, Z. Zhang F. N. C. Wong F. X. Kärtner F. Loehl and H. Schlarb: *Long-term femtosecond timing link stabilization using a single-crystal balanced cross correlator*. Optics Letters, 32:1044–1046, 2007.

[KL06] Kim, J.-W.; Kaertner, F. X.; and F. Ludwig: *Balanced optical-microwave phase detectors for optoelectronic phase-locked loops*. Optics Letters, 31:3659–2662, 2006.

[KM04] Kim, J.-W.; Ilday, F. Ö.; Kärtner F. X.; Mücke O.; Perrott M. H.; Graves W. S. and D. E. Moncton: *Large-Scale Timing Distribution and RF-Synchronization for FEL Facilities*. In *FEL Conference Trieste, Italy*, 2004.

[Lee89] Lee et. al., C. E.: *Optical-fiber Fabry-Perot embedded sensor*. Opt. Lett., 14:1225–1227, 1989.

[LHL+06] Loehl, F., K. Hacker, F. Ludwig, H. Schlarb, B. Schmidt and A. Winter: *A sub 100 fs Electron Bunch Arrival-Time Monitor System for FLASH*. In *Proceedings of the EPAC 2006 conference, Edinburgh, UK*, 2006.

[Lie05] Liepe, M.: *Superconducting RF and RF Control*. In *ERL 2005 Workshop, Newport News, USA*, 2005.

[Loh93] Loh, W. H.; Atkinson, D.; Morkel P. R.; Hopkinson M.; Rivers A.; Seeds A. J.; Payne D. N.: *All-solid-state subpicosecond passively mode locked erbium-doped fiber laser*. Appl. Phys. Lett., 64, 1993.

[Löh07] Löhl, F. private communication, 2007.

[Lor] Lorbeer, B.; Mueller, J.; Ludwig F.; Loehl F.; Schlarb H.; Winter A.: *Noise and Drift Characterization of critical components for the laser based synchronization system at FLASH*. In *Proceedings of DIPAC 2007, Venice, Italy*.

[ME88] Milloni, P. W. and J. H. Eberly: *Lasers*. Wiley, New York, 1988.

[MGK01] M. Guina, N. Xiang, A. Vainionpää O. G. Okhotnikov T. Sajavaara and J. Keinonen: *Self-starting stretched-pulse fiber laser mode locked and stabilized with slow and fast semiconductor saturable absorbers*. Optics Letters, 26:1809–1811, 2001.

[RSTW01] Richard, F., J. R. Schneider, D. Trines and A. Wagner (Editors): *TESLA Technical Design Report*. Technical Report, DESY, March 2001. DESY 2001-011.

[SAL+05] Schlarb, H., V. Ayvazyan, F. Ludwig, D. Noelle, B. Schmidt, S. Simrock, A. Winter and F. X. Kärtner: *Next Generation Synchronisation System for the VUV-FEL at DESY*. In *27th FEL Conference, Stanford, USA*, 2005.

[SCG+02] Schreiber, S., J.-P. Carneiro, Ch. Gerth, K. Honkavaara, M. Hüning, Ph. Piot, E. Schneidmiller and M. Yurkov: *IMPROVED OPERATION OF THE TTF PHOTOINJECTOR FOR FEL OPERATION*. In *Proceedings of the EPAC 2002*, Paris, France, 2002.

[Sch07] Schlarb, H.: *FLASH upgraded - Preparing for the European XFEL -*. In *Proceedings of the FEL 2007 Conference, Novosibirsk, Russia*, 2007.

[Sim05] Simrock, S.: *Overview of options for RF control & state of the art simulation results and performance test results*. In *ERL 2005 workshop, Newport News, USA*, 2005.

[Ste07] Steffen, B.: *Electro-Optic Methods for Longitudinal Bunch Diagnostics at FLASH*. PhD thesis, Universität Hamburg, 2007.

[TES02] TESLA Test Facility FEL team, The: *SASE FEL at the TESLA Test Facility, Phase 2*. Technical Report, DESY, 2002. TELSA-FEL 2002-01.

[TN93] Tamura, K.; Ippen, E. P.; Haus H. A. ; and L. E. Nelson: *77-fs pulse generation from a stretched-pulse mode-lockedall-fiber ring laser*. Optics Letters, 18:1080–1082, 1993.

[UKdA93] U. Keller, K. J. Weingarten, F. X. Kärtner D. Kopf B. Braun I. D. Jung R. Fluck C. Hönninger N. Matuschek and J. A. der Au: *Semiconductor Saturable Absorber Mirrors (SESAM's) for Femtosecond and Nanosecond Pulse Generation in Solid-State Lasers*. IEEE J. Selected Top. in Quantum Electron., 2:435–445, 1993.

[vdL86] Linde, D. von der: *Characterization of the noise in continuously operating mode-locked lasers*. Appl. Phys. B, 39:201, 1986.

[Win04] Winter, A.: *Bunch length measurements using electro-optical sampling at the SLS Linac*. Master's thesis, RWTH-Aachen, DESY-THESIS-2004-027, 2004.

[Win05] Winter et. al., A.: *Femtosecond Synchronisation of Ultrashort Pulse Lasers to a Microwave RF Clock*. In *Proceedings of the PAC 2005, Knoxville, TN, USA*, 2005.

Acknowledgements

Without the great support I was given during the course of this thesis, its completion would not have been possible.
Firstly I would like to thank Prof. Dr. Peter Schmüser for his effort and enthusiasm in supporting my thesis in Hamburg.
Secondly my thanks go to Prof. Dr. F. X. Kärtner, who made my 1 year as a visitor to his laboratory at MIT possible. It was always a great pleasure to discuss with him and benefit from his great supply of ideas.
With Prof. Dr. F. Ömer Ilday, then a research associate in Prof. Kärtner's group, I spent countless hours in the lab where he taught me most things I know about fiber optics. Our discussions often extended to the (unfortunately) few restaurants around MIT and we spent many evenings in café's discussing ideas and proposals, a perfect combination of our appreciation for physics and good food.
Many thanks go to Dr. Holger Schlarb, who guided the research as head of the synchronization effort for the many helpful discussions. Further thanks go to Dr. Bernhard Schmidt, who as group leader of the FLA group greatly supported the synchronization effort and at the same time greatly enhanced my knowledge of good wines.
The working atmosphere in the MIT group was extremely pleasant during my stay there. My thanks go to Dr. Felix Grawert, Dr. Oliver Mücke, Dr. Richard Ell, Dr. Ariel Gordon, Dr. Christian Jirauschek, Dr. Philip Wagenblast, Aleem Siddiqi, Jason Sickler and Jung-Won Kim for making this possible. For the opportunity to measure at the MIT Bates Lab, I am indebted to Daniel Cheever, Defa Wang, Bill Grawes and Townsend Zwart.
I would also like to thank the members of the synchronization team at DESY: Florian Löhl -fellow graduate student working on the fiber link stabilization-, Karl-Heinz Mathiesen, Frank Ludwig - his electronics expertise was invaluably helpful-, Matthias Felber, Bernd Steffen, Kirsten Hacker, Sebastian Schulz, Dr. Vladimir Arsov, Dr. Axel Knabbe. They were always supportive and the many discussions helped solve a lot of problems. Many thanks also go to Wojchiech Jalmuzna, who greatly supported me with the SIMCON software. Invaluable support came from all the technical staff that was involved with making the results of this thesis possible, namely Bernd Beyer, Albert Schleiermacher, Mattias Böttcher, Mathias Hoffmann, Kai Ludwig, Otto Peters and Jens Hansen. I am also greatful to Prof. Dr. Manfred Tonutti, who convinced

me to get involved with accelerator physics in the first place - a decision I have not come to regret. Finally, many thanks also go to Mrs. Ingrid Nikodem for help with administrative issues.
Last but not least I would like to thank my family, colleagues and friends for their support and tolerance of my lack of communication during the last months.